2018

MICRO-SCALE STUDY OF MULTI-COMPONENT IONIC TRANSPORT IN CONCRETE

Feng, Ganlin

University of Plymouth

MICRO-SCALE STUDY OF MULTI-COMPONENT IONIC TRANSPORT IN CONCRETE

by

GANLIN FENG

A thesis submitted to University of Plymouth
in partial fulfilment for the degree of

DOCTOR OF PHILOSOPHY

School of Engineering, Science and Engineering

December 2017

Abstract

Corrosion of reinforcing steel in concrete due to chloride ingress is one of the main causes of the deterioration of reinforced concrete structures, particularly in marine environments. It is therefore important to develop a reliable prediction model of chloride ingress into concrete, which can be used to predict the chloride concentration profiles accurately to help to assess the service life for reinforced concrete structures. Cementitious materials are porous media with a highly complex and active chemical composition. Ionic transport in cementitious materials is a complicated process involving mechanisms such as diffusion, migration, ionic binding, adsorption and electrochemical interactions taking place in the pore solution of the materials. The process is dependent on not only the microstructural properties of the materials such as porosity, pore size distribution and connectivity but also the electrochemical properties of the pore solution including ionic adsorption and ion-ion interactions. This thesis presents a numerical study on the multi-component ionic transport in concrete with the main focus on the microscopic scale.

This study first investigated the impact of the Electric Double Layer (EDL) on the ionic transport in cement-based materials. The EDL is a well-known phenomenon found in porous materials, which caused by the surface charges at the interface between solid surfaces and pore solutions. The numerical investigation is performed by solving the multi-component ionic transport model with considering the surface charges for a cement paste subjected to an externally applied electric field. The surface charge in the present model is taken into account by modifying the Nernst-Planck equation in which the electrostatic potential is dependent not only on the externally applied electric field

but also on the dissimilar diffusivity of different ionic species including the surface charges. Some important features about the impact of surface charge on the concentration distribution, migration speed and flux of individual ionic species are discussed.

Then a new one-dimensional numerical model for the multi-component ionic transport in concrete to simulate the rapid chloride migration test is proposed. Advantages and disadvantages of the traditional methods used to determine the local electrostatic potential, i.e. electro-neutrality condition and Poisson's equation, are illustrated. Based on the discussion a new electro-neutrality condition is presented, which can avoid the numerical difficulties caused by the Poisson's equation, and remain the non-linearity of the electric field distribution. This model with the new electro-neutrality condition is employed to simulate the RCM test to prove its applicability. The new model is promising in solving the multi-component ionic transport problems especially in microscopic scale.

Lastly, a one-dimensional numerical investigation on the chloride ingress in a surface-treated mortar with considering the penetration of sealer induced porosity gradient was performed. The numerical model was carefully treated to apply governing equations of ionic transport to this situation of two pore structures, with every parameter clearly defined on the microscopic scale.

List of Abbreviations

1-D - One Dimensional

2-D - Two Dimensional

3-D - Three Dimensional

C_3A - $3CaO \cdot Al_2O_3$

C_4AF - $2CaO \cdot Al_2O_3 \cdot Fe_2O_3$

C_2S - $2CaO \cdot SiO_2$

C_3S - $3CaO \cdot SiO_2$

C-S-H - Calcium Silicate Hydrate

DEF - Delayed Ettringite Formation

EDL - Electric Double Layer

ECE - Electrochemical Chloride Extraction

ECR - Electrochemical Chloride Removal

ITZ - Interfacial Transition Zone

MRI - Magnetic Resonance Imaging

NPP - Nernst-Planck/Poisson

OPC - Ordinary Portland Cement

RCM - Rapid Chloride Migration

RCPT - Rapid Chloride Permeability Test

REV - Representative Elementary Volume

w/c - water/cement

List of Parameters

C - chloride concentration in the pore solution

C_b - concentration of bound chloride ions

C_f - concentration of free chloride ions

C_i - concentration of the ith species in the pore solution

C_k - concentration of the kth species in the pore solution

C_{ko} - concentration of ionic species k in the bulk zone

C_o - chloride concentration on the exposed surface

C_s - concentration of surface charge on the pore surface

D - diffusion coefficient of chloride ions

D_c - diffusion coefficient of substrate layer

D_i - diffusion coefficient of the ith species in the pore solution

D_k - diffusion coefficient of the kth species in the pore solution

D_s - diffusion coefficient of surface coating layer

D_w - empirical constant

$D(\theta)$ - hydraulic diffusivity

F - Faraday constant

J - diffusion flux of chloride ions

J_i - total ionic flux of the ith species in the pore solution

J_k - total ionic flux of the kth species in the pore solution

M_{cl} - molar mass of chloride

N - total number of ionic species in the pore solution

R - ideal gas constant

T - temperature

X - distance from the exposed surface

erfc - the complementary error function

t - penetration time

t_p - penetration depth of sealer

t_s - thickness of surface coating

v- water flow velocity

wp - chloride content in weight percentage

z_i - valence number of the ith species in the pore solution

z_k - valence number of the kth species in the pore solution

z_s - valence number of surface charge on the pore surface

α - material constants for ionic binding obtained by curve-fitting of the experiment data

β - material constants for ionic binding obtained by curve-fitting of the experiment data

ε_0 - permittivity of a vacuum

ε_r - relative permittivity of water at temperature 298K

ρ_{mor} - density of mortar sample

θ - volumetric water content (volume of water/bulk volume of the material)

θ_i - initial water content

θ_r - normalized water content

θ_s - water content at wetted surface

λ_D - Debye length

$\emptyset$ - porosity for a fully saturated material

$\emptyset_c$ - porosity of mortar substrate

$\emptyset_s$ - porosity of surface coating

Φ - electrostatic potential

Φ_b - electrostatic potential at the bulk solution

Φ_s - electrostatic potential at the solid surface

List of Contents

Table of Figures

List of Tables

Acknowledgement

I wish to express my sincere appreciation to those who have contributed to this thesis and supported me in one way or the other during this amazing journey.

First and foremost, I owe my deepest gratitude to my first supervisor and mentor, Prof. Long-yuan Li, for giving me this great opportunity to study and research at Plymouth University, as well as a role model to be a respectable scholar. His immense knowledge and insightful suggestions inspire and guide me throughout my PhD career. I also remain indebted for his understanding and patience during the times when I was really down and depressed. Without his consistent support, this thesis would have never been completed.

My sincere thanks also go to Dr Boksun Kim, my second supervisor, for her invaluable comments and encouragement. Despite her busy schedule, she was always able to go through my drafts of papers several times in detail.

I would also like to appreciate Dr Jin Xia from Zhejiang University and Dr Wujian Long from Shenzhen University, for their generous support and help during my visit in their universities for experiments.

I would like to acknowledge the financial support provided by School of Engineering, Plymouth University and China Scholarship Council for the PhD Scholarship, and European Union Research Council for the research grant (FP7-PEOPLE-2011-IRSES-294955).

Last but not the least, I would like to thank my parents for their constant unconditional support - both emotionally and financially, and my friends, whose support and encouragement was worth more than I can express on paper.

Author's Declaration

At no time during the registration for the research degree has the author been registered for any other University award, without prior agreement of the Doctoral College Quality Sub-Committee.

No work submitted for a research degree at University of Plymouth may form part of any other degree for the candidate either at the University or at another establishment.

This PhD study was financed with the aid of School of Engineering, Plymouth University, China Scholarship Council for the UK PhD scholar-ship and European Union Research Council for the research grant (FP7-PEOPLE-2011-IRSES-294955).

Word count of main body of thesis:

Signed: _____

Date: _____

Chapter One - Introduction

1.1 Motivation of Research on Ionic Transport in Concrete

Concrete made by mixing portland cement with fine aggregate (normally sand), coarse aggregate (normally gravel) and water is the most widely used construction material in the world (Taylor, 1997). Concrete structures often undergo significant degradation while interacting with the environment. Although modern cement-based materials are much improved in properties, the high and rising cost of replacement and renewal of infrastructure facilities caused by the degradation, placed pressures on ensuring durable constructions. Hence, the durability of concrete structures has received much more attention over the past decades (Shi *et al.*, 2012).

Chloride induced corrosion of reinforcing steel in concrete has been recognized as the most critical threat to the durability of reinforced concrete structures, particularly those exposed to chloride-rich environment such as marine and offshore infrastructures (Page, 1975). It is generally acknowledged that reinforcing steel bars embedded in concrete start to depassivate when the concentration of the surrounding chloride reaches a certain threshold value (Alonso *et al.*, 2000; Ann & Song, 2007; Glass & Buenfeld, 1997). The depassivation results in a significant corrosion rate of steel leading to cracking and spalling of the concrete cover, and eventually local failure of the structure. Therefore, it is important to understand how fast chloride ions can penetrate in the concrete, in order to predict the initial corrosion time and the service life of the structures in a given environment.

Cementitious materials are porous media with a highly complex and active chemical composition. Ionic transport in cementitious materials is a complicated process involving mechanisms such as diffusion, migration, ionic binding, adsorption and electrochemical interactions taking place in the pore solution of the materials. The process is dependent on not only the microstructural properties of the materials such as porosity, pore size distribution and connectivity (Garboczi & Bentz, 1996; Li, 2014), but also the electrochemical properties of the pore solution including ionic adsorption and ion-ion interactions (Li & Page, 1998; Li & Page, 2000).

A large number of experimental and field tests have been carried out in order to get quantitative information on factors affecting the chloride penetration through concrete cover. In addition, theoretical advances have also been made to establish adequate models to reveal the underlying mechanisms. A reliable prediction model of chloride ingress through the concrete cover, which could predict the corrosion initiation time, is considered as the key point for assessment of durability of concrete (Glasser, Marchand & Samson, 2008). However, there are still deviations between existing prediction models and experimental evidences. The difference means that these models are not mature yet. In particular, the impact of microstructure properties of concrete on the ionic transport remains unclear.

1.2 Outline of This Dissertation

The aim of this work is to improve the understanding on the mechanisms of chloride penetration in concrete, with the main focus on the influences of factors based on the microscopic scale. The outline of this thesis is presented as follows:

Chapter Two reviews the research background relevant to this study. A brief description of the complex porous system in the concrete matrix is given. A summary of mechanisms of ionic transport through concrete is then provided. Experimental and numerical techniques developed to study ionic transport in concrete are also reviewed. Lastly the research gaps of existing research, based on this review, are summarised and the goals of the present study to fill some of those gaps are outlined.

Chapter Three investigates the effect of Electric Double Layer (EDL) on the electro-migration of chloride ions in cementitious materials using a numerical method. The investigation is performed by solving the multispecies ionic transport equations for a cement paste subjected to an externally applied electric field. Conventionally the Poisson-Boltzmann equation is used to determine ionic distribution in the perpendicular direction to the charged surface and hence it is limited to one dimension. However, the ionic distribution in the penetration depth through the pores is also important and hence a two-dimensional model is required. To extend the numerical simulation to two dimensions, the Nernst-Planck and Poisson's equations are used, coupled with a constant amount of surface charge on the pore walls as boundary conditions. Parameters affecting the implications of the EDL on multispecies ionic transport are examined. Interactions between the local electrostatic potential in the EDL and the global applied electric field are also discussed.

Chapter Four presents a two-dimensional, two-phase ionic transport model with a surface charge at solid-liquid interfaces. The present model is applied to investigate the effect of surface charges at the solid-liquid interface on the ionic transport in a cement paste when it is subjected to an externally applied electric field. The surface charge in

the present model is considered by modifying the Nernst-Planck equation in which the electrostatic potential is dependent not only on the externally applied electric field but also on the dissimilar diffusivity of different ionic species including the surface charges. Some important features about the effect of surface charge on the concentration distribution, migration speed and flux of individual ionic species are discussed.

Chapter Five proposes a new one-dimensional numerical model for the multi-component ionic transport in concrete to simulate the RCM test. Advantages and disadvantages of the traditional methods used to determine the local electrostatic potential, i.e. electro-neutrality condition and Poisson's equation, are illustrated. Then a new electro-neutrality condition is presented, which can avoid the numerical difficulties caused by the Poisson's equation, and remain the non-linearity of the electric field distribution. Lastly the model with the new electro-neutrality condition is employed to simulate the RCM test to prove its applicability. The new model is promising in solving the multi-component ionic transport problems especially in microscopic scale.

Chapter Six presents a one-dimensional numerical investigation on the chloride diffusion in a surface-treated mortar with considering the penetration of sealer induced porosity gradient. Based on the simulation results, differences between cement sealers and coatings are examined and discussed

Chapter Seven summarize the main results and contributions of this thesis. Limitations of the present numerical study are discussed. Possible improvements for future work are also given in this Chapter.

Chapter Two - Research Background

This Chapter will review the research background relevant to this study. Firstly, a brief description of the complex porous system in the concrete matrix is given. A summary of mechanisms of ionic transport through such a complex porous matrix is then provided. Experimental and numerical techniques developed to study ionic transport in concrete are also reviewed. Lastly the research gaps of existing research, based on this review, are summarised and the goals of the present study to fill some of those gaps are outlined.

2.1 Brief Introduction of Concrete

Microstructure properties of porous media such as cement-based materials are at the heart of modern material science. Unlike other engineering materials, concrete has a highly heterogeneous and complex microstructure. This section will give a brief introduction of the complex porous system in the concrete matrix.

2.1.1 Composition of Concrete

Portland cement, the main raw material of concrete, is a grey power produced by pulverizing a clinker with calcium sulfate. The major chemical compounds of a clinker are C_3S ($3CaO{\cdot}SiO_2$), C_2S ($2CaO{\cdot}SiO_2$), C_3A ($3CaO{\cdot}Al_2O_3$) and C_4AF ($2CaO{\cdot}Al_2O_3{\cdot}Fe_2O_3$). When portland cement is dispersed in water, a number of complex chemical reactions commonly called hydration will result in formation of various hydration products. The hydration products with the capillary pore system between them form the phase called bulk cement paste. Therefore, concrete may be

considered as a two-phase material, consisting of aggregate particles dispersed in a matrix of cement paste (Sun *et al.*, 2011). However, there is also an Interfacial Transition Zone (ITZ) near the surface of coarse aggregate which is weaker than either of the main components of concrete, usually taken as the third phase (Mehta & Monteiro, 2006).

As the main component of concrete, hydrated cement paste contains four principal phases. The most important phase is calcium silicate hydrate (C-S-H), which makes up 50-60 percent of the volume of solids in a fully hydrated portland cement paste and acts as the primary binding phase. C-S-H has a poorly crystallized structure, and the exact structure of C-S-H still remains unknown. Calcium hydroxide (portlandite) makes up 20-25 percent of the volume of solids in the cement paste. It tends to form large crystals but has considerably lower surface area compared with C-S-H. Another major phase is calcium sulfoaluminates, which constitute 15-20 percent of the solid volume in the cement paste. The most important substance of this type is Ettringite, which is a trisulfate ($3CaO \cdot Al_2O_3 \cdot 3CaSO_4 \cdot nH_2O$) formed during the early stage of hydration and may eventually transform to monosulfate. Both Ettringite and monosulfate play an important role in degradation phenomenons of concrete such as sulfate attack. The last phase of concern is the unhydrated clinker grains. During hydration, the hydration products tend to crystallize close to the surface of large size cement particles, which may forms a coating around them and remaining the unhydrated clinker grains.

2.1.2 Microstructure of Concrete

The bulk cement paste contains several types of voids. Among these voids, capillary voids and gel pores in the C-S-H are of the greatest concern. Capillary voids are the space not filled by solid hydration products. The size of capillary pores range from 10 to 50nm in low water/cement ratio pastes (Mehta & Monteiro, 2006). With high water/cement ratio, capillary voids may be as large as 3 to 5μm. Gel pores in C-S-H are very small, (Brunauer *et al.*, 1970) suggested that the size may vary from 0.5 to 2.5nm. Most researchers use the total volume of capillary pores and gel pores to calculate the porosity, which is an important parameter to consider the pore structure features of cement-based materials. Another important criterion for evaluating the characteristics of pore structure is the pore size distribution, which can be obtained from mercury intrusion test (Winslow & Liu, 1990).

2.2 Mechanisms of Ionic Transport in Concrete

The penetration of chloride ions into concrete is a complicated process which involves diffusion, migration, convection and capillary suction through the pore solution and microcracking network, accompanied by interaction between ions in the pore solution and the solid phase of the pore structure, e.g. physical adsorption and chemical binding (Yuan *et al.*, 2009). In addition, the imbalance of ionic fluxes of different ionic species in the pore solution will generate an electrostatic potential, which also will affect the transport of chloride ions (Li & Page, 1998; Li & Page, 2000). It is important to understand individual transport mechanisms in order to establish appropriate models in different conditions. The main mechanisms of ionic transport in concrete are reviewed in this section.

2.2.1 Diffusion

Ionic diffusion is a mass transfer of ions driven purely by concentration gradients. Early models used Fick's Law to describe chloride diffusion (Collepardi, Marcialis & Turriziani, 1972; Saetta, Scotta & Vitaliani, 1993). The mathematical expression is:

$$\frac{\partial C}{\partial t} = -\nabla J = -\nabla(-D\nabla C) \tag{2-1}$$

where C is the chloride concentration in the pore solution, t is penetration time, D is the diffusion coefficient and J is the diffusion flux of chloride ions. The analytical solution of Eq. (2-1) for a one-dimensional semi-infinite problem is given by (Carslaw, Jaeger & Feshbach, 1962; Crank, 1975):

$$C = C_0 erfc\left(\frac{x}{\sqrt{4Dt}}\right) \tag{2-2}$$

where C_o is surface chloride concentration, x is the distance from the exposed surface and *erfc* is the complementary error function. With this solution, the diffusion coefficient can be determined by measured chloride profiles in field or experiments with curve fit. As will be discussed in the following sections, diffusion coefficient obtained from simply considering Fick's Law cannot accurately describe chloride transport in concrete. More sophisticated model is needed to account for various other factors.

2.2.2 Migration

The migration of ionic species is peculiar to electrochemical systems or systems containing charged species. In the migration process, the electric field creates a driving force for the motion of charged species. Pore solution in concrete contains many kinds of ionic species. Unlike molecules, charged particles do not move independently of one another in solution (Marchand & Samson, 2009). The local electro-neutrality needs to

be preserved at any point in an ionic solution which will create local electric field and affects the diffusion process. The externally applied electric field will also accelerate the ionic movement. The mutual effect of diffusion and electrochemical migration of ions can be described by the well-known Nernst-Planck equation:

$$J_i = -D_i \nabla C_i - D_i C_i \frac{F z_i}{RT} \nabla \Phi \qquad (2\text{-}3)$$

where J_i is the total ionic flux, C_i is the concentration of species i in the pore solution, D_i is the diffusion coefficient of species i, Φ is electrostatic potential whose gradient is the negative of the electric field, z_i is the valence number of species i, F is Faraday constant, R is the ideal gas constant, T is the temperature. The first term on the right side of Eq.(2-3) is the diffusion flux, the second term is the migration flux. In the migration flux, $z_i F$ is the charge per mole on a species. Multiplication by the electric field $-\nabla\Phi$ gives the force per mole. Multiplication by the mobility D_i/RT gives the migraiton velocity, and finally multiplication by the concentration C_i gives the contribution to the net flux J_i due to the migration caused by electric field (Newman & Thomas-Alyea, 2012).

This relation should be applied to every ionic species in the pore solution. And the local electrostatic potential can be determined using Poisson's equation (Liu *et al.*, 2012; Samson, Marchand & Beaudoin, 1999; Samson, Marchand & Snyder, 2003; Xia & Li, 2013):

$$\nabla^2 \Phi = -\frac{F}{\varepsilon_0 \varepsilon_r} \sum_{i=1}^{N} z_i C_i \qquad (2\text{-}4)$$

where ε_0 is the permittivity of a vacuum, ε_r is the relative permittivity of water at temperature 298K. Mathematically, there is a numerical difficulty in solving the Poisson's equation together with the Nernst-Planck equations, because the coefficient $F/\varepsilon_0\varepsilon_r$ in the righ-hand-side of Eq. (2-4) is a very large number with the scale to 10^{14}. The approximate replacement of Poisson's equations adopted by many researchers is the electro-neutrality condition, which is:

$$\sum_{i=1}^{N} z_i C_i = 0 \qquad (2\text{-}5)$$

More detailed discussion about these two methods to determine the electrostatic potential will be given later in Chapter 5.

It should be mentioned here that the Nernst-Planck equation (2-3) is only precise in dilute ideal electrolytes. A chemical activity term is needed to adjust the flux when the ionic strength of the pore solution is high which is not discussed here (Li & Page, 1998; Samson *et al.*, 1999). And most importantly, the Nernst-Planck/Poisson equations apply regardless of whether an external electric potential exists.

2.2.3 Convection

Concrete is rarely saturated except in submerged parts of marine structures (Nielsen & Geiker, 2003). In an unsaturated condition, pore solution can transport in porous concrete by means of capillary suction (McCarter, Ezirim & Emerson, 1992; Sabir, Wild & O'Farrell, 1998). This type of bulk movement of pore solution as a fluid is called convection. Clearly, transport of pore solution which is the principal medium of aggressive agents, such as chloride ions, is responsible for the deterioration of unsaturated concrete.

If neglecting the osmotic effect of ionic concentration on the transport of water, the ionic solution movement can be simplified as water movement. Mathematically, the penetration of water into porous media can be described by unsaturated flow theory based on extended Darcy equation and Richards equation (Hall, 1989; Hall, 2007; Lockington, Parlange & Dux, 1999; Samson *et al.*, 2005; Wang & Ueda, 2011; Wang, Li & Page, 2005). This unsaturated flow theory is originally developed for water transport in soils, but later has been applied to construction materials due to the similar water profiles of soils and building materials found in the MRI (Magnetic Resonance Imaging) experiments (Gummerson *et al.*, 1979; Hazrati *et al.*, 2002; Roels *et al.*, 2004).

The governing equation is:

$$\frac{\partial \theta}{\partial t} = \nabla\left(D(\theta)\nabla\theta\right) \tag{2-6}$$

where θ is the volumetric water content (volume of water /bulk volume of the material), $D(\theta)$ is a material property called hydraulic diffusivity, which is commonly approximated by an exponential-law (Carmeliet *et al.*, 2004):

$$D(\theta) = D_w \exp(n\theta_r) \tag{2-7}$$

where D_w and n are the empirical constants, $\theta_r = (\theta - \theta_i)/(\theta_s - \theta_i)$ is normalized water content, with θ_i the initial water content ($\theta_i = 0$ for dry initial condition), θ_s the water content at wetted surface (it is considered as equal to volume fraction porosity when the surface is fully wetted). The flux density of a species by convection is given by:

$$J_i = C_i \cdot \mathbf{v} = C_i \cdot \left[- D(\theta) \nabla \theta \right] \qquad (2\text{-}8)$$

where $\mathbf{v}$ is the water flow velocity, then equations (2-6), (2-7) and (2-8) can be used to consider the effect of convection on ionic transport in addition to other mechanisms.

2.2.4 Ionic Binding

During transport in pore structure of concrete, chloride may be partially immobilized due to chemical bound with concrete C_3A (tricalcium aluminate) or C_4AF phases (forming Friedel's Salt), or physical adsorption by the surface of hydration products such as C-S-H (Berman, 1972; Buenfeld *et al.*, 1998; Delagrave *et al.*, 1997; Luping & Nilsson, 1993). This chloride binding effect removes chloride ions from the pore solution, which slows down the rate of penetration. If chloride binding is not considered, the diffusion coefficients obtained from experiments and numerical models are underestimated (Geiker, Nielsen & Herfort, 2007; Jensen *et al.*, 1999; Justnes, 1998; Loser *et al.*, 2010; Lu, Li & Zhang, 2002; Martın-Pérez *et al.*, 2000; Shi *et al.*, 2012; Yuan *et al.*, 2009).

In experiments, water-soluble and acid-soluble chlorides are referred as free and total chlorides respectively. Theoretically only free chloride ions in the pore solution are responsible for the corrosion of the steel. However, bound chlorides can be released by the change of pH in the pore solution, which indicates that bound chloride ions may also present threat to steel (Glass & Buenfeld, 1997; Glass & Buenfeld, 2000; Kayyali & Haque, 1995; Reddy *et al.*, 2002; Suryavanshi, Scantlebury & Lyon, 1998).

The relationship between free and bound chloride ions during ionic transport can be described by the Langmuir isotherm, which is derived from physical chemistry. The non-linear relationship is (Wang, Li & Page, 2005):

$$C_b = \frac{\alpha C_f}{(1+\beta C_f)} \tag{2-9}$$

Where C_b is the concentration of bound chloride ions, C_f is the concentration of free chloride ions, α and β are material constants which can be obtained by curve-fitting of the experimental data (Sergi, Yu & Page, 1992). Different types of binding mechanisms are also proposed and discussed, However none of them can accurately fit the experimental data with different exposed chloride concentration conditions, including the Langmuir isotherms (Yuan *et al.*, 2009). It should be mentioned here that binding experimental data obtained from crushed concrete specimens may overestimate the chloride-binding capacity, because a real concrete pore structure would have lower specific surface than a crushed specimen (Jiřičková & Černý, 2006; Shi *et al.*, 2012).

2.2.5 Mixed Mechanisms

There is usually more than one transport mechanism involved in the chloride penetration process in concrete depending on the concrete properties and the exposed condition. Chloride diffusion coefficients calculated based on a single mechanism or combined mechanisms are often used to evaluate the chloride resistance (Marchand & Samson, 2009).

2.3 Experimental Techniques for Evaluating Chloride Ingress

Performance based approach to service life design is increasingly replacing the deterministic approach. This has led to propose a number of tests which are used to assess the chloride penetration in cement-based materials (Šavija, Luković & Schlangen, 2014).

These methods can generally be classified into three categories. One is the tests based on natural diffusion, including the salt ponding test (AASHTO-T259, 2006) and the bulk diffusion test (NT-BUILD443, 1995). The second one is migration tests, which include the rapid chloride permeability test (ASTM-C1202, 2010) and the rapid migration test (NT-BUILD492, 1999). The other group includes different indirect measurement such as correlating the electrical resistivity of concrete to the resistance of chloride penetration (Andrade *et al.*, 1994; Mercado, Lorente & Bourbon, 2012). The natural diffusion test and migration test are the main methods adopted to evaluate the chloride resistance of concrete in Construction Standards.

Natural diffusion tests are long-term tests and time-consuming. The AASHTO-T259 salt ponding test setup is shown in Figure 2-1. This test may be influenced by the absorption effect and difficult in developing a sufficient chloride profile for some higher quality concretes (Stanish, Hooton & Thomas, 1997).

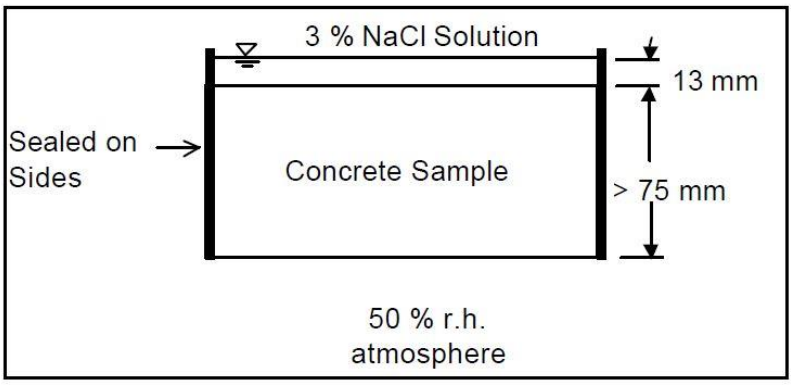

Figure 2-1. AASHTO-T259 salt ponding test setup (AASHTO-T259, 2006).

Compared to the diffusion tests, the migration tests have relatively short duration and are mostly used in research and engineering practice nowadays. The rapid chloride permeability test (RCPT) measures the total charge passed the specimen which is subjected to a 60V applied DC voltage for 6 hours as shown in Figure 2-2. It is apparent that the current passed is related to all ions in the pore solution not just the chloride ions, thus the application of this test in evaluating the chloride ingress is highly questionable (Andrade, 1993; Pfeifer, McDonald & Krauss, 1994).

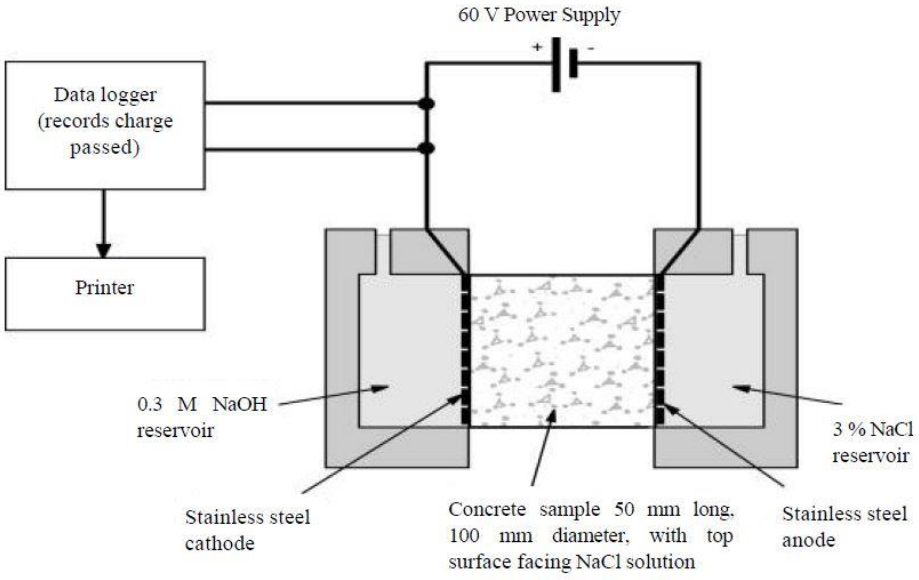

Figure 2-2. RCPT setup (ASTM-C1202, 2010)

Another migration test based on the similar principal is the rapid migration test (RCM), which was originally developed by (Tang & Nilsson, 1993) and shown in Figure 2-3. Instead of measuring the total passed charge, the RCM test measures the chloride penetration depth using silver nitrate solution as a colorimetric indicator (Baroghel-Bouny *et al.*, 2007; He *et al.*, 2012; Yang & Chiang, 2009), then the diffusion coefficient is calculated by the depth based on the mathematical solution of the Nernst-Planck equation (Luping, 1996). RCM test does address the criticisms of the RCPT related to measurement of actual chloride ion movement. However, the theory used to calculate the diffusion coefficient still ignores many influencing factors such as interaction between different ionic species in the pore solution and the pore structure features.

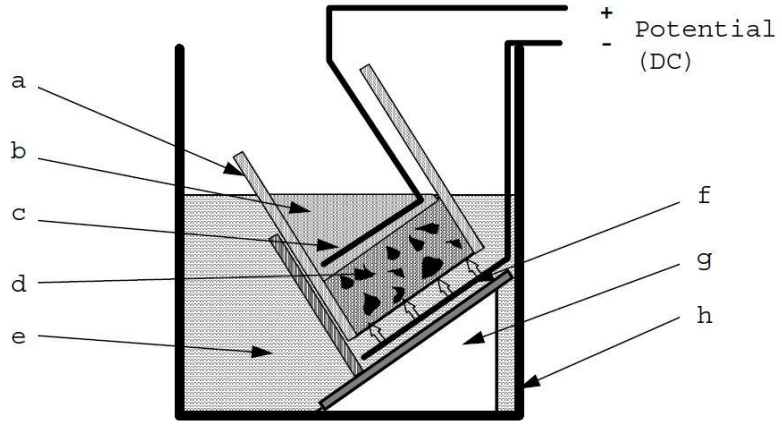

Figure 2-3. RCM setup (NT-BUILD492, 1999)

2.4 Numerical Simulation of Chloride Penetration in Concrete

From the review of experimental techniques developed to evaluate the chloride penetration rate in concrete, we can see that the main mechanisms considered are ionic

diffusion and ionic migration. The diffusion and migration of ionic species in an electrolytic solution can be described by Fick's Law and Nernst-Planck equation, respectively. However, the governing equations of the mechanisms mentioned above are mainly discussed and adopted at the microscopic scale in the pore solution (Xi & Bazant, 1999). Accurate definition of ionic transport in the pore solution may not fully describe the test results at large scale. Before reviewing the recent numerical modelling developments, some important definitions about the scales are introduced which should be considered before applying the mathematical equations.

2.4.1 Multi-Scale Modelling

The two main phases of concrete, hydrated cement paste and aggregate, are neither homogeneously distributed with respect to each other, nor homogeneous within themselves (as shown in Figure 2-4). Therefore, it is very difficult to constitute realistic models of its microstructure, from which the behaviour of the material can be reliably predicted. Many attempts have been made to find a reliable method which can be used to consider the effects of pore structure.

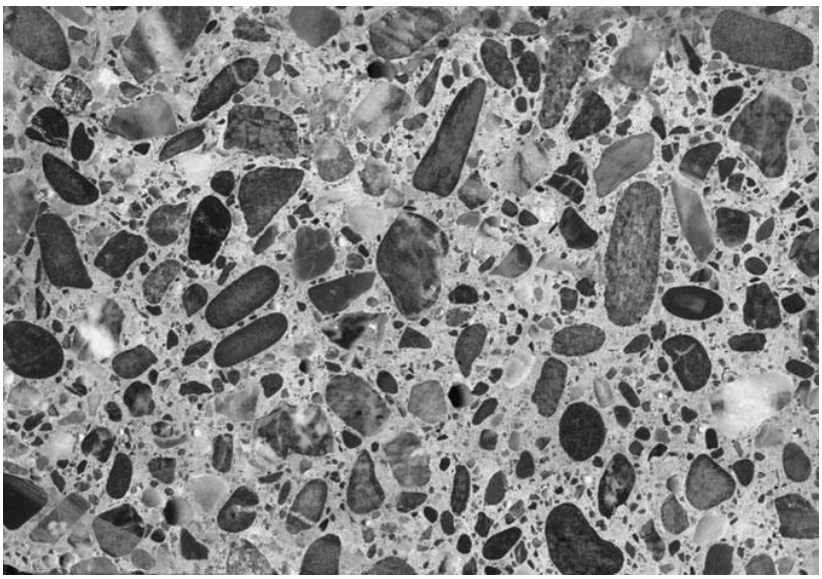

Figure 2-4. Polished section of a concrete specimen (Mehta & Monteiro, 2006)

To take into account of the concrete material properties, three different scales are introduced (Caré & Hervé, 2004; Sun *et al.*, 2011):

- The microscopic scale, based on the order of magnitude from 10^{-9} m to 10^{-7} m, deals with the micro pore network features of concrete. These features can be characterized by many pore structure parameters such as porosity, tortuosity and constrictivity. A simple explanation of the parameters affecting the ionic transport path is shown in Figure 2-5. Interactions between ions in the pore solution and the solid phase of the pore structure, e.g. physical adsorption and chemical binding, should also be measured in microscopic scale.(Tournassat & Steefel, 2015)
- The mesoscopic scale, based on the order of magnitude from 10^{-6} m to 10^{-3} m, considers the concrete as a composite material with three phases as shown in Figure 2-6. The aggregates are assumed to be randomly distributed in a continuous cement paste matrix. Both aggregate and cement paste can be approximately considered as homogeneous. Interfacial transition zone (ITZ) is usually taken as the third phase at the mesoscopic scale as the interface is different from the cement paste phase. Experimental results demonstrated that ITZ is an interface with a gradient of porosity and complex compounds (Gao *et al.*, 2005).The diffusivity of concrete is determined by diffusivities of all the three phases and their volume fraction involving different composite material theories.
- The macroscopic scale, based on the order of magnitude 10^{-2}m, corresponds to the size of experimental specimens. Chloride profiles obtained from steady-state experiments are analysed with the Fick's first law to determine the effective chloride diffusion coefficient. The coefficient is then expressed as an empirical

function with experimental factors such as water/cement ratio (Atkinson & Nickerson, 1984; Hobbs, 1999).

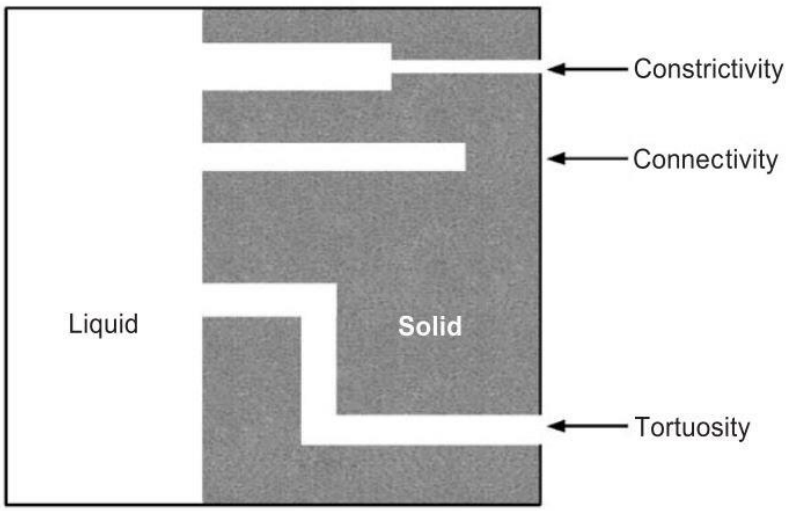

Figure 2-5. Schematic of pore structure parameters (Shane *et al.*, 1999; Van Brakel & Heertjes, 1974).

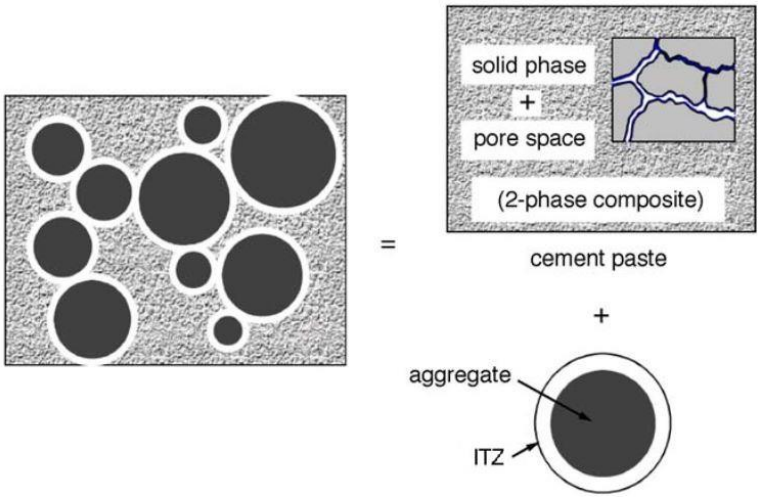

Figure 2-6. Three-phase composite at the mesoscopic scale (Oh & Jang, 2004).

2.4.2 Representative Elementary Volume

In order to link the mathematical transport equations derived at the pore scale to the macroscopic performance of concrete, homogenization methods are used to clarify the theoretical definition of the state variables (Samson, Marchand & Beaudoin, 1999). The basis of homogenization method relies on the concept of representative elementary volume (REV).

By definition, the representative elementary volume is an infinitesimal part of the three-dimensional material system. More precisely, if L and l are the characteristic lengths of the structure and the elementary volume respectively, the condition $l \ll L$ guarantees the relevance of the use of the tools of differential calculus offered by a continuum description. Furthermore, the elementary volume is expected to be large enough to be representative of the constitutive material, which explains its name as representative elementary volume. It is intuitively understood that this property requires the characteristic size of the REV to be chosen so as to capture in a statistical sense all the information concerning the geometrical and physical properties of the physics at stake. Roughly speaking, if d is the characteristic length scale of the local heterogeneities, typically the pore size in a porous medium, the condition $d \ll l$ is expected to ensure that the elementary volume is representative. In summary, the two conditions on the size of the REV are (Dormieux, Kondo & Ulm, 2006):

$$d \ll l \ll L \tag{2-10}$$

In terms of concrete material, a valid REV should be large enough that the pore structure characteristics (such as porosity, paste fraction, etc) are representative of the material. A random REV of porous media is shown in Figure 2-7. Through REV, the equations

at the microscopic scale are then averaged over the entire volume of the material, which can be used to model the chloride penetration in experiment with clear definitions.

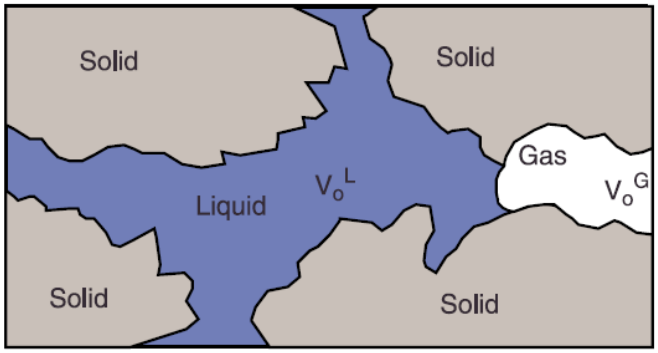

Figure 2-7. A simple illustration of REV (Samson *et al.*, 2005).

2.4.3 Multi-Component Migration Models

Over the past two decades, a number of models have been developed to numerically simulate the chloride penetration in concrete, ranging from classical mono-species diffusion models based on Fick's laws (Collepardi, Marcialis & Turriziani, 1972) to multi-species diffusion-migration models based on Nernst-Planck and Poisson's equations (Samson & Marchand, 1999; Xia & Li, 2013). The rapid developments in the field of chloride migration tests have heightened the need for precise migration models.

In the early migration models developed for cementitious materials the electrostatic potential used in the Nernst-Planck equation is merely determined by the externally applied electric field. In this case, the transport equations of individual ionic species in the material can be treated separately and solved independently (Atkinson & Nickerson, 1984; Dhir, Jones & Ng, 1998; Maheswaran & Sanjayan, 2004; Page, Short & El Tarras, 1981; Sergi, Yu & Page, 1992; Tang & Nilsson, 1993). The influence of ionic

interaction between different ionic species in cementitious materials on the electrostatic potential was considered first by Yu and Page (Yu & Page, 1996), then Li and Page (Li & Page, 1998; Li & Page, 2000), and followed by others (Elakneswaran, Nawa & Kurumisawa, 2009c; Friedmann, Amiri & Aït-Mokhtar, 2008a; Johannesson *et al.*, 2007; Krabbenhøft & Krabbenhøft, 2008; Truc, Ollivier & Nilsson, 2000a; Truc, Ollivier & Nilsson, 2000b; Xia & Li, 2013), in which the electrostatic potential is determined based on not only the externally applied electric field but also the internal electrostatic potential generated by the dissimilar diffusivity of different ionic species. Consequently, the transport equations of individual ionic species in the material are coupled each other and have to be solved dependently. Recently, the multicomponent transport model has been expanded from a single-phase model to two- and three-phases mesoscopic model to consider the heterogeneous nature of the cementitious materials (Dehghanpoor Abyaneh, Wong & Buenfeld, 2013; Dehghanpoor Abyaneh, Wong & Buenfeld, 2014; Li, Xia & Lin, 2012; Liu *et al.*, 2015; Liu *et al.*, 2012).

2.5 Control of Steel Corrosion Induced by Chloride Penetration

Many kinds of protective and rehabilitation methods have been used to control the corrosion of embedded steel in reinforced concrete structures caused by chloride penetration. This section provides a brief overview of the main physical and chemical techniques adopted in practice.

It is to be expected that when the embedded steel is protected from external environment by an adequately thick concrete cover with low permeability, the corrosion of steel and other problems associated with it would not arise. Therefore, the most straightforward way to restrict chloride penetration from the environment is using

highly impenetrable concrete. But considering the cost efficiency and the complexity to adjust concrete mixture parameters, surface protection method is often considered to be the alternative and more effective way to enhance durability characteristic of concrete. According to EN standard (Uni, 2004), surface protection can be used as a protection system in new concrete structures and also as a repair method for old structures. Different classifications have been made in previous published literatures for concrete surface protection materials, concerning performance of surface treatments on concrete (Basheer *et al.*, 1997; Buenfeld & Zhang, 1998; Ibrahim *et al.*, 1997) (Maslehuddin *et al.*, 2005; Safiuddin & Soudki, 2011; Seneviratne, Sergi & Page, 2000; Thompson *et al.*, 1997). In general, surface treatment for concrete includes coatings, penetrants and sealers. Concrete surface coatings form a continuous film on concrete surface, penetrants line the pore walls of concrete to render it hydrophobic and sealers penetrate concrete substrate and may form a thin layer on the surface (Zhang & Buenfeld, 2000a). Either way, the surface treatments aim to make the concrete cover less permeable to aggressive substances or cut off the water transportation into the concrete cover, which provides the path for chloride ions.

Instead of conventional repairs and physical protections provided by surface treatment, electrochemical techniques such as cathodic protection and electric chloride removal are also effective methods to control the corrosion of embedded steel. Steel corrosion in concrete occurs by the movement of electric charge from the anode (a positively charged area of steel where the steel is dissolving and forming rust) to the cathode (a negatively charged area of steel where oxygen and water are turned into hydroxyl ions). The best known and most established technique to control this electrochemical corrosion process is cathodic protection. Cathodic protection systems aim to suppress

the current flow in the corrosion area either by supplying externally a current flow in the opposite direction or by using sacrificial anodes. Unlike localized patch repairs which may accelerate corrosion in adjoining areas due to the incipient anode effect, cathodic protection system prevents corrosion across the whole of the protected area of the structure (Broomfield, 2006).

In the case of corrosion control against chloride penetration, another effective electrochemical method is electrochemical chloride removal (ECR), which is also frequently called electrochemical chloride extraction (ECE). Generally, the chloride removal process involves applying a high but temporary DC current through concrete cover between the reinforcing steel and an external anode (Li & Page, 1998; Li & Page, 2000; Liu *et al.*, 2014; Wang, Li & Page, 2001). The electric force will drive the negative chloride ions from the steel surface, which is the cathode, towards the external anode. The aim of electrochemical chloride removal is to remove the chloride ions around the steel surface as much as possible and within a comparatively short time (a few weeks normally). Although electrochemical methods mentioned above are more effective than conventional repairs, there are still some limitations for them to apply in practice. The electrochemical methods are more expensive than conventional repairs and must be used with great care in different conditions. More standards and specifications for electrochemical methods are needed.

2.6 Research Gap in Microscopic Scale Modelling of Chloride Penetration in Concrete

Despite the considerable amount of experimental and numerical work published on chloride penetration in concrete, far too little attention has been paid to the micro-scale level investigation on the penetration mechanism of chlorides. Therefore, the main objective in this section is to outline the research gaps in the literature and to introduce research goals that will fill some of those gaps in this thesis.

2.6.1 Influence of Electric Double Layer on Chloride Penetration in Concrete

The Electric Double Layer (EDL) is a well-known electrochemical phenomenon, which can be found at the interface of the solid hydrates surface and the electrolytic pore solution in cementitious materials (Viallis-Terrisse, Nonat & Petit, 2001).

Due to the mixed mechanisms such as ionization, ionic adsorption and ionic dissolution, the cement hydrates will develop a surface charge when brought into contact with the pore solution (Elakneswaran, Nawa & Kurumisawa, 2009c). The charge imbalance near the surface will create a local electric potential difference. Ions in the pore solution of opposite charge to that of the surface (counter-ions) are attracted towards the charged surface, while ions of like charge (co-ions) are repelled from the surface due to the electric force. However, of finite size, the centre of an ion can only approach the surface to within its hydrated radius without becoming specifically absorbed, which creates an inner layer called ‘stern layer’. Beyond the stern layer to the unaffected pore solution, the electric attraction and repulsion is combined by the mixing tendency resulting from the random thermal motion of the ions. These ions are then distributed in a ‘diffuse’ manner and this layer is called ‘diffuse layer’. The stern layer and diffuse layer form

the structure of EDL (Probstein, 2005). The local electric charge and potential imbalance in the EDL have a great impact on ionic transport in porous media, especially in fine pores (Appelo & Wersin, 2007; Kari *et al.*, 2013). Therefore, the surface charge on the pore surface is another important factor that should be taken into account in the ionic transport in concrete.

However, so far, there has been little work on the effect of the EDL on the ionic transport in cementitious materials. Several researchers (Nägele, 1985; Zhang & Buenfeld, 1997; Zhang & Buenfeld, 2000b) have reported the measurement of significantly high membrane potentials caused by the surface charge at the interface. This local electric potential and surface charge may have a great impact on the ionic distribution and ionic migration, especially in finely porous media.

2.6.2 Influence of Various Pore Structure on the Ionic Transport

The physical resistance of concrete to chloride penetration is highly dependent on the pore structure of concrete in terms of porosity, pore size, pore distribution and interconnectivity of the pore system, which are determined by many factors such as type of cement, w/c ratio, supplementary cementing materials, compaction, curing, stress conditions, shrinkage, etc. It should be mentioned here that these pore structure parameters are not intrinsic fixed numbers. During the service life of concrete structures, continuing hydration of cement, shrinkage due to the loss of water in the pores or thermal changes, stress condition changes and chemical attacks when exposed to detrimental environment may cause continuous changes of concrete pore structure (Dehghanpoor Abyaneh, Wong & Buenfeld, 2013; Spiesz & Brouwers, 2013; Sun *et al.*, 2011).

Also, when concrete is subjected to surface treatment, which has been proved as an efficient barrier system for concrete structures, normally the chloride ions need to pass through two materials with different pore structures to reach the reinforcing steel. This process cannot be simply described by the models based on single porous medium. It should be carefully treated to apply ionic transport models in this situation of two pore structures, with every parameter clearly defined on the microscopic scale.

2.6.3 Influence of Other Degradations on Chloride Penetration in Concrete

While interacting with external environment, concrete often undergoes significant alterations (such as carbonation, leaching and sulfate attack) which have adverse consequences on its engineering properties. Most of the alterations including the pore structure changes come from the detrimental chemical reactions (Glasser, Marchand & Samson, 2008).

Concrete is a porous material made of a rigid solid matrix and a liquid phase (pore solution). The solid is a composite mixture of complex crystallized hydrated compounds. The liquid phase in concrete is a highly charged ionic solution containing mainly OH^-, Na^+, SO_4^{2-} and Ca^{2+} ions. During the service-life of the concrete structure, the chemical composition of the concrete pore solution can be modified by the penetration of external ions and/or the leaching of ions already present in the pore solution. The modification of the pore solution chemical composition readily leads to a series of dissolution/precipitation reactions, which can significantly alter the pore structure of concrete. These microstructure alterations will then in turn affect the ionic

transport in the pore solution. A brief overview of the various types of chemical reactions is presented in following sections.

2.6.3.1 Sulfate Attack

Cement-based materials exposed to ground waters with sulfate may undergo substantial degradation, which is called external sulfate attack (Taylor, 1997). On the other hand, sulfates present in the original mix can also damage the material by the form of delayed ettringite formation (DEF), which is called internal sulfate attack (Taylor, Famy & Scrivener, 2001). It is commonly accepted that the main reactions in sulfate attack occur between sulfate ions and ionic species of pore solution to precipitate gypsum ($CaSO_4 \cdot 2H_2O$), ettringite ($3CaO \cdot Al_2O_3 \cdot 3CaSO_4 \cdot 32H_2O$), thaumasite ($Ca_3[Si(OH)_6 \cdot 12H_2O] \cdot (CO_3) \cdot SO_4$) or mixtures of these phases. The formation of gypsum and ettringite may cause expansion and ultimately cracking, spalling and other degradation phenomenon. Experimental results showed that high sulfate concentrations exposure condition leads to precipitation of gypsum, while lower sulfate concentration exposure condition leads to no or only little gypsum precipitation (Planel *et al.*, 2006; Schmidt *et al.*, 2009). Although the exact origin of the pressure causing macroscopic expansion is still controversial, ettringite precipitation is usually recognised as the predominant cause.

Depending on the cation type associated with the sulfate solution (i.e., Na+ or Mg^{2+}), the mechanism of sufate ingress is different (Gollop & Taylor, 1995). Santhanam et al. (Santhanam, Cohen & Olek, 2002; Santhanam, Cohen & Olek, 2003) summarized the experimental results from a comprehensive research study on sulfate attack and

proposed different mechanisms of attack resulting from sodium and magnesium sulfate solutions which are shown in schematic diagram in Figure 2-8 and Figure 2-9.

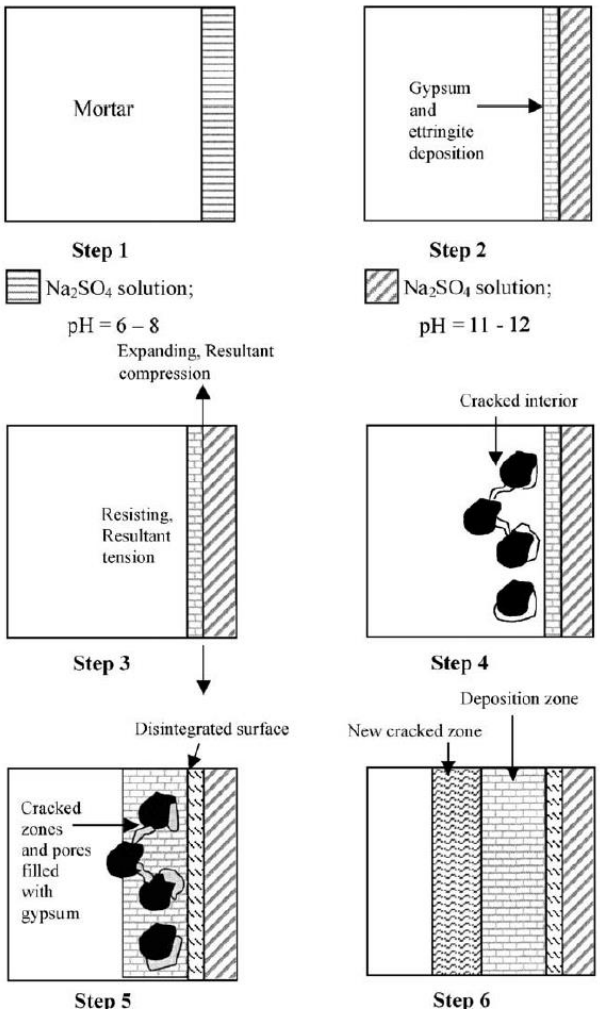

Figure 2-8. Proposed mechanism of sodium sulfate attack (Santhanam, Cohen & Olek, 2003).

In the case of sodium sulfate attack, the expansion follows a two-stage process. During the initial stage, the expansion is very slow. There is a sudden increase in the expansion rate in the second stage and this rate keeps nearly constant until failure. On the other hand, in the case of magnesium sulfate attack, expansion occurs at a continuously increasing rate. Main reason of the difference between sodium and magnesium sulfate attack is that, the conversion of calcium hydroxide to gypsum is accompanied by the

simultaneous formation of magnesium hydroxide (brucite), which is insoluble and reduces the alkalinity of the system. In the absence of hydroxyl ions in the solution, C-S-H is no longer stable and converts to the non-cementitious magnesium silicate hydrate (M-S-H). The magnesium sulfate attack is therefore more severe on cement-based materials.

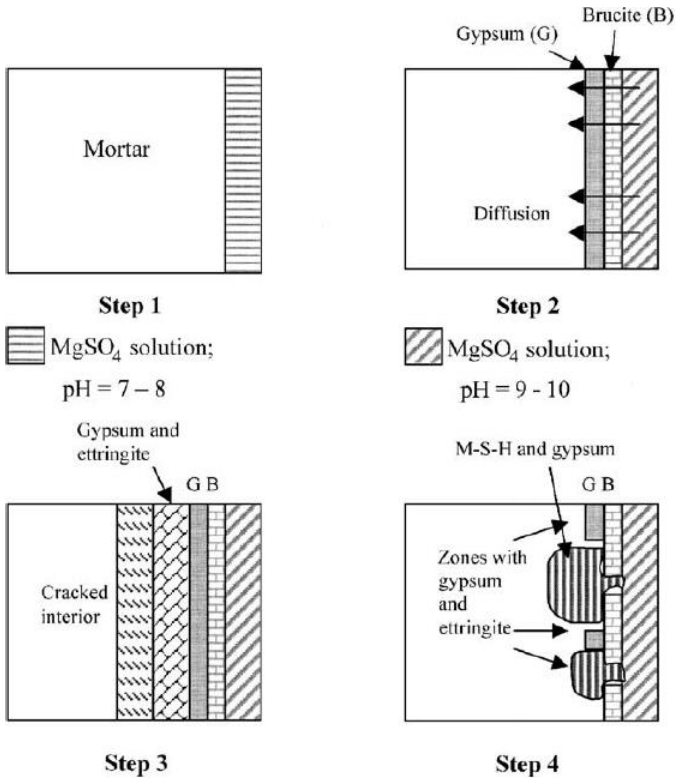

Figure 2-9. Proposed mechanism of magnesium sulfate attack (Santhanam, Cohen & Olek, 2003).

Many other factors can influence the degradation of concrete by sulfate attack such as water/cement ratio, the mineralogy of cement, supplementary cementing materials and temperature. Thus, modelling the microstructural alterations is a challenging task due to the complicated mechanism of sulfate attack.

The mostly accepted model capable of treating multi-species reactive transport problems is given by (Moranville, Kamali & Guillon, 2004), where the current chemical equilibrium state is obtained locally by means of a chemical equilibrium code (coupled chemical-transport models). Such numerical tools turn out to be essential when the degraded states of the material have to be precisely predicated in terms of the time evaluation of volume fraction of the various hydrate products dissolved or precipitated at each point of the material. These tools are also crucial in the case of complex aggressive solutions containing different species, which generally cannot be directly considered by simplified approaches involving only a limited number of species (Lothenbach *et al.*, 2010).

$$Ca^{2+}_{(aq)} + 2OH^{-}_{(aq)} = Ca(OH)_{2_{(s)}} \tag{2-11}$$

In terms of dissolution/precipitation reaction, such as reaction (2-11), the algebraic chemical equilibrium equation used to model this reaction can be derived as (Rubin, 1983; Samson, Marchand & Beaudoin, 2000):

$$K = \gamma_1 c_1 \gamma_2^2 c_2^2 \tag{2-12}$$

Unlike other chemical equilibrium, the solid phase concentration does not appear in Eq. (2-12) in the dissolution/precipitation process. Therefore, it is more precise to express it as an inequality:

$$\gamma_1 c_1 \gamma_2^2 c_2^2 \begin{cases} = K \; if \; precipitation \; is \; present \\ < K \; if \; there \; is \; no \; precipitaition \end{cases} \tag{2-13}$$

Considering this chemical equilibrium, (Marchand *et al.*, 2002) used five major solid phases involving in the sulfate attack process to model the influence of precipitation/dissolution reactions on the transport process. The equilibrium constants are given in Table 2-1.

Table 2-1. Equilibrium constants for solid phases in hydrated cement systems (Marchand *et al.*, 2002)

Name	Chemical composition	Expression for equilibrium	Value of equilibrium constant ($-\log K_{sp}$)
Portlandite	$Ca(OH)_2$	$K_{sp} = \{Ca\}\{OH\}^2$	5.2
C–S–H	$1.65CaO \cdot SiO_2 \cdot (2.45)H_2O$[a]	$K_{sp} = \{Ca\}\{OH\}^{2}$[b]	5.6[b]
Ettringite	$3CaO \cdot Al_2O_3 \cdot 3CaSO_4 \cdot 32H_2O$	$K_{sp} = \{Ca\}^6\{OH\}^4\{SO_4\}^3\{Al(OH)_4\}^2$	44.0
Hydrogarnet	$3CaO \cdot Al_2O_3 \cdot 6H_2O$	$K_{sp} = \{Ca\}^3\{OH\}^4\{Al(OH)_4\}^2$	23.0
Gypsum	$CaSO_4 \cdot 2H_2O$	$K_{sp} = \{Ca\}\{SO_4\}$	4.6

Chemical reactions can also modify the transport of ions by affecting the pore structure. One way to consider this impact is to link the porosity with the diffusion coefficient, which is proposed by (Garboczi & Bentz, 1992):

$$\frac{D_i}{D_i^u} = 0.001 + 0.07\emptyset_{cap}^2 + 1.8 * H(\emptyset_{cap} - 0.18)\,(\emptyset_{cap} - 0.18)^2 \quad (2\text{-}14)$$

where $\emptyset_{cap}$ is the capillary porosity of the paste, D_i^u is the diffusion coefficient of the ionic species *i* in the free solution. The initial capillary porosity of the material can be calculated by the water/cement ratio and degree of hydration (Powers & Brownyard, 1946). The influence of chemical reaction on the capillary porosity can be calculated as follows:

$$\emptyset_{cap} = \emptyset_{cap}^{init} + \sum_{s=1}^{M}(V_s^{init} - V_s) \quad (2\text{-}15)$$

where $\emptyset_{cap}^{init}$ is the initial capillary porosity, V_s is the volume of a given solid phase, per unit volume of cement paste, and *M* is the total number of solid phases.

2.6.3.2 Leaching

Among the various kinds of chemical deterioration, leaching is a progressive extraction of calcium from the cementitious material resulting from the contact with an external solution having pH significantly lower than that of the alkaline pore solution (such as de-ionised water) (Adenot & Buil, 1992; Bentz & Garboczi, 1992). In the first stage of the process, hydroxyl ions in the pore solution tend to be leached out of the system under the electrochemical potential gradient. In order to restore the local chemical equilibrium, calcium hydroxide, $Ca(OH)_2$, will dissolve thus releasing OH^- and Ca^{2+} ions to the pore solution. As calcium leaches from the solid phases of concrete, it may cause efflorescence (i.e., the surface formation of calcium carbonate or calcium sulfate). More importantly, the dissolution of calcium hydroxide and possibly decalcification of C-S-H also lead to corresponding porosity increase and accelerated penetration of other detrimental ions (Feng, Miao & Bullard, 2014). Numerous concrete structures are exposed to this simple form of chemical degradations and the ingress of sulfate ions into cementitious materials is generally coupled with calcium leaching since ground water are usually near the neutral state with $pH \approx 7$ (Planel *et al.*, 2006; Rozière *et al.*, 2009).

Leaching can also be simulated by the thermodynamic equilibrium as the sulfate attack. (Feng, Miao & Bullard, 2014) extended a 3-D thermodynamically guided microstructure model of cement hydration to simulate leaching of well-hydrated cement. The model can be readily extended to analyse other types of degradation such as sulfate and carbonation, once validated for leaching phenomena.

2.6.3.3 Carbonation

The whole carbonation process involves a series of different steps. Gaseous carbon dioxide first penetrates the partially saturated concrete and dissolves in the pore solution mainly as HCO_3^- and CO_3^-. The CO_3^- species then reacts with dissolved calcium in the pore solution to precipitate calcite, $CaCO_3$, as well as other CO_2-based solid phases (Glasser, Marchand & Samson, 2008). The carbonation process will result in a pH drop in the pore solution, which leads to the dissolution of portlandite. On one hand, the formation of calcite in replacement of portlandite reduces the porosity of the material since calcite has a higher molar volume (36.9 cm^3/mol compared to 33.1 cm^3/mol for portlandite), which may favour formation of a protective layer at the surface of concrete. On the other hand, the drop of pH associated with the process can potentially have a detrimental effect on reinforced concrete structures by destroying the passive layer around steel rebars (Kwon & Song, 2010; Morandeau, Thiéry & Dangla, 2014).

2.6.3.4 Wetting and Drying Cycles

As discussed in previous section 2.2.3, in unsaturated condition, convection driven by the capillary suction is one of the major means by which the detrimental ions can penetrate into the deeper part of the cementitious materials. This type of ionic transport is also called absorption and plays an important role when the materials are intermittently subjected to wetting and drying cycles (Arya, Bioubakhsh & Vassie, 2013; Arya, Vassie & Bioubakhsh, 2013; Polder & Peelen, 2002).

When external water (possibly containing chlorides) encounters a dry surface, it will be drawn into the pore structure through capillary suction. It does serve to bring chlorides quickly to some depth in the concrete and reduce the distance that they must diffuse to

reach the rebar (Hong & Hooton, 2000; Hong & Hooton, 1999). On the other hand, the detrimental ions may be concentrated by evaporation of water, which is called wicking effect by certain researchers (Boddy *et al.*, 1999; Nilsson & Ollivier, 1995). An experimental illustration of the effects of wetting and drying cycles on the chloride penetration is given in Figure 2-10. Similar profiles can also be found in concrete cores from field structures (Hong & Hooton, 2000).

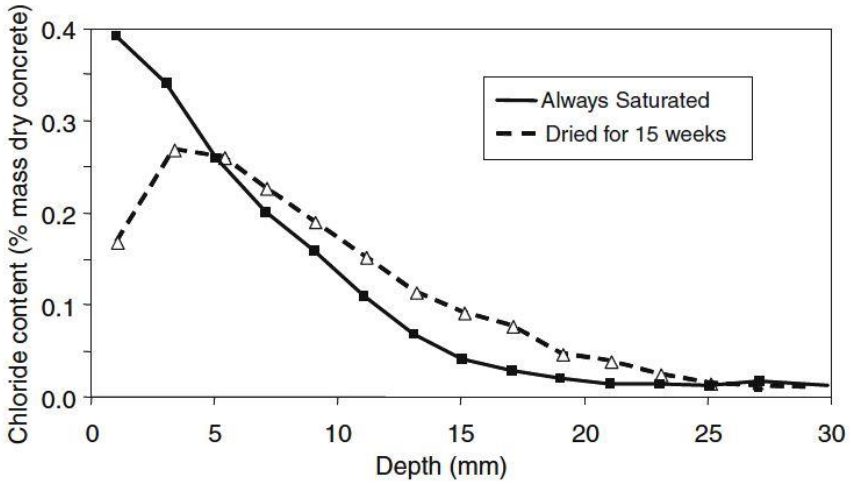

Figure 2-10. Impact of drying on the chloride distribution in concrete. (Marchand & Samson, 2009)

As shown in Figure 2-10, two chloride penetration profiles were obtained from samples subjected to two different conditions. One set of samples were kept saturated during the experiment, anther series of samples were subjected to an additional drying process. The chloride distribution profile measured from the saturated samples has the typical smooth shape predicted by Fick's law, which is discussed in section 2.2.1. In the case of samples subjected to drying process, the maximum chloride concentration is not measured at the surface of the sample but a little deeper in the material, and the penetration of chloride deeper within the material is also affected. A possible explanation of this phenomenon is that the loss of water at the surface contributes to locally reduce chloride concentration which turns the profile into a bell-shaped curve

quite distinct from what could be predicted by Fick's diffusion model (Marchand & Samson, 2009). The results indicate that the classic Fick' approach cannot predict the chloride penetration accurately when concrete is subjected to wetting and drying cycles, especially around the surface area.

Chapter Three – Simulation of Single-Phase Multi-Component Ionic Transport in Cement Paste Considering Electric Double Layer

In this Chapter, the effect of Electric Double Layer (EDL) on the electro-migration of chloride ions in cementitious materials is investigated using a numerical method. The work is performed by solving the multispecies ionic transport equations for a cement paste subjected to an externally applied electric field. Conventionally the Poisson-Boltzmann equation is used to determine ionic distribution in the perpendicular direction to the charged surface and hence it is limited to one dimension. However, the ionic distribution in the penetration depth through the pores is also important and hence a two-dimensional model is required. To extend the numerical simulation to two dimensions, the Nernst-Planck and Poisson's equations were used, coupled with a constant amount of surface charge on the pore walls as boundary conditions. Parameters affecting the implications of the EDL on multispecies ionic transport are examined. Interactions between the local electrostatic potential in the EDL and the global applied electric field are also discussed.

3.1 Introduction

The EDL is a well-known phenomenon found in porous materials, which occurs at the interface between solid surfaces and pore solutions. When brought into contact with an aqueous medium, substances will acquire a surface electric charge. Cementitious

materials also develop a surface charge at the surface when they are in contact with electrolyte pore solutions. This phenomenon is due to the mixed mechanisms of ionization, ion adsorption and ion dissolution. As descripted in Section 2.6.1, the charge imbalance near the surface caused by the surface charge will create a local electric potential difference, which can influence the distribution of nearby ions in the solution (Probstein, 2005). And the special electrochemical structure formed near the surface is called Electric Double Layer (Stern, 1924).

The earliest theoretical model of the EDL was proposed by Quincke (Quincke, 1861) and Von Helmholtz (von Helmholtz, 1879), in which the interface was described as a plane condenser. The model was improved by Chapman (Chapman, 1913) and Gouy (Gouy, 1910) by taking into account the random thermal motion of ions, in which the counter-ions (with opposite charge sign to that of the surface) are attracted toward the surface, while co-ions (with the same charge sign to that of the surface) are repelled from the surface. In the meantime, the random thermal motion of the ions tends to disperse the ions. This combined tendency leads to the formation of the EDL. Consequently, in the region close to the charged surface, the amount of counter-ions is larger than that of co-ions.

Chatterji and Kawamura (Chatterji, 1996; Chatterji & Kawamura, 1992) investigated the impact of the EDL on the ionic transport in a hydrated cement-electrolyte system. In their work, the pore solution contains two parts, namely a double layer solution and a bulk solution. The transport of counter-ions was assumed to be mostly through the double layer solution while the transport of co-ions was mainly through the bulk pore solution. Zhang and Buenfeld (Zhang & Buenfeld, 1997; Zhang & Buenfeld, 2000b)

reported the measurement of membrane potentials, which were between 20 and 45 mV across the OPC (Ordinary Portland Cement) mortar specimens. They later found that a positive membrane potential accelerated the chloride diffusion while a negative membrane potential decelerated the chloride diffusion. Elakneswaran *et al.* (Elakneswaran, Nawa & Kurumisawa, 2009a; Elakneswaran, Nawa & Kurumisawa, 2009c; Elakneswaran, Nawa & Kurumisawa, 2009b) also found that the hydrated cement paste with or without the blast furnace slag has a positive surface charge. However, other researchers (Castellote, Llorente & Andrade, 2006; Ersoy *et al.*, 2013; Florea & Brouwers, 2012; Hocine *et al.*, 2012; Labbez *et al.*, 2011; Nägele, 1985), who took C-S-H suspensions and cement as experiment subjects, found that the surface of the C-S-H gel is negatively charged. A common explanation for this controversy is that the formal surface charge of C-S-H remains negative because the charges of the bridging silica tetrahedral are not always compensated (Florea & Brouwers, 2012), but the reversal of the surface charge may happen when the amount of calcium ions increases. Labbez *et al.* (Labbez *et al.*, 2011) pointed out that the calcium ions are not chemically but physically adsorbed to the C-S-H surface, which means that the multivalent counter-ions will accumulate to the C-S-H surface to influence the sign of the surface charge when the content of calcium ions is relatively high. Nevertheless, more experiments are needed in order to draw general conclusions about the sign and magnitude of the surface charge in various cementitious materials.

Based on a simplified solution of the Poisson-Boltzmann equation, Friedmann *et al.* (Friedmann, Amiri & Aït-Mokhtar, 2008c; Friedmann, Amiri & Aït-Mokhtar, 2012) demonstrated the effect of the EDL on ionic fluxes in the pore solution. They found that gel pores with pore diameters close to the Debye length have a large influence on the

ionic transport due to the overlapping of the EDL. Nguyen and Amiri (Nguyen & Amiri, 2014) investigated the EDL effect on chloride penetration in unsaturated concrete with fly ash. The work was performed by solving the multispecies ionic transport equations coupled with that of humidity. The results showed that the chloride concentration increases more in concrete with negative EDL than in that with positive EDL. The EDL effect reduces in unsaturated concrete due to the discontinuity of the liquid phase, but increases in concrete containing slag when compared to that with fly ash due to the high ionic strength of the pore solution caused by the ferrous ions in the slag. Arnold *et al.* (Arnold *et al.*, 2013) developed a numerical solution of the full nonlinear Poisson-Boltzmann equations for asymmetric electrolyte solutions. They claimed their numerical solution was more accurate and applicable than the linearized approximation with symmetric electrolyte solution. They also discussed the impact of pore size on the effect of the EDL and the possible mechanisms behind the disparate cation and anion diffusivities.

In this Chapter, the effect of an EDL on the electro-migration of chloride ions in cementitious materials is investigated using a numerical method. The work is performed by solving the multispecies ionic transport equations for a cement paste subjected to an externally applied electric field. The problem investigated is very similar to that used in the rapid chloride migration (RCM) test for cement and concrete materials. However, due to the involvement of the external electric field, there is an interaction between the local electrostatic potential in the EDL and the global applied electric field, the problem of which has not been discussed in the existing literature.

3.2 Two-Dimensional Single-Phase Multi-Component Ionic Transport Model with Electric Double Layer

Current models for a quantitative description of the EDL theory are mostly based on the simplified one-dimensional Poisson-Boltzmann equation. With the assumption of an ideal symmetric electrolyte, the distribution of ions along the axis perpendicular to the charged surface is expressed by the Boltzmann equation. However, whether the Boltzmann equation can be applied to the case of a multi-component ionic solution in more than one-dimensional domains is not known.

Consider the transport of individual ionic species in the pore solution in a saturated cement-based material. According to mass conservation, the ionic concentration of each individual species in the pore solution should satisfy the following Nernst-Planck equation (Liu *et al.*, 2012; Xia & Li, 2013):

$$\frac{\partial C_k}{\partial t} = \nabla \cdot \left[D_k \nabla C_k + \left(\frac{F \nabla \Phi}{RT} \right) z_k D_k C_k \right] \qquad \text{k} = 1, 2, \ldots \text{N} \qquad (3\text{-}1)$$

where C_k is the concentration of the k-th ionic species, D_k is the diffusion coefficient of the k-th ionic species, z_k is the valence number of the k-th ionic species, Φ is the electrostatic potential, F is the Faraday constant, R is the ideal gas constant, T is the absolute temperature, t is the time, and N is the total number of ionic species in the pore solution. The first and second terms in the bracket in the right-hand-side of the equation represent the diffusion and migration fluxes, respectively. Note that ionic binding is not taken into account in Eq. (3-1). Thus, the diffusion coefficient used in Eq. (3-1) should be referred as to the apparent diffusion coefficient of ions.

The electrostatic potential can be determined using Poisson's equation as follows:

$$\nabla^2\Phi = -\frac{F}{\varepsilon_o\varepsilon_r}\sum_{k=1}^{N}(z_k C_k + z_s C_s) \qquad (3\text{-}2)$$

where ε_o is the permittivity of a vacuum, ε_r is the relative permittivity of water at temperature of 298K, z_s and C_s are the valence number and concentration of the surface charge, respectively. Note that C_s exists only on the surface of liquid phase and is taken as zero in the pore solution. The governing equations (3-1) and (3-2) are applied to a two-dimensional domain shown in Figure 3-1, which represents the one-direction migration test of a cement paste. Generally, in chloride migration tests, the axially symmetric cross-section of the specimen is in the size of 50x50 mm (for a cylindrical specimen of diameter 100 mm and length 50 mm). However, the influence area of EDL is much smaller, which is about tens nanometre to a few micrometres. In order to minimise the size effect and focus on the influence of EDL on ionic transport along the penetration depth, compromised solution domain of 5x1 (x-y) mm is chosen. The upper (y = 1 mm) and lower boundaries (y = 0) of the domain shown in Figure 3-1 are the interfaces between the solid and liquid phases where surface charges exist. These two boundaries are assumed to be sealed and thus the boundary conditions there are zero-flux conditions, in other words, Cauchy boundary conditions. The left-hand boundary (x = 0) is exposed to an external NaCl solution where a cathode is placed. The right-hand boundary (x = 5 mm) is exposed to an external NaOH solution where there is an anode. A constant voltage is applied between the anode and cathode. Hence, the boundary conditions are *Dirichlet* conditions. Table 3-1 shows the initial and boundary conditions as well as the diffusion coefficients of the ionic species considered in this numerical study. The diffusion coefficients of potassium, sodium, chloride and hydroxyl ions used in this study are taken from corresponding values of them in dilute

solution but divided by a factor of 50 to take into account the retardation that arises from the constriction and tortuosity of the pore path through which the ions are travelling (Xia & Li, 2013).

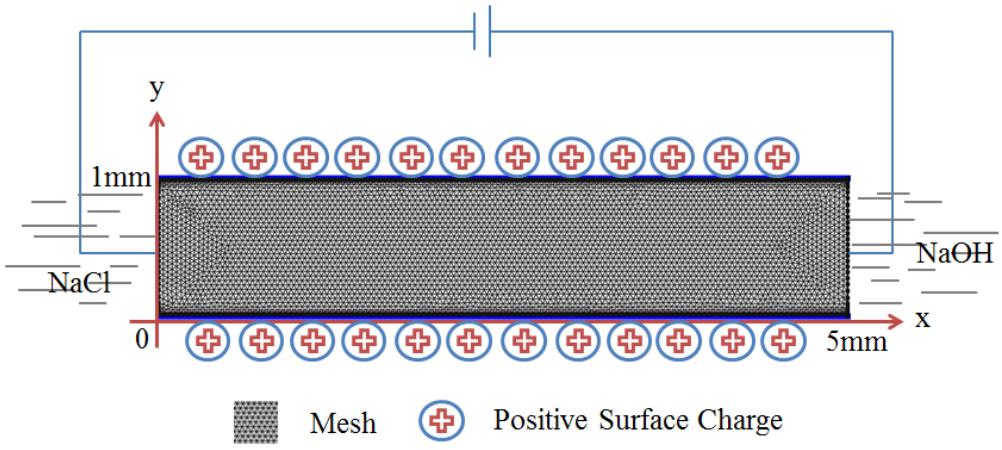

Figure 3-1. Schematic of the two-dimensional model

The voltage normally used in the RCM test is about 24 V for a specimen length of 50 mm. However, since the model used in this study is only for the liquid phase, the dimensions of the model are much smaller than those of a typical specimen used in the migration test. In order that the potential gradient created in the liquid phase is similar to that in the specimen used in the migration test, the voltage should be reduced accordingly. By using an identical proportional factor, the voltage used in the present model is 2.4 V for the model specimen length of 5 mm.

The governing equations (3-1) and (3-2) together with the initial and boundary conditions defined in Table 3-1 can be used to solve for the electrostatic potential Φ and ionic concentrations C_k (k = 1, …, N) numerically. A commercial computational software package called COMSOL is used, from which one can get the electrostatic potential Φ and ionic concentrations C_k at any coordinate points at any time.

Table 3-1. Properties and conditions considered in the numerical study

Variables	Chloride (mol/m^3)	Hydroxyl (mol/m^3)	Potassium (mol/m^3)	Sodium (mol/m^3)	Voltage (V)
Initial conditions	0	400	300	100	-
Boundary at x = 0 mm	400	0	0	400	0
Boundary at x = 5 mm	0	400	0	400	2.4
Valence number	-1	-1	1	1	-
Diffusion coefficient $x10^{-11}$ m^2/s	4.064	10.546	3.914	2.668	-

3.3 Simulation Results and Discussion

The transport of ions in a liquid phase can be driven by the electrostatic potential gradient and/or the concentration gradient. Note that, at the initial time, the charge is balanced in the domain but not at the boundaries of y = 0 and y = 1 mm where the surfaces have a positive charge of 400 mol/m^3. Thus, the ionic transport takes place not only in the x-direction but also in the y-direction.

The ionic transport along x-direction is due to the action of the externally applied electric field applied between the two boundaries of x = 0 and x = 5 mm, which forces positively charged ions (potassium and sodium) to move from anode to cathode and negatively charged ions (chloride and hydroxyl) to move from cathode to anode.

The ionic transport along y-direction is due to the charge imbalance in the regions near the boundaries of $y = 0$ and $y = 1$ mm. This charge imbalance causes negatively charged ions to move closer to the boundaries and positively charged ions to move away from the boundaries, so that the positive charge on the solid phase can be balanced by the negative charge ions in the liquid phase. However, due to the fact that the charge imbalance is highly localised, the ionic transport in the *y*-direction is rather quick and it occurs only in narrow regions very close to the two boundaries (i.e. $y = 0$ and $y = 1$ mm). This is demonstrated by the ionic concentration distribution profiles plotted at $x = 2.5$ mm along the *y*-axis at two different times shown in Figure 3-2. It can be seen from the figure that, near to the solid surface the hydroxyl concentration increases from 400 mol/m^3 to 580 mol/m^3, whereas the potassium concentration drops from 300 mol/m^3 to 210 mol/m^3 and sodium concentration drops from 100 mol/m^3 to 70 mol/m^3. However, the thickness where the concentrations vary from the boundary to inner bulk region is only about 0.02 mm, which defines the effect zone of the EDL. The charge imbalance in this effect zone creates an electrostatic potential gradient along the *y*-axis, which is plotted in Figure 3-3. Interestingly, the numerical results plotted in Figure 3-2 and Figure 3-3 for the ionic concentration and electrostatic potential distributions can be approximately described using the Debye-Hückel approximation (Probstein, 2005) and Boltzmann distribution function as follows:

$$\Phi = \Phi_b + \Phi_s \exp\left(-\frac{y}{\lambda_D}\right) \tag{3-3}$$

$$C_k = C_{ko} \exp\left(\frac{-z_k F(\Phi - \Phi_b)}{RT}\right) \tag{3-4}$$

where Φ_b is the electrostatic potential at the bulk solution, $\Phi_s = 9.15$ mV is the electrostatic potential at the solid surface, λ_D is the Debye length (A value of 7 μm is

determined in this study.), and C_{ko} is the concentration of ionic species k in the bulk zone.

The transport of chloride ions under the action of an externally applied electric field is plotted in Figure 3-4. It can be seen from the figure that, due to the effect of the EDL, chloride ions are also pulled to the two boundaries of $y = 0$ and $y = 1$ mm while they are moving from the cathode to the anode. However, except for the variation of concentration in the effect zones of the EDL, the main transport behaviour of chloride ions in the x-direction is similar to what was reported previously for the case without the EDL (Xia & Li, 2013), i.e. the transport is dominated by the electro-migration. This indicates that the EDL has almost no effect on the chloride migration in the x-axis, particularly in the bulk zone. This finding can be further confirmed by the transport speeds of chloride ions in the x-direction in both the EDL effect zone and bulk zone, which are nearly identical, although the concentrations in the two zones are significantly different.

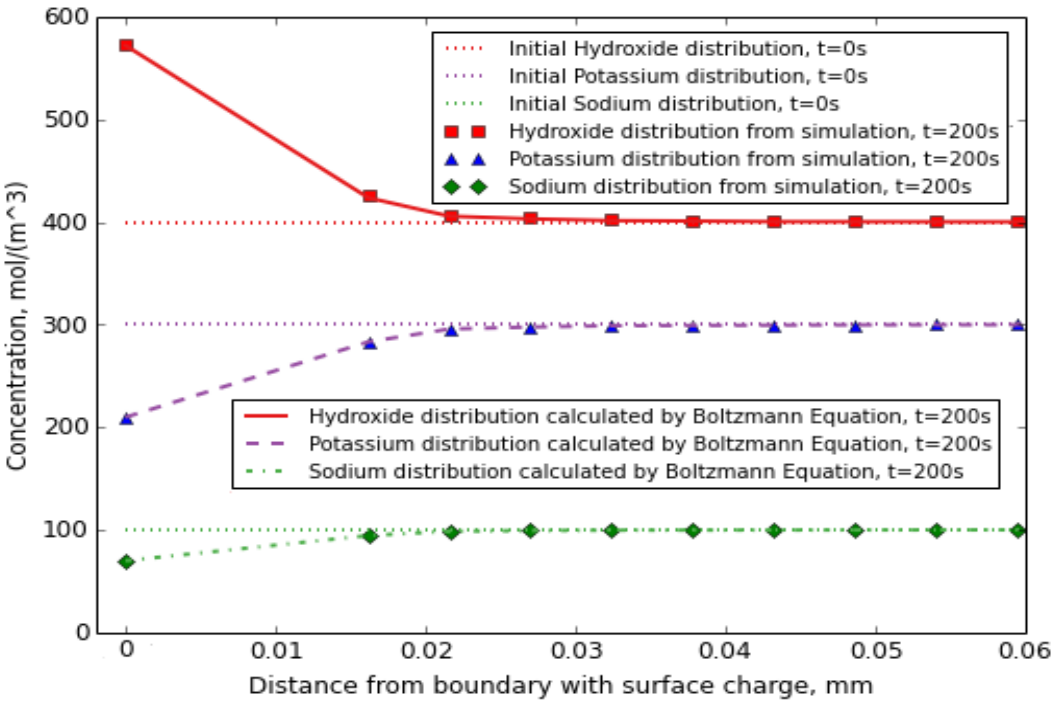

Figure 3-2. Ionic distribution near the charged surface at x=2.5 mm

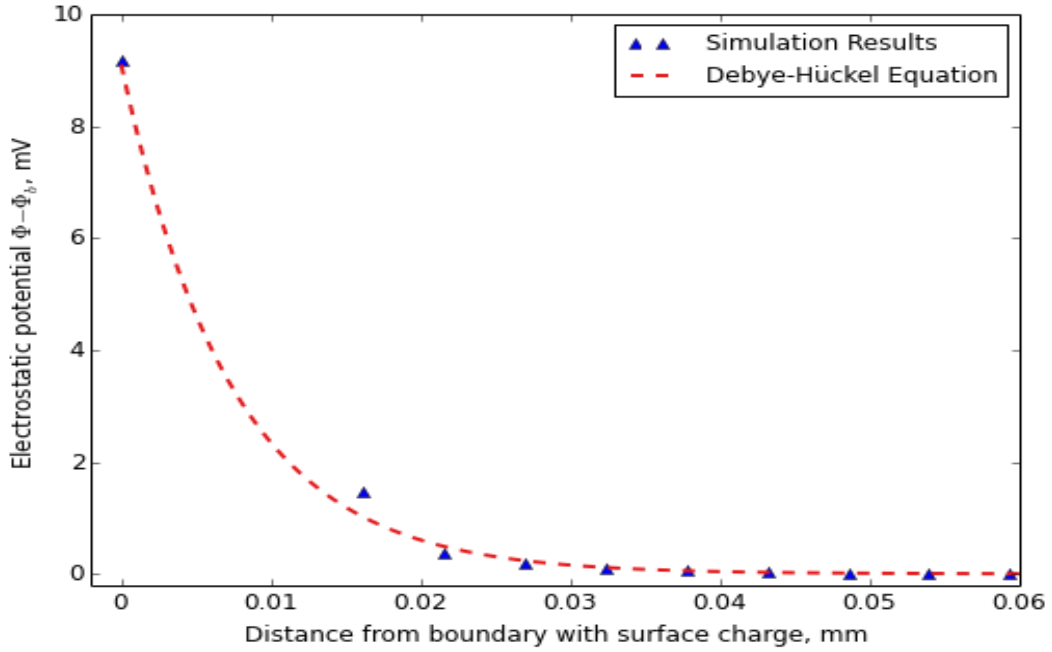

Figure 3-3. Electrostatic potential distribution near the charged surface at x = 2.5 mm (t =200 s), Φ_b is the electrostatic potential in the bulk solution at x = 2.5 mm (t =200 s)

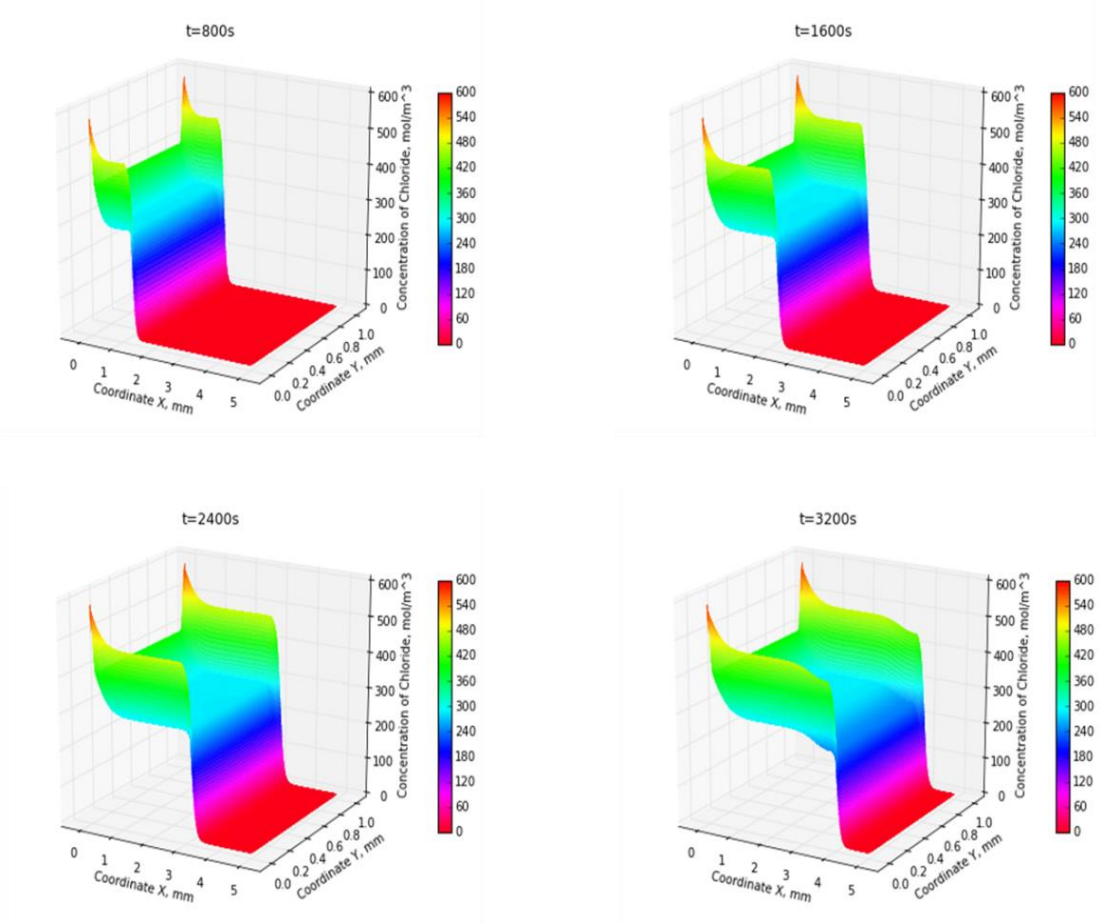

Figure 3-4.Chloride concentration profiles at four different times.

Note that the ionic flux is proportional to the flow speed and the ionic concentration. Hence, the flux of chloride ions will be larger in the EDL effect zone than in the bulk zone. This implies that the EDL with positively charged surface will increase the transport of chloride ions in the liquid phase.

Figure 3-5 provides a further quantitative comparison of chloride concentration distribution profiles along the *x*-axis, in which the three profiles represent the concentration at the boundary ($y = 0$), the average concentration along the *y*-axis, and the average concentration along the *y*-axis obtained when the surface charge was ignored in the simulation. It can be seen from the figure that the migration velocities of

chloride ions in the three profiles are almost the same. Also, although the chloride concentration at the boundary is much higher than that in the other two profiles the average concentration when the surface charge is considered is only about 2% higher than the average concentration when the surface charge is ignored. The latter is probably because the effect zone of the EDL is very narrow when compared to the bulk zone.

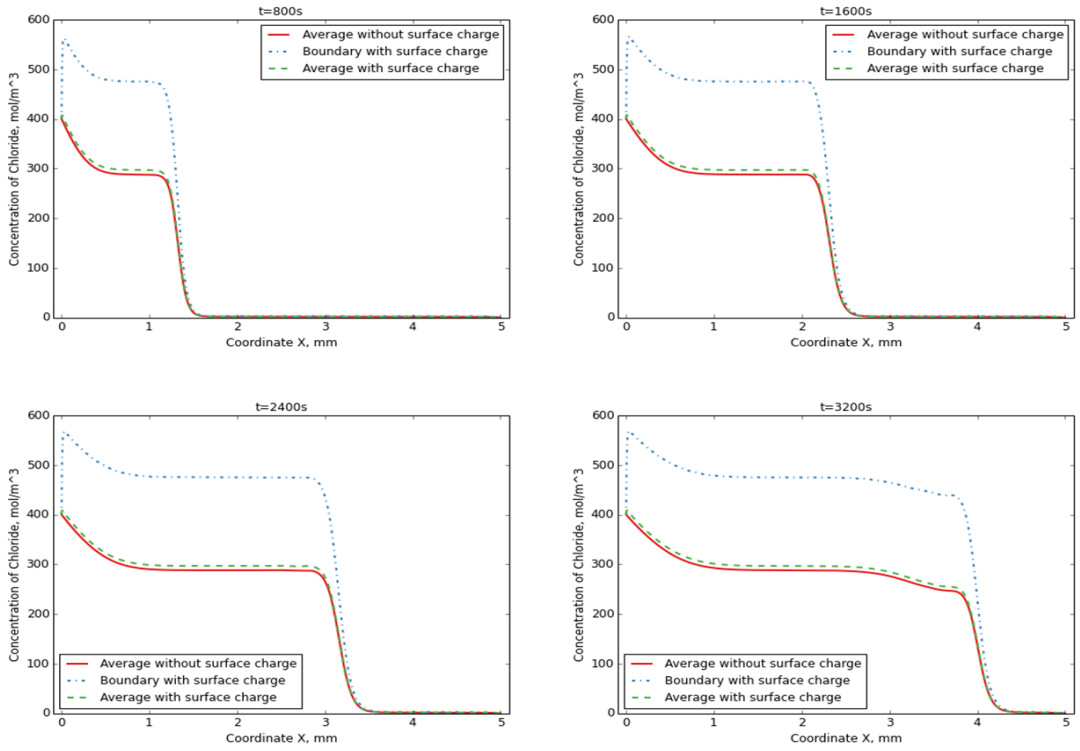

Figure 3-5. Comparison of chloride concentration profiles along the x-axis

Figure 3-6 shows a similar comparison of hydroxyl concentration distribution profiles along the *x*-axis, in which the three profiles represent the concentration at the boundary ($y = 0$), the average concentration along the *y*-axis, and the average concentration along the *y*-axis obtained when the surface charge is ignored. Similar to the chloride ions, the hydroxyl ions also have a higher concentration at the boundary ($y = 0$). However, in terms of the average concentration, the effect of the EDL is also not significant. It is

noticed from the figure that the migration velocity of hydroxyl ions is almost the same as that of chloride ions although its diffusion coefficient is about 2.5 times that of chloride ions, which indicates that there is a strong electro-interaction between different ionic species. This further demonstrates the importance of using multi-component transport model when an electric field is involved in the ionic transport problem, which has been proved by many authors (Li & Page, 2000; Liu *et al.*, 2015; Yu & Page, 1996). Although in previous multi-component ionic transport studies, the EDL effect was not considered.

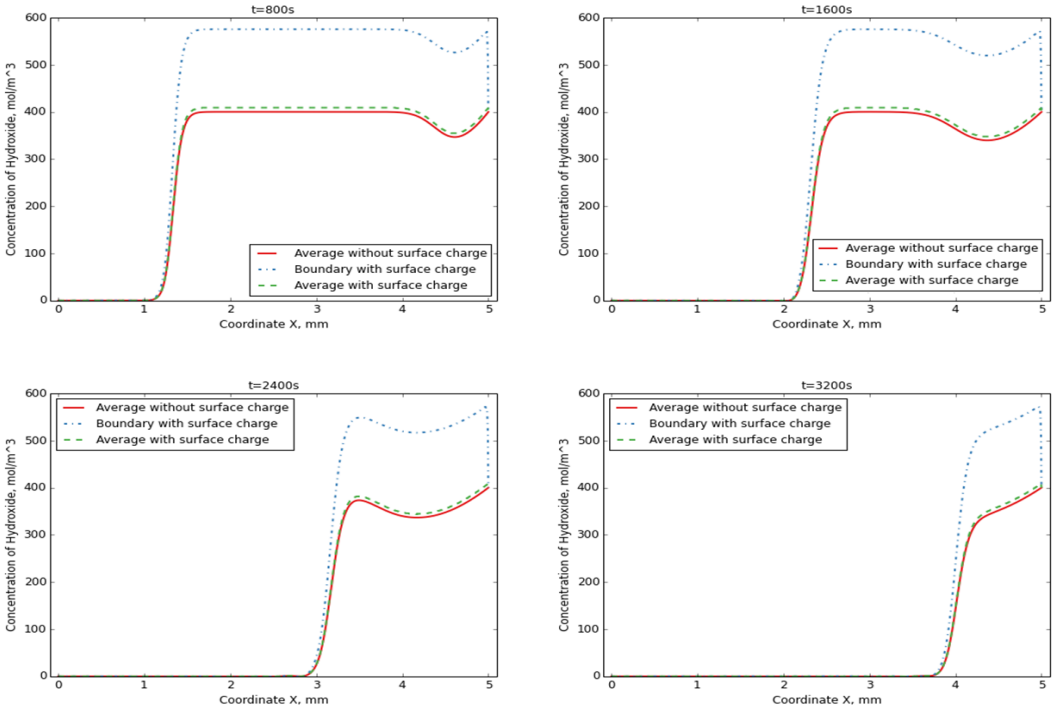

Figure 3-6. Comparison of hydroxyl concentration profiles along the x-axis

As it is expected, the positively charged ions (potassium and sodium) are repelled from the charged surfaces, leading to lower concentrations at the boundaries ($y = 0$ and $y = 1$ mm), as is demonstrated in Figure 3-7 and Figure 3-8. It can be seen from the figures that the influence of the EDL on the average concentrations of potassium and sodium

ions are less significant than that on the average concentrations of chloride and hydroxyl ions. Interestingly, Figure 3-7 and Figure 3-8 show that the migration velocities of potassium and sodium ions are clearly smaller than that of the chloride or hydroxyl ions. In addition, it can be observed from the figures that the wave fronts of potassium and sodium ions are not very steep, indicating that the diffusion has a moderate contribution in the ionic transport. The reason that the transport of the positively charged ions is somehow different from the transport of the negatively charged ions is mainly due to the electrostatic potential, the gradient of which is not uniformly distributed along the x-axis (Xia & Li, 2013).

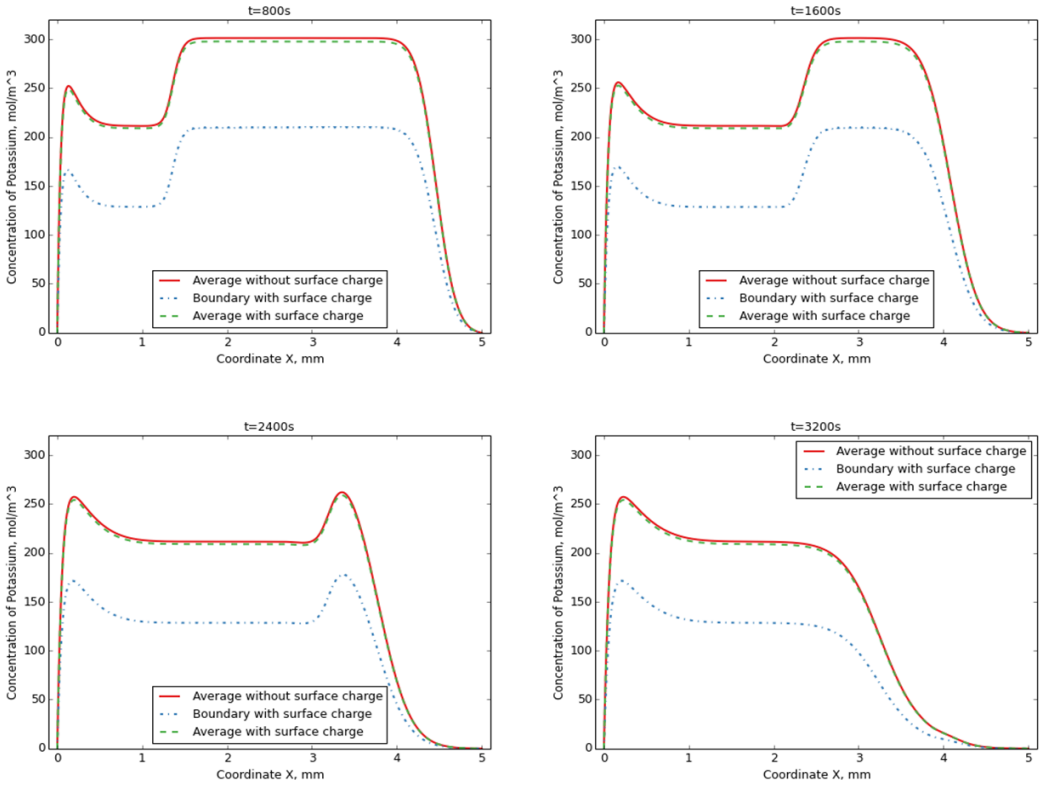

Figure 3-7. Comparison of potassium concentration profiles along the x-axis

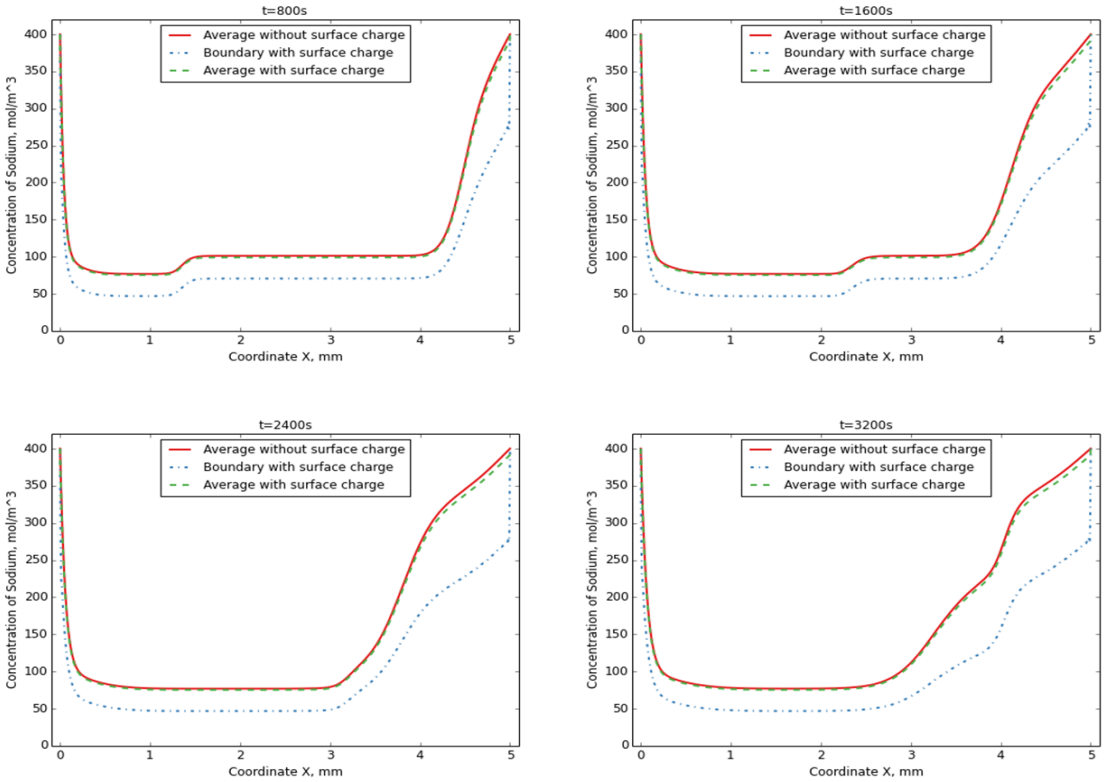

Figure 3-8. Comparison of sodium concentration profiles along the x-axis

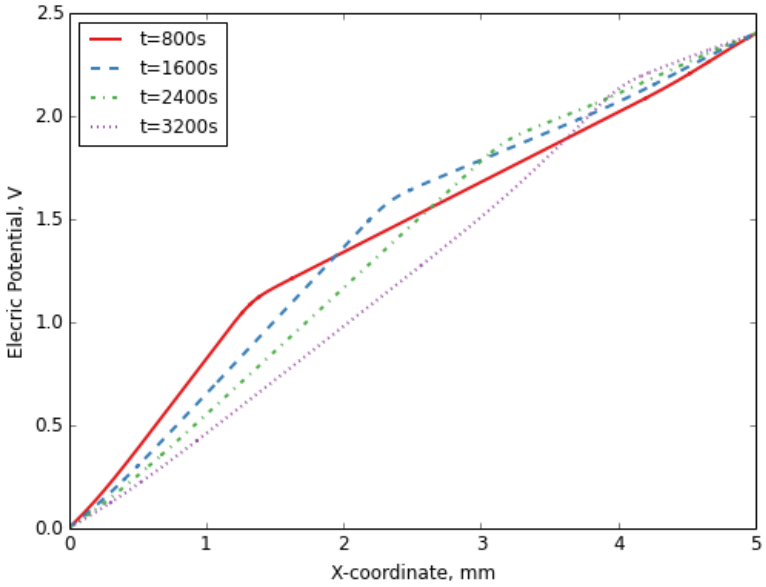

Figure 3-9. Electrostatic potential distribution along the x-axis at y = 0.5 mm

Figure 3-9 shows the electrostatic potential distribution plotted at y = 0.5 mm. It can be seen from the figure that the electrostatic potential gradient is larger in the region near the cathode than in the region near the anode. When the ionic wave front is located in the region with a comparatively small electrostatic potential gradient, the ionic migration speed reduces. The smaller the migration speed is, the more contribution the diffusion will have, and thus the less steep the wave front will be in the ionic profile.

Figure 3-10 shows the influence of the externally applied voltage on the transport of chloride ions along the charged surface (y = 0). Three voltages ranging from 0.6 to 2.4 V are used herein. Note that, when the voltage is reduced, the transport time needs to be increased proportionally because the migration speed is linearly related to the applied voltage. It can be seen from the figure that the higher the externally applied voltage, the steeper the wave front appeared in the concentration distribution profile. This is to be expected, as the migration speed of ions is proportional to the externally applied voltage. Also, it can be seen from the figure that the concentration in the plateau seems to be independent of the externally applied voltage, whereas the position of the wave front is merely dependent on the product of the externally applied voltage and the transport time. This indicates that the migration speed of chloride ions is almost linearly proportional to the externally applied voltage.

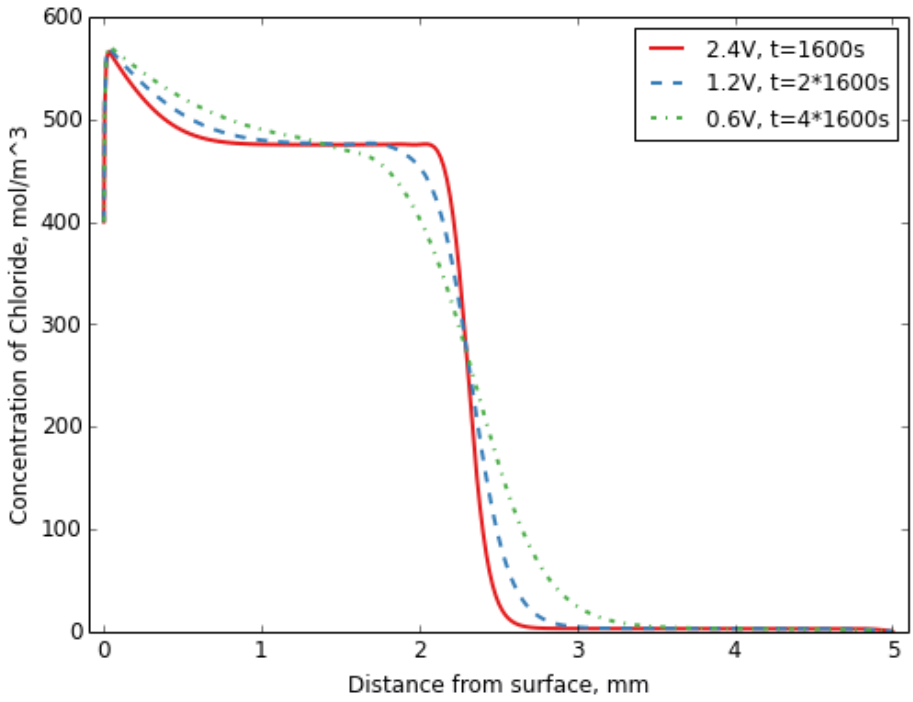

(a)

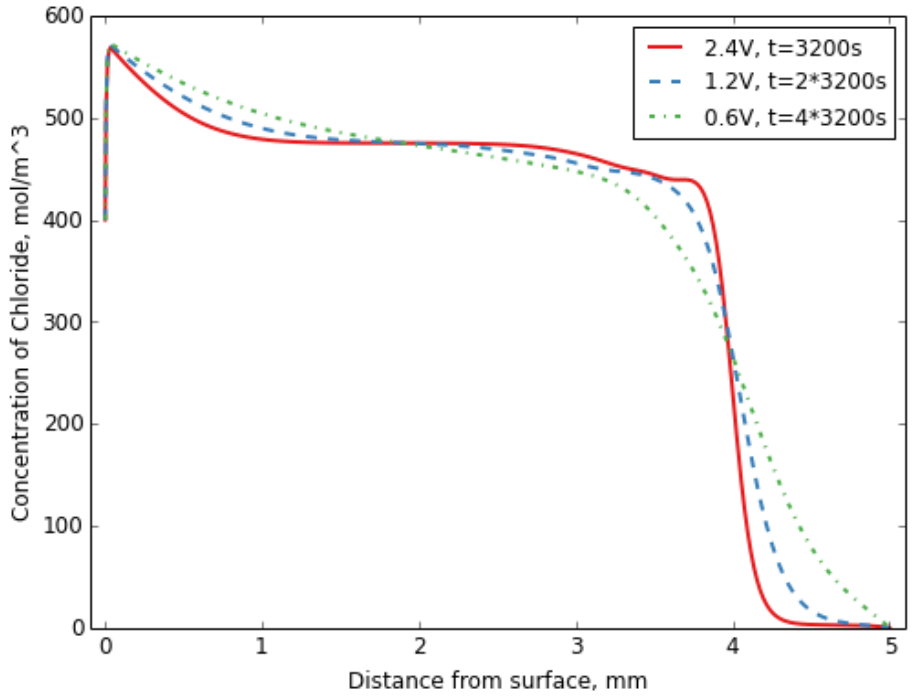

(b)

Figure 3-10. Influence of externally applied voltage on the transport of chloride ions along the charged surface (y = 0). (a) t = 1600 s based on 2.4V and (b) t = 3200 s based on 2.4V

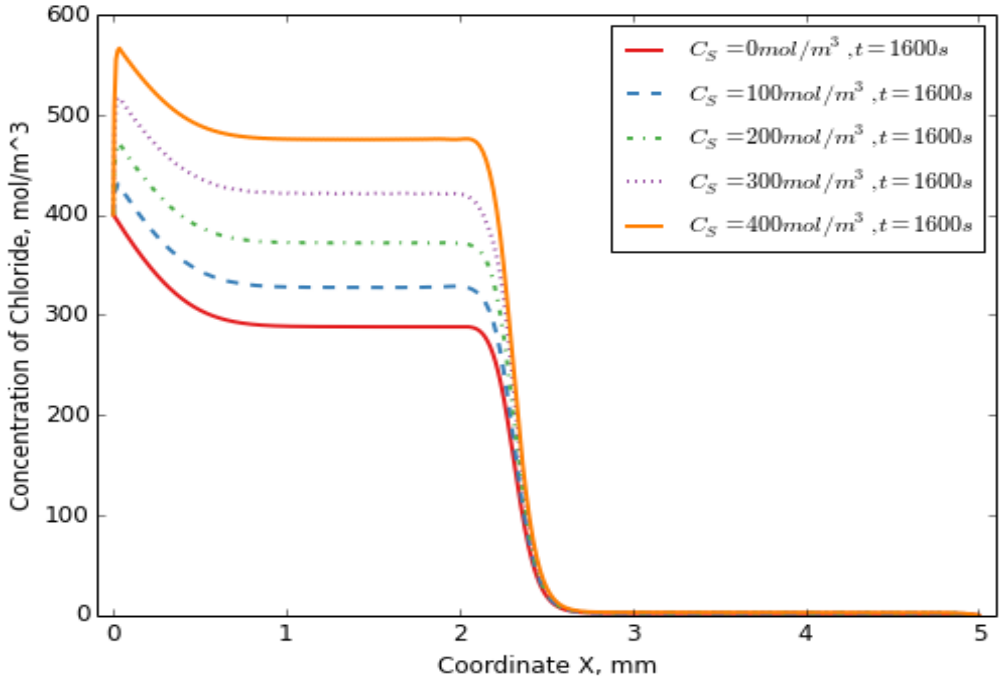

(a)

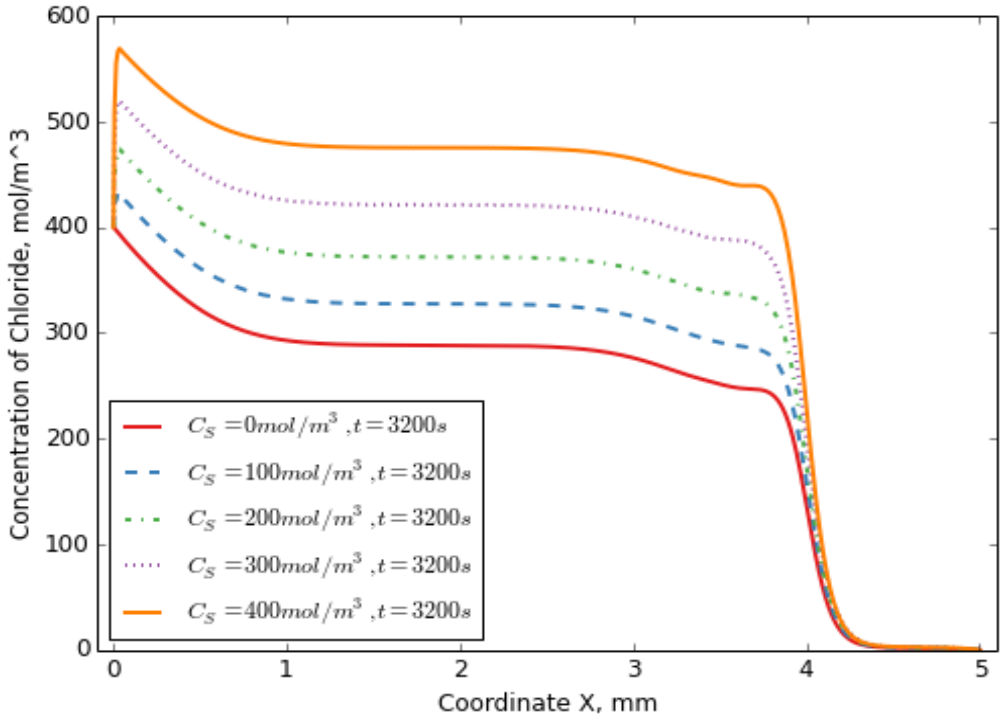

(b)

Figure 3-11. Influence of surface charge on the transport of chloride ions along the charged surface (y = 0). (a) t = 1600 s and (b) t = 3200 s

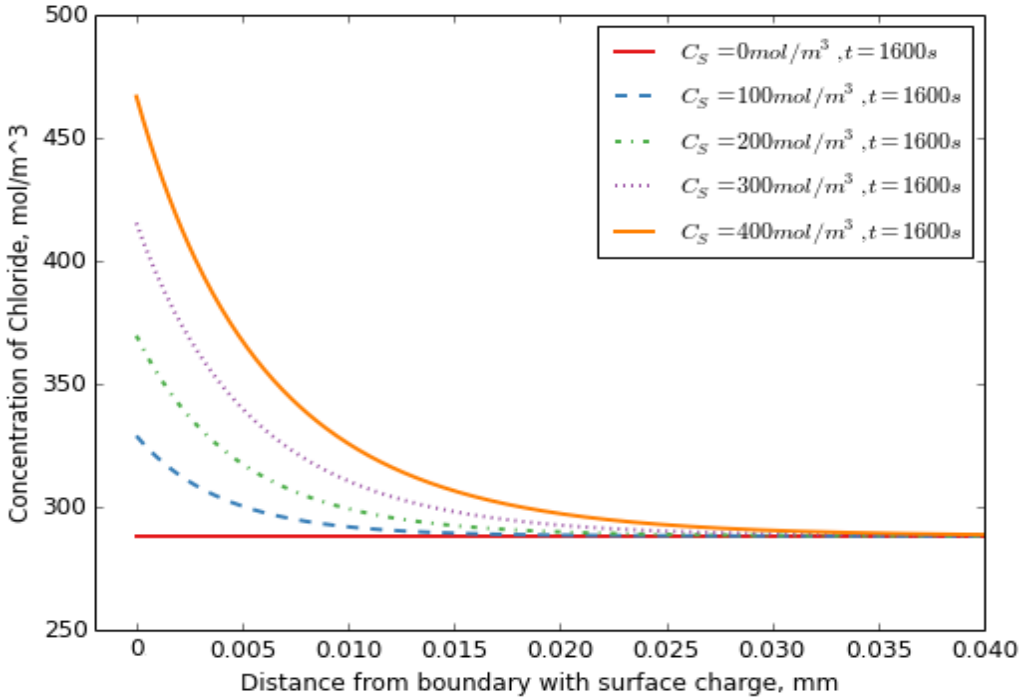

Figure 3-12. Influence of surface charge on the thickness of the EDL zone

Figure 3-11 shows the influence of surface charge on the transport of chloride ions along the charged surface (y = 0). It can be seen from the figure that the larger the surface charge, the higher the chloride concentration in the plateau. However, the surface charge has almost no influence on the migration speed of chloride ions in the x-axial direction.

Figure 3-12 shows the effect of the surface charge on the thickness of the EDL zone. It is seen from the figure that the thickness of the effect zone increases with the surface charge.

3.4 Conclusions

This study has presented a numerical investigation on the effects of the EDL on the ionic transport in cement paste when subjected to an externally applied electric field. Instead of using the zeta potential and the Boltzmann equation to determine the ionic distribution close to the charged surface, the present model uses Nernst-Planck and Poisson's equations coupled with a constant amount of surface charge on the pore walls as the EDL boundary conditions. In addition, the simulation is extended to a two-dimensional geometry. From the present study the following conclusions can be drawn:

- The present numerical model gives almost the same ionic distributions of both counter-ions and co-ions along the axis perpendicular to the charge surface as described by the Boltzmann equation, which proves that this model is valid to evaluate the effects of the EDL on the migration of ionic species in concrete.
- The extension of the diffuse layer according to the numerical results reaches as far as 40 μm, which is much greater than that estimated using the Debye length based evaluation theory (7 μm).
- When positive surface charges were applied, the negatively charged ionic species have higher concentrations in the EDL effect zones than in the bulk zone; while the positively charged ionic species have lower concentrations in the EDL effect zones than in the bulk zone. However, in terms of the average concentration along the y-axis, the effect of the EDL seems not to be very significant as the difference is within 2%.
- The change of the amount of externally applied electric potential has little influence on the EDL effects but has great influence on the shape of the wave front of ionic profiles.

- As the amount of the surface charge increases, the effect of the EDL on the ionic penetration also increases. In particular, the increase of surface charge leads to an increase of ionic flux of negatively charged ions.
- Overall, it was shown that the EDL has little effect on the migration speed of ions but a significant effect on the ionic flux.

Chapter Four - Simulation of Two-Phase Multi-Component Ionic Transport in Cement Paste with Electric Double Layer

This Chapter presents a two-dimensional, two-phase ionic transport model with a surface charge at solid-liquid interfaces. The present model is applied to investigate the effect of surface charges at the solid-liquid interface on the ionic transport in a cement paste when it is subjected to an externally applied electric field. The surface charge in the present model is considered by modifying the Nernst-Planck equation in which the electrostatic potential is dependent not only on the externally applied electric field but also on the dissimilar diffusivity of different ionic species including the surface charges. The coupled transport equations of individual ionic species are solved numerically using a finite element method built in commercial software COMSOL. Some important features about the effect of surface charge on the concentration distribution, migration speed and flux of individual ionic species are discussed.

4.1 Introduction

In the past decade, much effort has been made to investigate the surface charge of various cement hydrate phases. Due to lack of direct test methods, most studies determined the sign and the amount of the surface charge by measuring the zeta potential, which is the potential at the shear surface between the stern and diffuse layers and is closely related to the surface charge. Many researchers conducted zeta potential measurement on synthetic C-S-H suspensions (Castellote, Llorente & Andrade, 2006;

Hocine *et al.*, 2012; Labbez *et al.*, 2011), which are the main hydration products of cement-based materials. They found that the surface of C-S-H gel is negatively charged at low concentrations of Ca2+ in solution with a negative zeta potential. However, the zeta potential becomes positive when the concentration of Ca2+ is higher than a certain value. Elakneswaran et al. (Elakneswaran, Nawa & Kurumisawa, 2009a; Elakneswaran, Nawa & Kurumisawa, 2009b) studied the surface potential characteristics of different major mineral phases of hydrated cement paste. It was reported that Friedel's salt and portlandite have positive surface charge while others show negative surface charge in water. Overall, the hydrated cement paste shows positive net surface charge by dissociation and adsorption. Nevertheless, the experimental results and theory of the surface charge are still not strong enough to make a general conclusion about the sign and the magnitude of the surface charge in cementitious materials.

Typically, the ionic and electric potential distributions in the EDL can be estimated by a linearized version of the Poisson-Boltzmann equation, which is only applicable at low potentials. With a constant electric potential boundary condition, one can get the results of electric potential distribution perpendicular to the charged surface, which is called the Debye-Hückel approximation. Then the ionic concentration distribution can be calculated by using the Boltzmann equation. However, the zeta potential measurements of cementitious materials indicate that the magnitude of the surface potential is relatively high for the linearization to be applicable (Probstein, 2005). Arnold et al. (Arnold *et al.*, 2013) presented a numerical solution of the full nonlinear Poisson-Boltzmann equations and examined the implications of EDL on the ionic diffusion in discrete pore geometries. The scheme is more applicable than the analytical Debye-Hückel approximation in cementitious materials. Friedmann et al. (Friedmann, Amiri

& Aït-Mokhtar, 2008b) developed an analytical solution of the Poisson-Boltzmann equation by replacing the Poisson's equation with the electro-neutrality approximation. They demonstrated that the overlapping of two diffuse layers in gel pores strongly influence the EDL effect on ionic transport. Nguyen and Amiri (Nguyen & Amiri, 2014) investigated the EDL effect on chloride penetration in unsaturated concrete by solving the multi-species ionic transport equations coupled with that of humidity. The EDL effect is introduced by modifying the ionic concentration with influencing parameters, which are mainly dependent on the zeta potential and the pore diameter. Their numerical results showed that the EDL effect reduces in unsaturated concrete due to the discontinuity of liquid phase but increases in the concrete containing slag when compared to that with fly ash due to the high ionic strength of pore solution caused by the ferrous ions of slag.

In this Chapter, a two-dimensional numerical model is developed to simulate the transport of multiple species in a cement paste with surface charges. The model is used to simulate the ionic transport taking place in a cement paste when it is subjected to a rapid chloride migration (RCM) test. The numerical results show that there is an interaction between the local electric field generated by the surface charges and the global electric field generated by the externally applied voltage. The effect of surface charges at the pore surfaces on the ionic transport, in particular, the chloride penetration, in the two-dimensional model of cement paste is examined and discussed, through which the importance of using two-dimensional geometry is highlighted.

4.2 Two-Dimensional Two-Phase Multi-Component Ionic Transport Model with Surface Charges

It is assumed that the cement paste to be studied herein is fully saturated and there are no chemical reactions such as ionic adsorption/desorption between solid and liquid phases and ion-solvent molecules interactions in the pore solution. The transport of ionic species in the cement paste is the balance of the competing effects between the random thermal motion of the ions and the electric force, which is valid not only in the diffuse layer of EDL but also in the bulk solution where the effect of the surface charge can be ignored. The conventional Poisson-Boltzmann equation incorporates both the thermal and electric effects to describe the influence of surface charges but is only applicable to one-dimensional problems, in which the local electrostatic potential generated by the EDL is not affected by the externally applied bulk electric field. For cementitious materials, however, the connective pores where ionic transport takes place are randomly distributed in the materials. When an external electric field is applied, the bulk electric field is generally not perpendicular to the local electric filed generated by the surface charge at randomly distributed pore surfaces. Therefore, the local and bulk electric fields may disturb each other. The interactive nature of these two electric fields may affect the transport of ions in the pore solution, the problem of which has not been addressed in the existing literature and is to be discussed here.

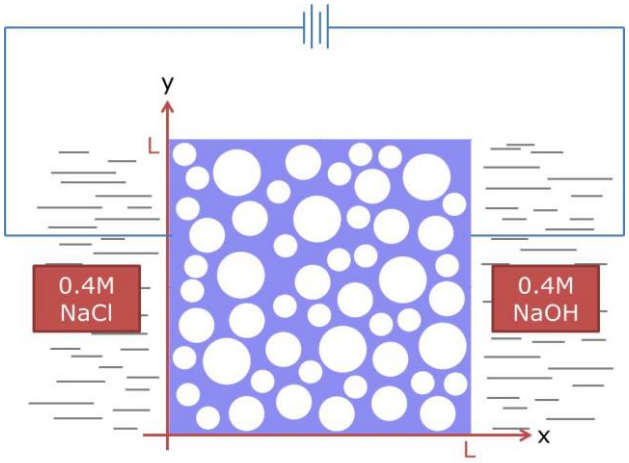

Figure 4-1. 2-D, two-phase model used in simulation.

Here a cylindrical cement paste specimen used in the RCM test is considered. Because of the symmetry, the transport of ions in the specimen can be treated as a two-dimensional problem as shown in Figure 4-1, where the cement paste is represented by a two-phase porous material. The solid phase represents the solid part in the specimen where ionic transport cannot take place, whereas the liquid phase represents the transport medium where ionic transport can take place. The interface between the solid and liquid phases represents the pore surfaces where a surface charge exists. The specimen is exposed to NaCl and NaOH solutions on its left and right sides, respectively. The top and bottom sides of the specimen are sealed and therefore there is no ionic transport across these two boundaries. An external electric field is applied between the cathode placed in the NaCl solution and the anode placed in the NaOH solution as shown in Figure 4-1.

The ionic flux of individual species in the liquid phase due to diffusion and migration can be expressed as follows:

$$J_k = -D_k \nabla C_k - D_k \frac{z_k F C_k}{RT} \nabla \Phi \qquad \text{k} = 1, 2, \ldots \text{N} \qquad (4\text{-}1)$$

where J_k is the flux, D_k is the diffusion coefficient, C_k is the concentration, z_k is the valence number, F = 96480 C/mol is the Faraday constant, Φ is the electrostatic potential, $R = 8.314\ \text{J/(mol} \cdot \text{K)}$ is the ideal gas constant, T = 298 K is the absolute temperature, subscript k stands for the k-th ionic species, and N is the total number of ionic species considered in the solution. The first and second terms in the right-hand-side of the equation represent the flux due to diffusion and migration, respectively. Note that the electrostatic potential in Eq. (4-1) is generated not only by the externally applied electric field but also by the dissimilar diffusivity of different ionic species involved in the solution including the surface charges. By using the conventional Poisson's equation with considering the surface charges, the electrostatic potential in the solution domain can be determined as follows:

$$\nabla^2 \Phi = -\frac{F}{\varepsilon_o \varepsilon_r} \sum_{k=1}^{N} (z_k C_k + z_s C_s) \qquad (4\text{-}2)$$

where $\varepsilon_0 = 8.854 \times 10^{-12}\ \text{C/(V} \cdot \text{m)}$ is the permittivity of a vacuum, $\varepsilon_r = 78.3$ is the relative permittivity of water at temperature 298K, z_s and C_s are the valence number and concentration of the surface charge, respectively. Note that the surface charge exists only at the interfaces between solid and liquid phases and is taken as zero in the solution. The effect of the stern layer is not taken into account in this study for the sake of numerical simplicity. It is assumed that the thickness of stern layer is negligible compared to the size of the cement pores and the surface potential is equivalent to the zeta potential at the shear surface between the stern layer and diffuse layer (Arnold *et al.*, 2013).

The mass conservation of individual ionic species in a representative elementary volume in the liquid phase requires the following equation:

$$\frac{\partial C_k}{\partial t} = -\nabla \cdot J_k \qquad \text{k = 1, 2, … N} \qquad (4\text{-}3)$$

where t is the time. Substituting Eq. (4-1) into (4-3), it yields,

$$\frac{\partial C_k}{\partial t} = \nabla \cdot \left[D_k \nabla C_k + D_k \frac{z_k F C_k}{RT} \nabla \Phi \right] \qquad \text{k = 1, 2, … N} \qquad (4\text{-}4)$$

Equations (4-4) and (4-2) are the governing equations applied to the liquid phase, which can be used to solve for the electrostatic potential Φ and the concentrations C_k (k = 1, 2, … N) of individual ionic species if the initial and boundary conditions of Φ and C_k are defined.

The above-described model is applied to simulate the ionic transport in the cement paste with pore surface charges when it is subjected to an RCM test. Note that, in RCM tests, the axially symmetric cross-section of the specimen is normally in the size of 50x50 mm (for a cylindrical specimen of diameter 100 mm and length 50 mm). However, the size of EDL is much smaller, which is about tens nanometre to a few micrometres. In order to minimise the size effect and enlarge the effect of EDL on ionic transport to be studied, a compromised solution domain of 5x5 mm is chosen (see Figure 4-1), in which the solid and liquid phases are assumed to have an equal volume fraction, which represents a cement paste of water-to-cement ratio 0.54. Four ionic species, namely potassium, sodium, chloride and hydroxyl are considered. The initial and boundary conditions of the four ionic species are given in Table 4-1. The externally applied voltage normally used in RCM tests is about 24 V, which produces a voltage gradient across the specimen of 48 V/cm. In order to make the solution domain have the same

voltage gradient, the externally applied voltage employed in the present simulation is reduced to 2.4 V. The detailed boundary conditions of the electrostatic potential at four boundaries used in the simulation are also given in Table 4-1.

Table 4-1. Initial and boundary conditions and parametric values used in the simulation.

Variables	Chloride (mol/m^3)	Hydroxyl (mol/m^3)	Potassium (mol/m^3)	Sodium (mol/m^3)	Voltage (V)
Initial conditions	$C = 0$	$C = 400$	$C = 300$	$C = 100$	-
Boundary conditions at $x = 0$ mm	$C = 400$	$C = 0$	$C = 0$	$C = 400$	$\Phi = 0$
Boundary conditions at $x = 5$ mm	$C = 0$	$C = 400$	$C = 0$	$C = 400$	$\Phi = 2.4$
Boundary conditions at $y = 0$ mm	$J = 0$	$J = 0$	$J = 0$	$J = 0$	əΦ/əy=0
Boundary conditions at $y = 5$ mm	$J = 0$	$J = 0$	$J = 0$	$J = 0$	əΦ/əy=0
Valence number	$z = -1$	$z = -1$	$z = 1$	$z = 1$	-
Diffusion coefficient $x10^{-11}$ m^2/s	D =4.064	D =10.546	D =3.914	D =2.668	-

The surface charges on the interfaces between solid and liquid phases are assumed to be positive monovalent ions (i.e. z_s = 1) with a constant concentration of C_s = 400 mol/m^3, which matches to the surface potential used in other studies, for example, (Elakneswaran, Nawa & Kurumisawa, 2009a; Elakneswaran, Nawa & Kurumisawa, 2009c; Elakneswaran, Nawa & Kurumisawa, 2009b; Viallis-Terrisse, Nonat & Petit, 2001).

The diffusion coefficients of the potassium, sodium, chloride and hydroxyl ions used in the present simulation are shown in Table 4-1, which are taken from corresponding values of them in dilute solution but divided by a factor of 50 to take into account the retardation that arises from the constriction and tortuosity of the pore path through which the ions are travelling.

Note that the ionic transport takes place in the liquid phase only. Hence, the finite element mesh is made also only in the liquid phase. The external boundary conditions described above are applied to the four sides (x = 0, x = 5 mm, y = 0, y = 5 mm). For the interface boundaries between the solid and liquid phases a zero-flux boundary condition is used. It can be recognised that the electrode setting, geometry of the specimen and the external boundary conditions are symmetric about the horizontal central line. Hence, for the simplification of investigation, only a half of the specimen, is modelled. To avoid the numerical difficulty caused by the sudden change in concentration of the charge from the interface to bulk solution, extremely small element sizes (see Figure 4-2) are used in the regions near to the interfaces. In order to examine the effect of element size on the numerical results, trials of different element sizes ranging from 10^{-7} m to 10^{-5} m were conducted. The final mesh was adopted when the

further reduction of the chosen element size has almost no effect on the obtained results and also remain convergence of the numerical solution.

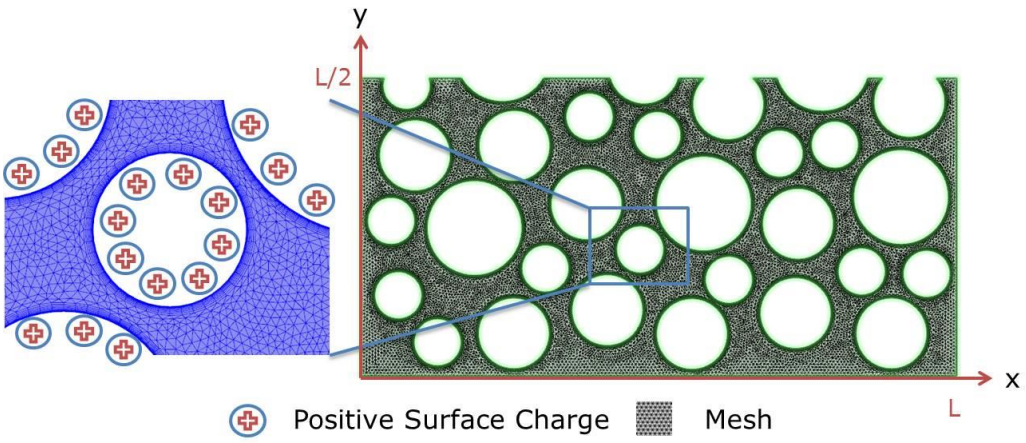

Figure 4-2. Schematic of finite element mesh and surface charge.

4.3 Simulation Results and Discussion

The governing equations (4-2) and (4-4) with initial and boundary conditions defined in Table 4-1 are solved using the commercial software COMSOL. The details of the COMSOL software can be found in the COMSOL website and thus are not given further here. Instead, in what follows, only results and the discussion of the results are provided.

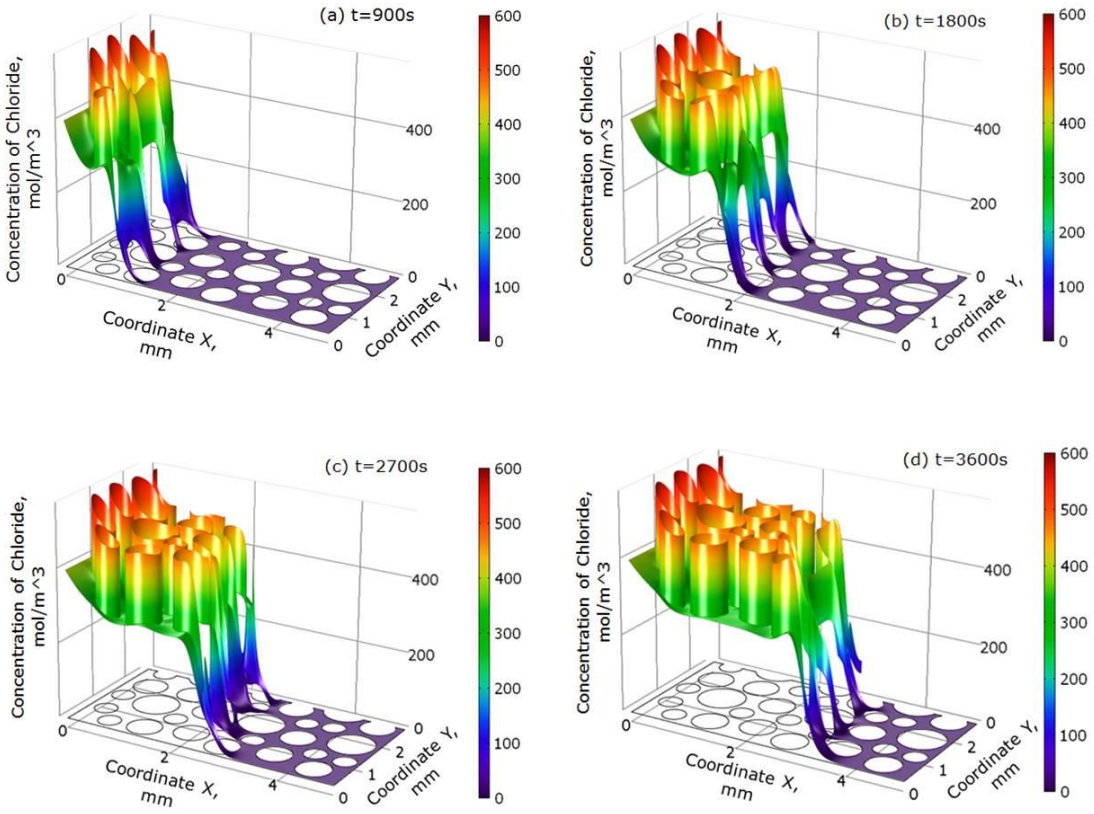

Figure 4-3. Chloride concentration profiles at four different times.

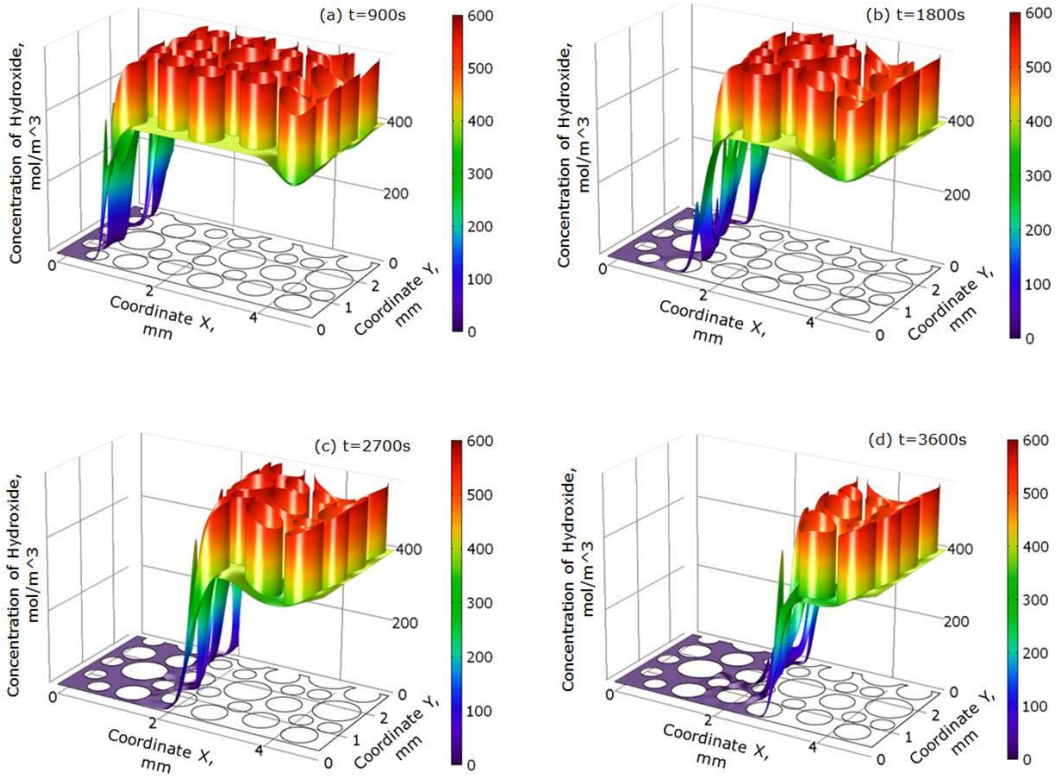

Figure 4-4. Hydroxyl concentration profiles at four different times.

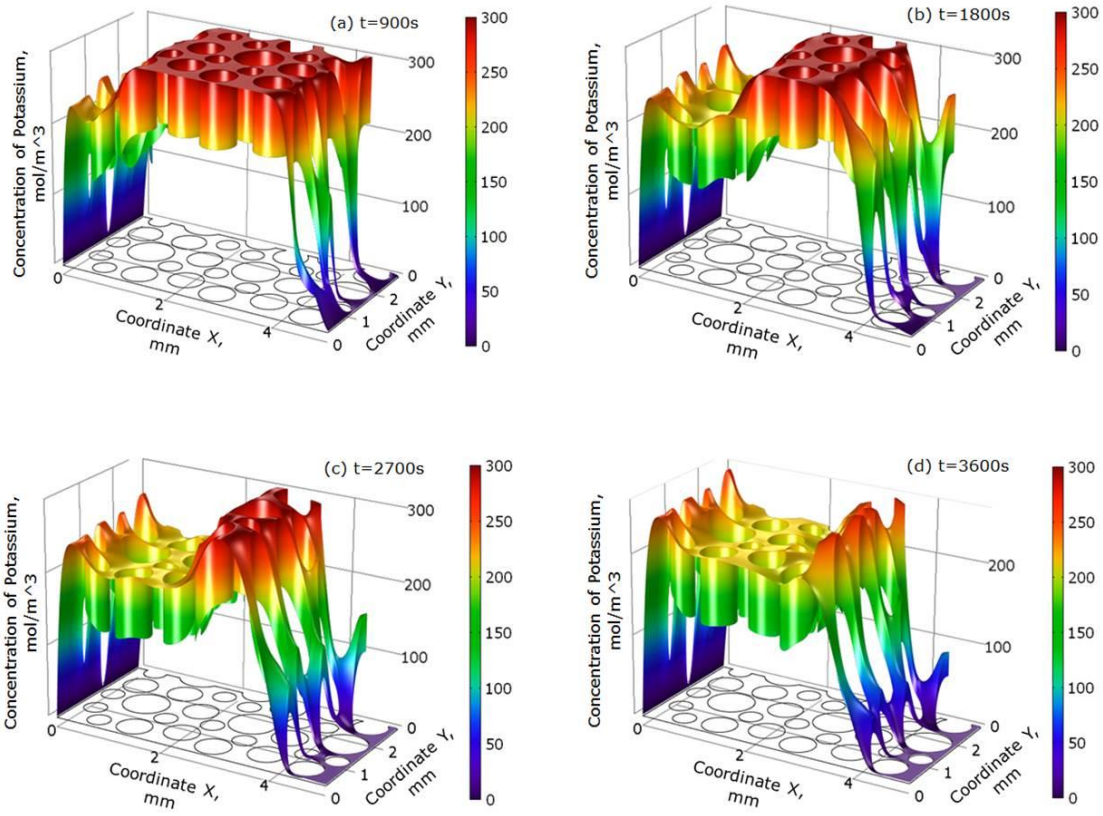

Figure 4-5. Potassium concentration profiles at four different times.

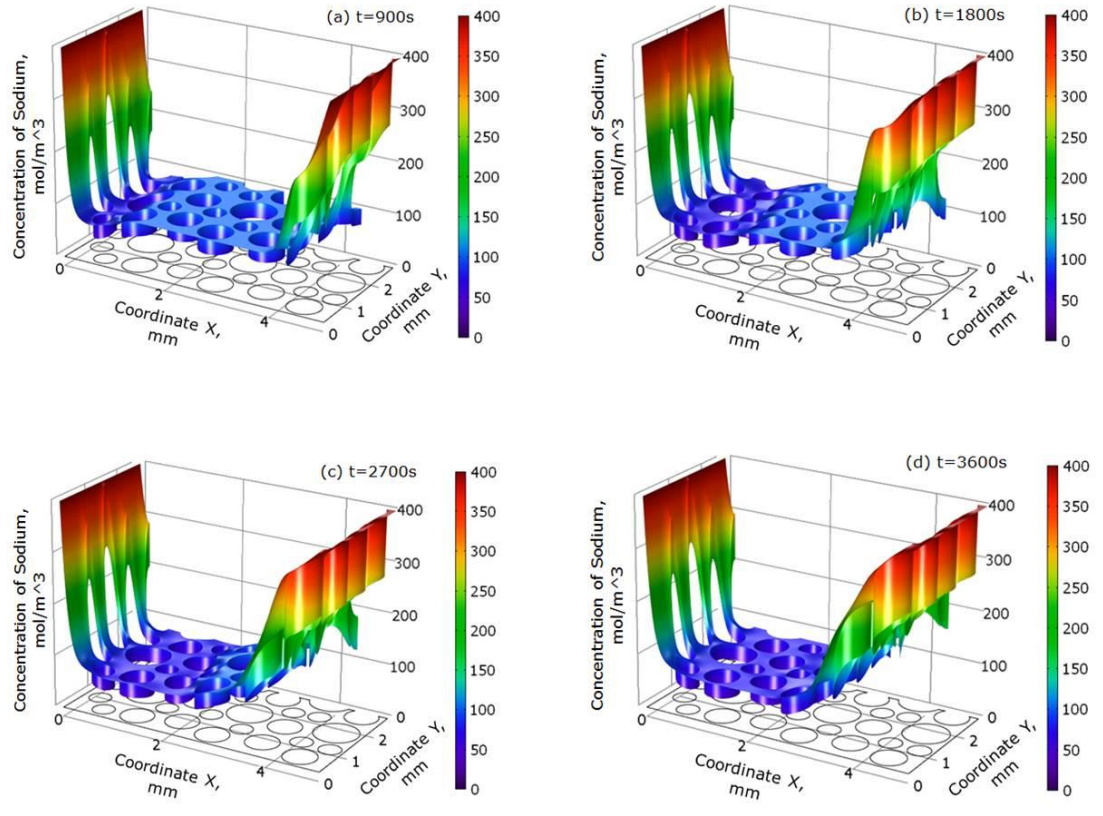

Figure 4-6. Sodium concentration profiles at four different times.

Figure 4-3 to Figure 4-6 show the concentration distribution profiles of the chloride, hydroxyl, potassium, and sodium ions in the liquid phase at four different times, in which the z-axis is the ionic concentration, the x- and y-axes represent the coordinate point (x, y), respectively. These 3-D plots clearly illustrate the evolution of ionic transport with the time. Special attention is focused on the effect of the surface charges on the concentration distributions of the four ionic species, particularly in the regions near the charged surfaces (edge of the circles in the numerical model). It can be seen from the figures that, under the action of the externally electric field applied between the two boundaries at $x = 0$ and $x = 5$ mm, the negatively charged ions (chloride and hydroxyl) are forced to move from the cathode to the anode, while the positively charged ions (potassium and sodium) move from the anode to the cathode. In addition, due to the charge imbalance at the solid-liquid interfaces caused by the positive charge, the negatively or positively charged ions also move towards to or away from the charged surfaces while they are moving from one electrode to another. The electric attraction and repulsion, together with the effect of the concentration gradient, results in that the ionic distribution near the surface is in a 'diffuse' manner as mentioned before. However, the charge imbalance is highly localised and occurs only in very narrow regions close to the charged surfaces. As shown in Figure 4-3 to Figure 4-6, the concentrations of chloride and hydroxyl increase steeply when approaching the solid-liquid interface, whereas the concentrations of potassium and sodium drop steeply. Note that the effect of the surface charge on the concentration distribution of individual ionic species is dependent not only on the amount of the surface charge but also on the ionic concentration in the bulk solution. The higher the concentration of an ionic species in the bulk solution, the larger the effect of the surface charge on the concentration distribution of that ionic species. The concentration increase of negatively charged ions

or the concentration decrease of positively charged ions around the charged surface could be interpreted as the adsorption or desorption of ions due to the chemical attraction or repulsion of ions.

In order to investigate the overall effect of the surface charge on the transport of each ionic species along the x-axial direction, Figure 4-7 to Figure 4-10 provide the 2-D plots of individual ionic species for a quantitative comparison of ionic concentration distributions along the x-axis. Three average concentrations in y-axis are used in the figures. One is the average concentration in the liquid phase obtained with considering the effect of EDL; one is the average concentration in the liquid phase obtained without considering the effect of EDL; and one is the average concentration obtained in the 1-D and one-phase model (i.e. neither the solid phase nor the surface charge is considered in the model). It can be seen from Figure 4-7 that, the transport of chloride ions slows down by a factor of about 1.5 when the solid phase is included in the model. This is probably due to the influence of tortuosity of the two-phase model. It is interesting to notice that, as far as the transport speed is concerned, the surface charge has almost no effect on the transport of chloride ions. However, in terms of the average concentration, the positively charged surface leads to chloride to have marginally higher average concentration. The reason of this is probably due to the high chloride concentration along the charged surfaces but their layers are very thin.

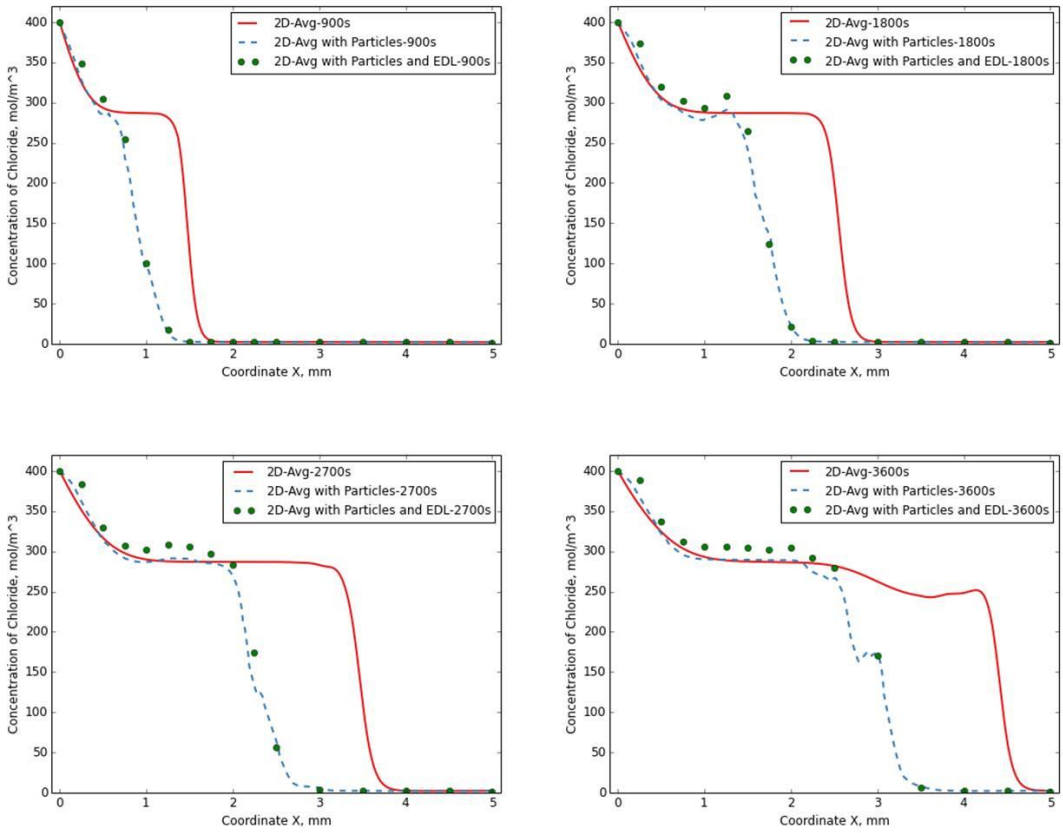

Figure 4-7. Comparison of average chloride concentrations.

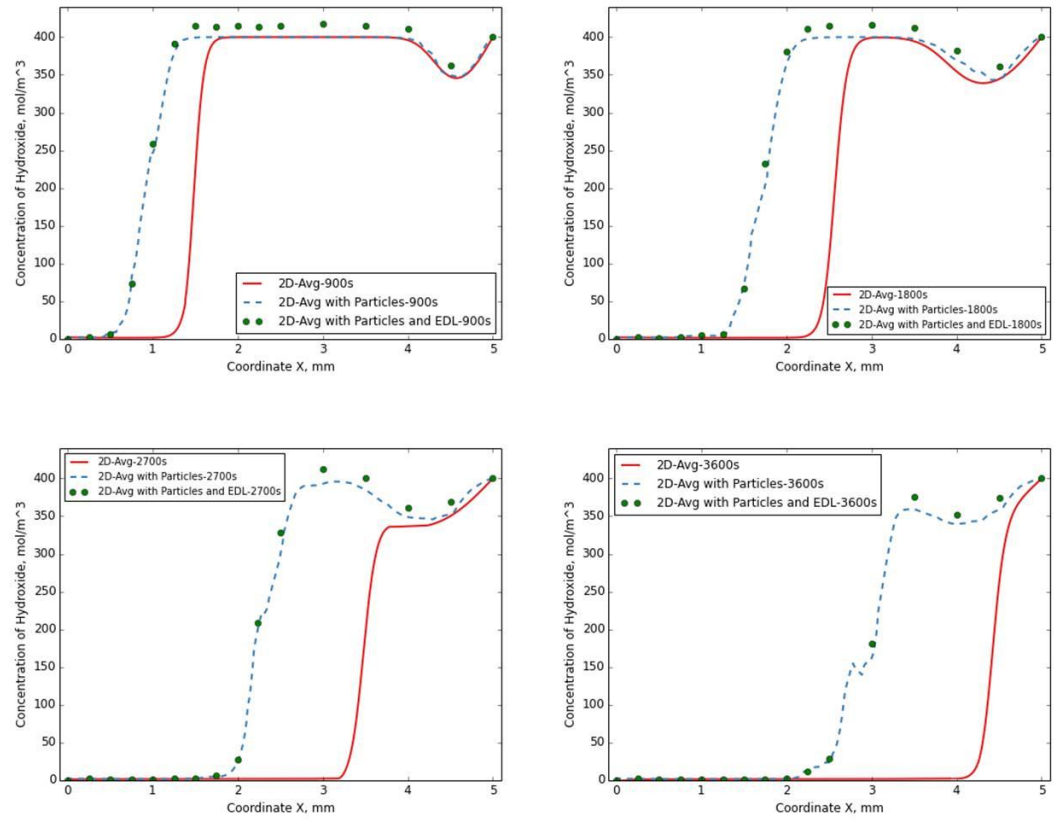

Figure 4-8. Comparison of average hydroxyl concentrations.

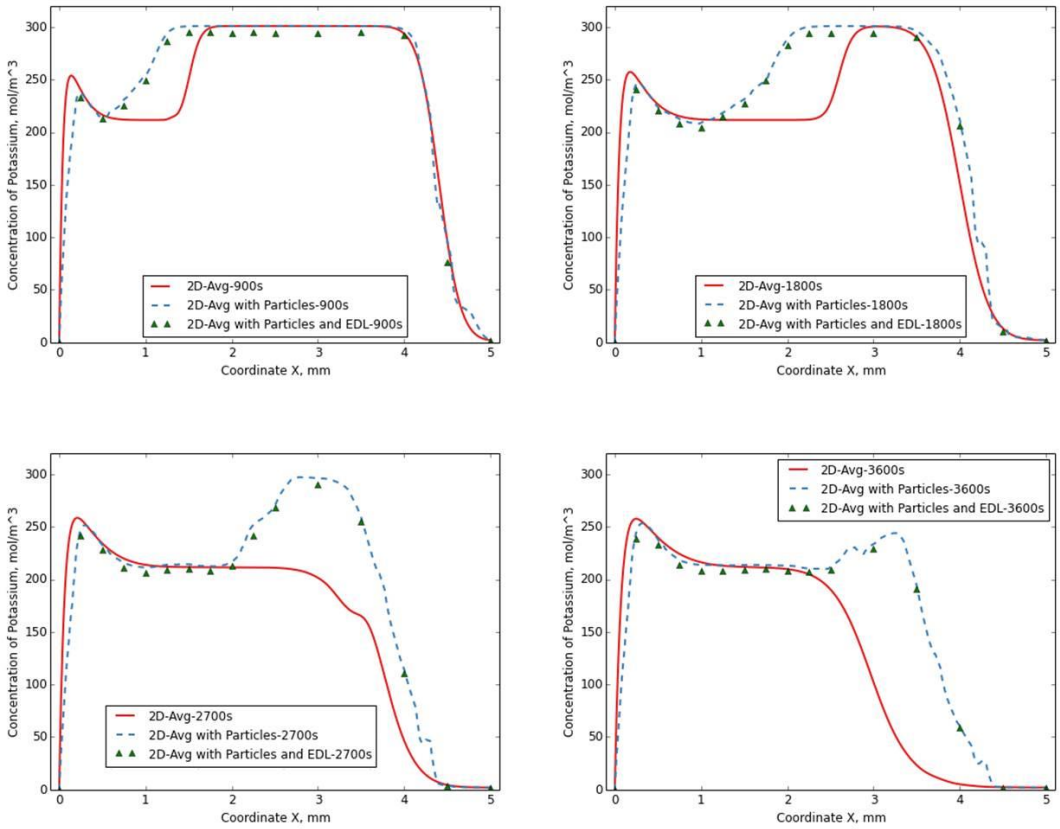

Figure 4-9. Comparison of average potassium concentrations.

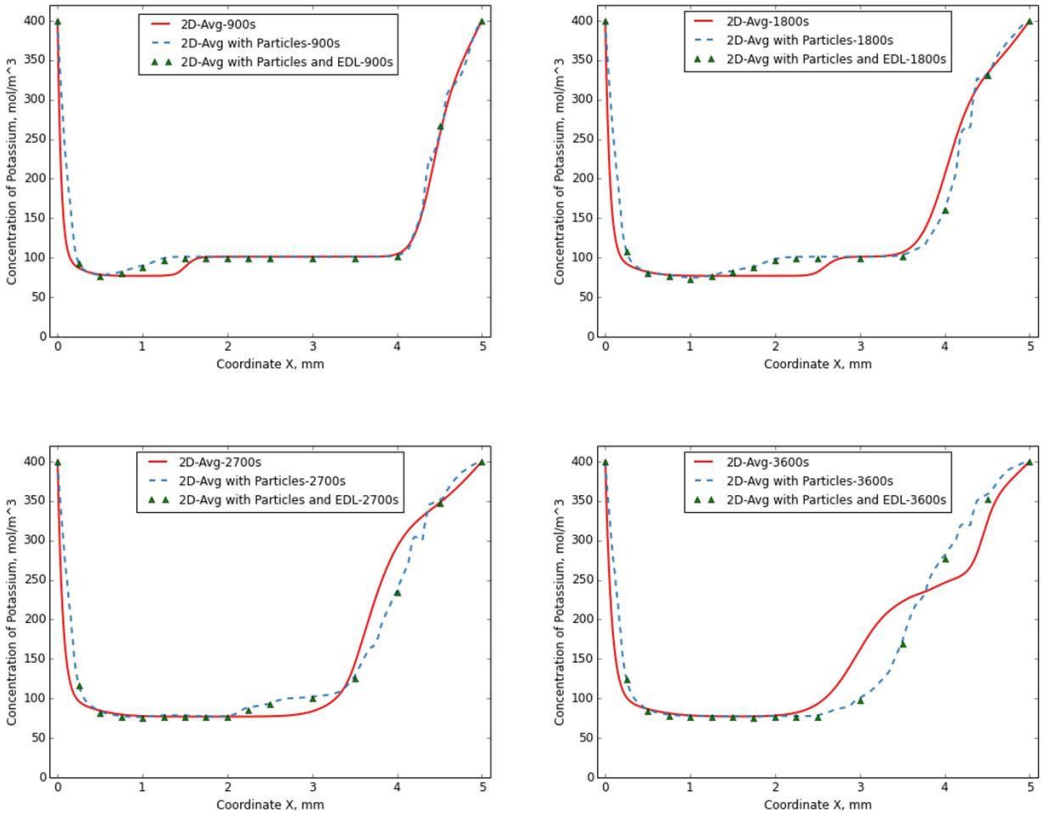

Figure 4-10. Comparison of average sodium concentrations.

The average concentrations shown in Figure 4-8 for hydroxyl ions provide similar features. It is noted from the figure that the migration speed of the hydroxyl ions is almost the same as that of the chloride ions, although the diffusion coefficient of hydroxyl ions is about 2.5 times as that of chloride ions. This indicates that the interaction between different ionic species has a strong influence on the transport of individual ionic species. Figure 4-9 and Figure 4-10 show the average concentrations of potassium and sodium ions. It can be seen from the figures that, the transport speed of these two ionic species are also reduced when the solid phase is included in the model. However, unlike the negatively charged chloride and hydroxyl ions, the positively charged potassium and sodium ions have slightly lower average concentrations when the solid and liquid interfaces have a positive surface charge. In summary, it is found that the positive surface charge has more influence on the transport of negatively charged ions than that of the positively charge ions.

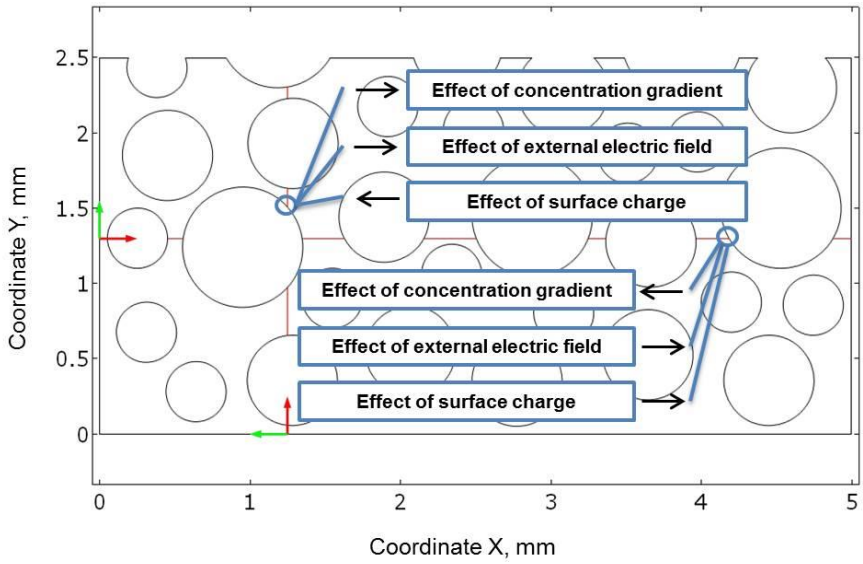

Figure 4-11. Factors affecting ionic flux at a point on solid-liquid interface.

In the RCM test, the dominant ionic flux is the migration flux, which is proportional to the migration speed and ionic concentration as described in Eq.(4-1). Figure 4-11 graphically shows the effects of the surface charge on the local ionic fluxes. The three ionic fluxes at the two points shown in the figure represent the fluxes induced by the diffusion, local electric field caused by the surface charge, and global electric field caused by the externally applied electric voltage, at a certain time. Of interest is the x-component of the flux of chloride ions since it is primarily concerned in the test. There are three types of driven forces, which have contributions to the x-component of the chloride flux at a single point at the charged surface as well as in the diffuse layer near the charged surface. They are the concentration gradient, externally applied electric field along the x-axis, and the local charge imbalance caused by the surface charge, respectively. It can been seen from Figure 4-11 that, the direction of the x-component of chloride flux resulting from the externally applied electric field along the x-axis remains the same across the whole domain. However, the direction of the x-component of chloride flux at the solid-liquid interface resulting from the concentration gradient and the surface charge is dependent on the normal direction of the charged surface. Thus, the x-component of the chloride flux will be influenced strongly by the pore geometry of the material. It is obvious that this feature cannot be explained by using the one-dimensional EDL model.

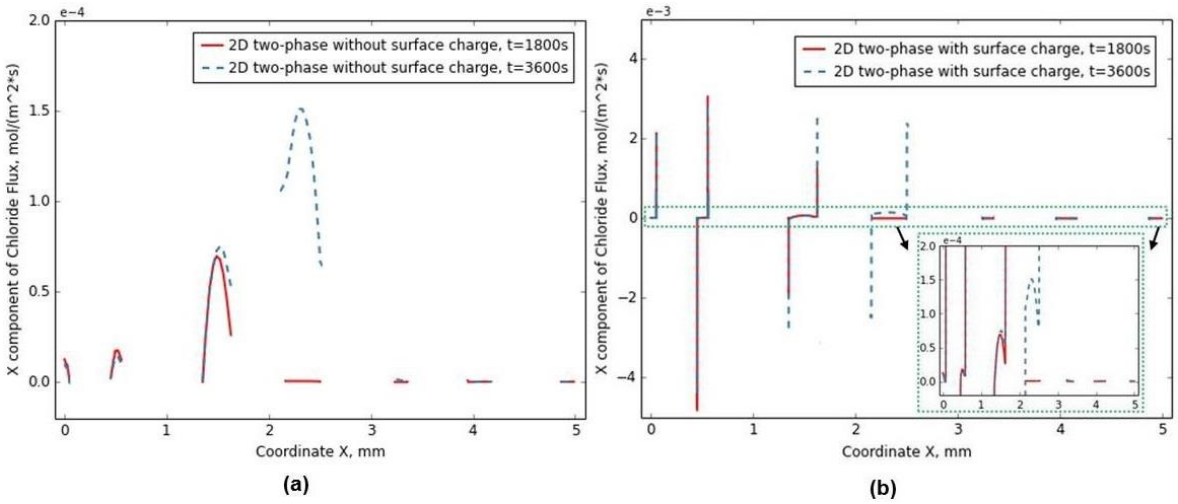

Figure 4-12. The x-component of chloride flux at line y = 1.3 mm at two different times, (a) without surface charge and (b) with surface charge.

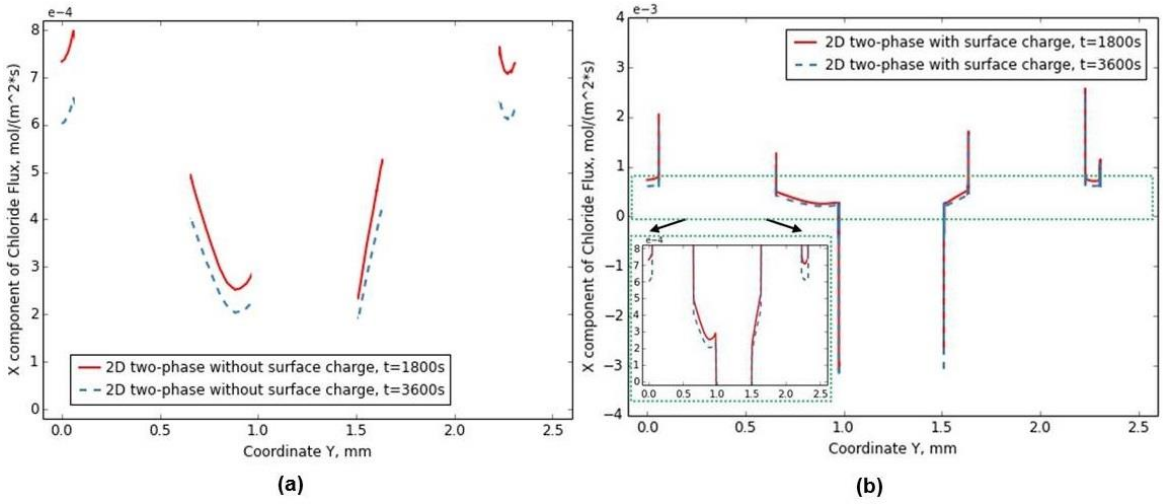

Figure 4-13. The x-component of chloride flux at line x = 1.25 mm at two different times, (a) without surface charge and (b) with surface charge.

The main purpose of the RCM tests is to determine the diffusion coefficient of chloride ions in the tested specimen. There are two exercises that are currently used in the tests. One is to obtain the apparent diffusion coefficient (Tang & Nilsson, 1993) based on the depth, to which the chloride ions have penetrated in the specimen; the other is to obtain the effective diffusion coefficient (Chung-Chia, 2004) based on the flux of chloride

ions, which has passed through the specimen. The former is controlled by the travel speed of chloride ions, whereas the latter is related to the flux of chloride ions, which is dependent on not only the speed but also the concentration of chloride ions. To examine the effect of the surface charge on the chloride flux, Figure 4-12 and Figure 4-13 show the comparison of x-components of chloride flux at two lines (x = 1.25 mm and y = 1.3 mm), obtained from the present simulation models with and without considering the surface charge. Note that, since the solid phase is discontinuous and impermeable to ions the flux profiles plotted are not continuous in these figures.

It can be seen from Figure 4-12(a) that, when the surface charge is not taken into account, the x-component of chloride flux at the line of y = 1.3 mm varies along x-axis. In general, the flux is lower at the place near to the solid surface and higher at the place far away from the solid surface, representing the obstacle effect of the solid phase on ionic transport in x-direction. In contrast, the x-component of chloride flux at the line of x = 1.25 mm shown in Figure 4-13(a) also varies along y-axis, but it is dependent on the pattern of solid phase. In some regions the higher flux is found at the place near to the solid surface and the lower flux is at the place far away from the solid surface. While in other regions the flux increases/decreases from one solid surface to another solid surface, representing the effect of ahead and rear solid particles on ionic transport in liquid phase of the material when an externally applied electric field is involved.

When the surface charge is taken into account, however, the x-components of chloride flux at the two lines (y = 1.3 mm and x = 1.25 mm) are found to be quite different (see Figure 4-12(b) and Figure 4-13(b) from those shown in Figure 4-12(a) and Figure 4-13(a). Firstly, the surface charge significantly alters the x-component value of

chloride flux in the region very close to a solid surface. Secondly, the scale value of the x-component of chloride flux close to a solid surface is about 10^{-3} mol/(m^2·s), which is about 10 times of that in the bulk solution. Thirdly, the effect of the surface charge on the x-component of chloride flux is only in very thin layer surrounding the solid surface as demonstrated in the zoom plots shown in Figure 4-12(b) and Figure 4-13(b). Note that the effect of the surface charge on the x-component of chloride flux is different at the different points on the surface of a solid particle. For example, as is shown in Figure 4-12(b), the x-component of chloride flux reduces at the front point of a solid particle, but increases at the rear point of the solid particle. However, as is shown in Figure 4-13(b), the x-component of chloride flux could increase or decrease at the upper or lower point of a solid particle, depending on the pattern of the pore structure used in the model (i.e. the sizes and positions of its ahead and rear solid particles).

4.4 Conclusions

A 2-D, two-phase multicomponent ionic transport model has been developed in this Chapter. The present model has been applied to investigate the effect of surface charges at the solid-liquid interface on the ionic transport in a cement paste when it is subjected to an externally applied electric field. The surface charge in the present model is considered by modifying the Nernst-Planck equation in which the electrostatic potential is dependent not only on the externally applied electric field but also on the dissimilar diffusivity of different ionic species including the surface charges. The coupled transport equations of individual ionic species are solved numerically by using commercial software COMSOL. From the present study, the following conclusions can be drawn:

- The surface charge has a significant influence on the concentration distribution of ionic species but only in the region close to the charge surface. A positive surface charge increases the concentration of negatively charged ions but decreases the concentration of positively charged ions.
- The overall migration speed of ionic species in the two-phase model is found to be slower than that in the single-phase model because of the effect of tortuosity when the solid phase is involved. The surface charge at the solid-liquid interfaces seems to have very little influence on the overall migration speed of ionic species. This is mainly due to the layer of effect zone of EDL that is very thin when compared to its bulk solution zone.
- The surface charge has great influence on the chloride flux; but it is also only in the region close to the charge surface. A positive charge surface increases the x-component of chloride flux at the rear point of a solid particle, but decreases the x-component of chloride flux at the front point of a solid particle. A positive charge surface could increase or decrease the x-component of chloride flux at the upper or lower point of a solid particle, depending on the pattern of the solid and liquid phases used in the model.

Chapter Five – A Novel 1-D Numerical Model for Multi-Component Ionic Transport in Concrete

In this Chapter, a new one-dimensional numerical model for the multi-component ionic transport in concrete is presented. Advantages and disadvantages of the traditional methods used to determine the local electrostatic potential, i.e. electro-neutrality condition and Poisson's equation, are illustrated. Then a new electro-neutrality condition is presented, which can avoid the numerical difficulties caused by the Poisson's equation, and remain the non-linearity of the electric field distribution. Lastly the model with the new electro-neutrality condition is employed to simulate the RCM test to prove its applicability. The new model is promising in solving the multi-component ionic transport problems especially in microscopic scale.

5.1 Introduction

Since the early 1980s a considerable amount of laboratory and field tests have been carried out to investigate the mechanism of chloride ingress in concrete (e.g., (Atkinson & Nickerson, 1984; Audenaert, Yuan & De Schutter, 2010; Chen *et al.*, 2012; Chung-Chia, 2004; Dhir, Jones & Ng, 1998; Page, Short & El Tarras, 1981; Sergi, Yu & Page, 1992)). These experimental methods can be classified into two categories. One is the diffusion test, in which the main driving force of the chloride penetration is the concentration gradient. The other is the migration test, in which the dominant driving force of the chloride penetration is the electrostatic potential gradient generated by the externally applied electric field. Based on the obtained experimental results, many prediction models have also been developed to examine the influence of various involved factors on the penetration of chloride ions in cementitious materials (Andrade,

Castellote & d'Andrea, 2011; Baroghel-Bouny *et al.*, 2012; Bentz, Garboczi & Lagergren, 1998; Garboczi, Schwartz & Bentz, 1995; Halamickova *et al.*, 1995; Jiang *et al.*, 2013; Li, Xia & Lin, 2012; Li & Page, 1998; Li & Page, 2000; Liu & Shi, 2012; Mercado, Lorente & Bourbon, 2012; Pack *et al.*, 2010; Xia & Li, 2013; Yang & Weng, 2013; Ying *et al.*, 2013).

As aforementioned in the literature review in Chapter Two, in recent years there has been an increasing interest in developing and improving rapid chloride migration test and numerical models for chloride migration in concrete. The Rapid Migration Test (RCM) was first developed by Luping Tang and Nilsson (Tang & Nilsson, 1993), and then adopted by Nordtest as NT Build 492 (NT-BUILD492, 1999). Instead of measuring the total passed charge, the RCM test measures the chloride penetration depth using silver nitrate solution as a colorimetric indicator. Then the diffusion coefficient of chloride ion is calculated by the depth based on the mathematical solution of the Nernst-Planck equation. It should be pointed out here that the calculation of the chloride diffusion coefficient in RCM test is based on assumption of the constant electric field in the experiment sample, which means the migration speed of chloride ions is constant along the penetration depth. It does not take into account the electrostatic interactions between different ionic species in the pore solution.

The early attempts to consider the multi-species influences on the chloride penetration in concrete used the electro-neutrality to determine the electrostatic potential (Friedmann *et al.*, 2004; Frizon *et al.*, 2003; Lorente, Carcassè & Ollivier, 2003; Narsilio *et al.*, 2007; Toumi, François & Alvarado, 2007; Truc, Ollivier & Nilsson, 2000a; Truc, Ollivier & Nilsson, 2000b). However, the numerical results from the

models, in which the electro-neutrality was employed, showed that the electrostatic potential gradient was still constant. And the migration speed of different ions involved is also constant, which entirely depends on the diffusion coefficient and the applied external electric potential. The multi-component interactions are not fully presented with aforementioned models using electro-neutrality (Liu, 2014). It should be pointed out here that, the electro-neutrality condition is not a fundamental law of nature, a more nearly correct relationship would be Poisson's equation (Newman & Thomas-Alyea, 2012). Recently, a number of numerical studies have been carried out to simulate the chloride migration in concrete using the Nernst-Planck/Poisson's equation (NPP) system (Krabbenhøft & Krabbenhøft, 2008; Liu *et al.*, 2015; Liu *et al.*, 2012; Samson, Marchand & Snyder, 2003; Xia & Li, 2013). Despite the numerical difficulties caused by the Poisson's equation, the concentration distribution profiles of ionic species obtained from the NPP models are significantly different from those obtained from the models using electro-neutrality condition. And the electrostatic potential gradient calculated from the NPP model is not constant but regionally dependent, which means the Poisson's equation is more correct to describe the multi-component coupling. Nevertheless, Poisson's equation makes the NPP model highly non-linear and therefore it is very difficult to achieve convergent solutions unless the element size chosen for the finite element mesh is extremely small. This situation will get worse when the model is adopted to simulate micro-scale problems like the Electric Double Layer effects discussed in Chapter Three and Chapter Four.

In order to simplify the NPP model and keep the non-linear electric field distribution in the same time, a new one-dimensional ionic transport model will be presented in the

next section and it will aim to extend the applicability of the NPP model to more microscopic level modelling situations.

5.2 Description of the New Multi-Component Transport Model

Assume that the material is fully saturated and the pore solution is an ideal and dilute electrolyte solution, the flux of each ionic species in a multi-component electrolyte solution can be expressed using the Nernst-Planck equation as follows:

$$J_k = -D_k \nabla C_k - D_k \frac{z_k F C_k}{RT} \nabla \Phi \qquad \text{k = 1, 2, … N} \qquad (5\text{-}1)$$

where J_k is the flux, D_k is the diffusion coefficient, C_k is the concentration, z_k is the charge number, F = 9.648×10^4 C/mol is the Faraday constant, Φ is the electrostatic potential, $R = 8.314\ \mathrm{J/(mol \cdot K)}$ is the ideal gas constant, T = 298 K is the absolute temperature, subscript k represents the k-th ionic species, and N is the total number of ionic species considered in the solution. The transport of each ionic species in the material can be described by following the mass conservation equation:

$$\frac{\partial C_k}{\partial t} = -\nabla \cdot J_k \qquad \text{k = 1, 2, … N} \qquad (5\text{-}2)$$

where t is the time. Substituting Eq. (5-1) into (5-2), it yields,

$$\frac{\partial C_k}{\partial t} = \nabla \cdot \left[D_k \nabla C_k + D_k \frac{z_k F C_k}{RT} \nabla \Phi \right] \qquad \text{k = 1, 2, … N} \qquad (5\text{-}3)$$

If the interaction between chloride ions and other ionic species in the pore solution can be ignored, the gradient of electrostatic potential can be approximately calculated as the potential difference between the two sides of the specimen in the RCM test, which is $\nabla \Phi = \mathrm{V/L}$, where V is the externally applied electric potential and L is the distance between the two electrodes used in the RCM test. This approximation about

electrostatic potential distribution $\nabla\Phi = \mathrm{V/L}$ can also be calculated by adopting the assumption of the electro-neutrality condition as follows,

$$\sum_{k=1}^{N} z_k C_k = 0 \tag{5-4}$$

Otherwise the conventional Poisson's equation should be applied to calculate the electrostatic potential. For a medium of uniform dielectric constant, the electrostatic potential in the solution can be determined as follows:

$$\nabla^2\Phi = -\frac{F}{\varepsilon_o \varepsilon_r} \sum_{k=1}^{N} z_k C_k \tag{5-5}$$

where $\varepsilon_0 = 8.854 \times 10^{-12}\ \mathrm{C/(V \cdot m)}$ is the permittivity of a vacuum, $\varepsilon_r = 78.3$ is the relative permittivity of water at the temperature of 298K. The Poisson's equation relates the charge density to the Laplacian of the electrostatic potential. The proportionality constant in Eq. (5-5) is Faraday's constant *F* divided by the permittivity, which is a quite large value ($1.39 \times 10^{14}\ V \cdot m/mol$ for the relative permittivity constant of water 78.3). As mentioned in Section 6.1, the large value of the proportionality constant causes numerical difficulties in solving the NPP models. The partial differential equation (5-3) coupled with either Eq.(5-4) or Eq. (5-5) can be used to model the multi-component ionic transport. Both of them have disadvantages, which raise a question about whether there is a way to consider the multi-species interaction and avoid the numerical difficulties caused by the Poisson's equation at the same time.

5.2.1 A Numerical Demonstration of the Possibility to Simplify Poisson's Equation

In order to evaluate the influence of the proportionality constant in the Poisson's equation on modelling the ionic transport with NPP models, Eq. (5-3) and (5-5) are now used to simulate a rapid chloride migration test. In the RCM test, a cylindrical specimen is subjected to a constant voltage (normally 24V) between its two surfaces. One surface is exposed to an external NaCl solution, where a cathode is applied, and the other side is exposed to a NaOH solution, where an anode is applied. The schematic setting of the RCM test used in the demonstration simulation is shown in Figure 5-1. It can be assumed here that the chloride concentrations in the two external compartments remain unchanged during the migration test, because the volumes of the two external solutions are much greater than the pore volume of the specimen. Only three types of initial ionic species in the pore solution of the specimen will be included in the numerical demonstration study for simplicity. The parameters, initial and boundary conditions employed in this numerical demonstration are shown in Table 5-1. Eq. (5-3) and (5-5) together with the initial and boundary conditions can be solved using numerical methods. The numerical methods applied here are very similar to those used in the literature (Xia & Li, 2013), thus are not described here.

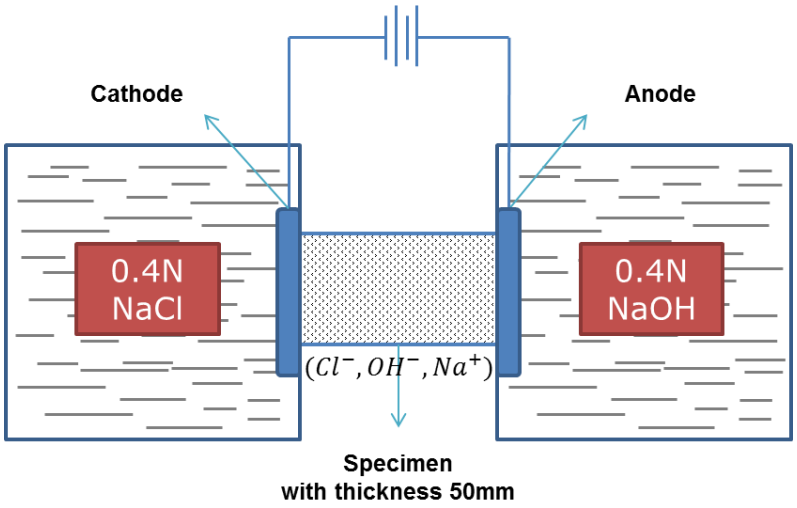

Figure 5-1. Schematic of the RCM test used in the numerical demonstration

Table 5-1. Initial and boundary conditions, valence number and diffusion coefficients of different ionic species considered in the numerical demonstration.

Variables	Chloride (mol/m^3)	Hydroxyl (mol/m^3)	Sodium (mol/m^3)	Voltage (V)
Initial conditions	$C = 0$	$C = 400$	$C = 400$	-
Boundary conditions at $x = 0$ mm	$C = 400$	$C = 0$	$C = 400$	0
Boundary conditions at $x = 50$ mm	$C = 0$	$C = 400$	$C = 400$	24
Valence number	$z = -1$	$z = -1$	$z = 1$	-
Diffusion coefficient $x10^{-10}$ m^2/s	D =2.032	D =5.260	D =1.334	-

In this numerical demonstration, different values of the proportionality constant $F/\varepsilon_0\varepsilon_r$ ranging from $1.39 \times 10^8\ V \cdot m/mol$ to $1.39 \times 10^{14}\ V \cdot m/mol$ are adopted. When the medium of ionic transportation is chosen to be water at the temperature of 298K, which is the real case in RCM test, the proportionality constant is $1.39 \times 10^{14}\ V \cdot m/mol$. When the medium of ionic transportation is changed to another material with a relative permittivity 10^6 times larger than water, which is not realistic at this moment but for comparison, the proportionality constant is $1.39 \times 10^8\ V \cdot m/mol$. Interestingly the simulations results obtained from NPP models with different values of $F/\varepsilon_0\varepsilon_r$ are nearly the same. Therefore, only simulation results of two cases, when $F/\varepsilon_0\varepsilon_r = 1.39 \times 10^8\ V \cdot m/mol$ and $F/\varepsilon_0\varepsilon_r = 1.39 \times 10^{14}\ V \cdot m/mol$, are shown in Figure 5-2. It is apparent from Figure 5-2 that concentration profiles of Cl^- and OH^- obtained from two NPP models with different proportionality constant $F/\varepsilon_0\varepsilon_r$ are almost identical.

This numerical demonstration is sufficient to prove that the involvement of the proportionality constant in the Poisson's equation is unnecessary, even the Poisson's equation is the fundamental law of nature. Then the question is why there is a difference between numerical results from the models using electro-neutrality conditions and those from NPP models? It is important to point out here that, in the electro-neutrality condition the net charge $\sum_1^N z_k C_k$ is assumed to be zero, which is reasonable because the net charge is very small. However, it does not imply that $\nabla^2\Phi = 0$, which completely ignored the nonlinearity of the electric field distribution in multi-component system.

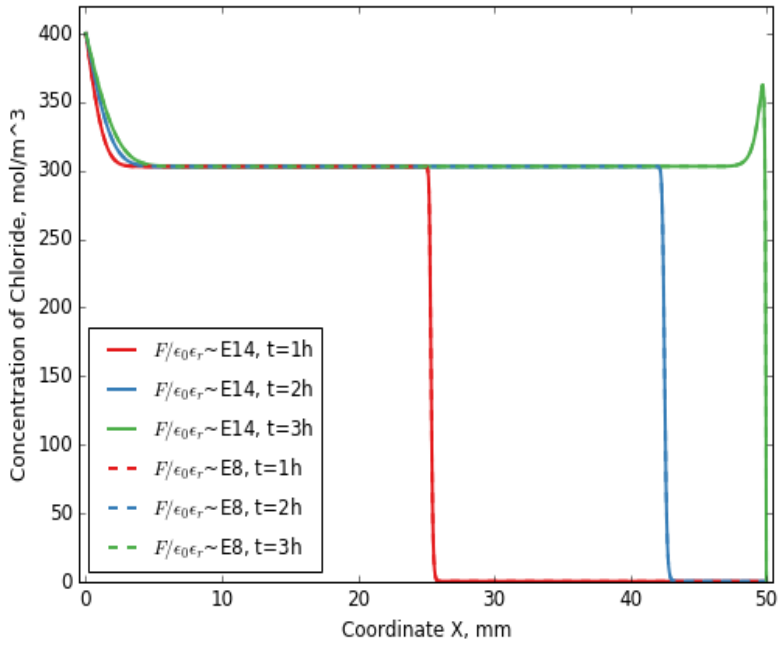

(a)

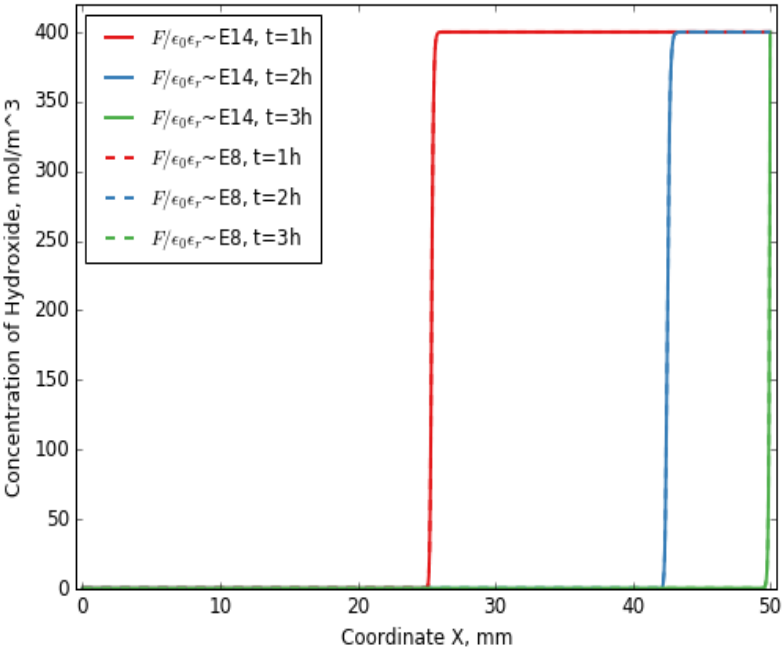

(b)

Figure 5-2. Comparison of results from NPP models with different values of proportionality constant $F/\varepsilon_0\varepsilon_r$. (a) Concentration distribution of Cl^- (b) Concentration distribution of OH^-.

5.2.2 The New Model for Multi-Component Ionic Transport in Concrete

The new model presented in this study will employ a new electro-neutrality condition to calculate the electrostatic potential in the multi-component solution. In the new electro-neutrality condition, Eq. (5-4) is adopted to replace the Poisson's equation in order to avoid the numerical difficulties. In addition, the electric field $\nabla\Phi$ will be calculated through the current density, instead of being set to constant which only depends on the externally applied voltage.

Current density is the flux of charge, that is, the rate of flow of charge per unit area perpendicular to the direction of flow, which can be described as follows,

$$I = F\sum_{k=1}^{N} z_k J_k \qquad \text{k = 1, 2, … N} \qquad (5\text{-}6)$$

where I is the current density, substituting Eq. (5-1) into Eq. (5-6) yields,

$$\nabla\Phi = \frac{RT}{F}\left(\frac{-I - F\sum z_k D_k \nabla C_k}{F\sum z_k^2 D_k C_k}\right) \qquad \text{k = 1, 2, … N} \qquad (5\text{-}7)$$

If the current density can be obtained, the electric field can be calculated through Eq. (5-7). It is a physical law of nature that electric charge is conserved. This fact is already built into the basic transport equations. Multiplication of Eq. (5-2) by z_kF addition over species yield,

$$\frac{\partial}{\partial t} F\sum_{k=1}^{N} z_k C_k = -\nabla \cdot F\sum_{k=1}^{N} z_k J_k \qquad \text{k = 1, 2, … N} \qquad (5\text{-}8)$$

In view of the assumption of electro-neutrality $\sum_1^N z_k C_k = 0$, the left term of Eq. (5-8) is equal to zero and the right term of (5-8) is the gradient of current density, Eq. (5-8) can be reduced to,

$$\nabla \cdot I = 0 \qquad \text{k} = 1, 2, \ldots \text{N} \tag{5-9}$$

It can be seen from Eq. (5-9) that the gradient of current density is zero, which means in the one-dimensional condition, the current density is constant with the assumption of electro-neutrality. With the current density being constant, it can be calculated from the integral of Eq. (5-7) along the penetration depth of ionic species as follows,

$$\Delta\Phi = \int_0^L \nabla\Phi dx = -\frac{RT}{F}\left(I\int_0^L \frac{1}{F\sum z_k^2 D_k C_k}\, dx + \int_0^L \frac{\sum z_k D_k \nabla C_k}{\sum z_k^2 D_k C_k}\, dx \right) \tag{5-10}$$

where $\Delta\Phi$ is the externally applied electric potential difference between the two electrodes. Now a finite difference method called The Forward Time Centred Space (FTCS) method (Hoffman & Frankel, 2001) can be employed here to solve the partial differential equations (5-3), with the new electro-neutrality condition described in this section. The flow chart of algorithm for the new model is presented in Figure 5-3. The code for this new model is written in MATLAB.

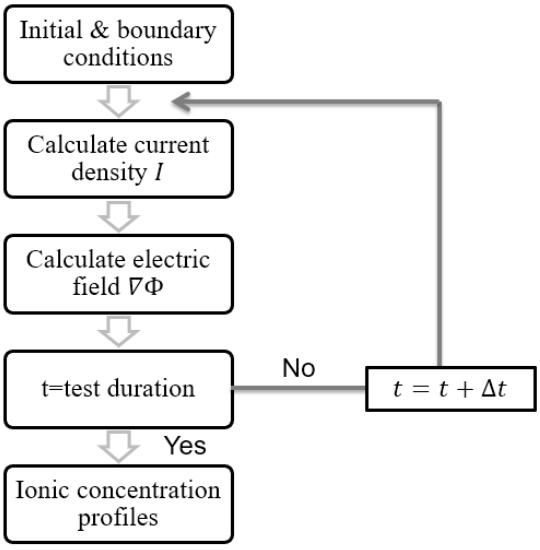

Figure 5-3. Flow chat of algorithm for solving the new model with new electro-neutrality condition.

A numerical example of using the model with the new electro-neutrality condition to simulate the RCM test is given here. The RCM test setup is similar with that described in Section 5.2.1. The numerical results obtained from the proposed new model are compared to those obtained from the NPP models, which are shown in Figure 5-4 and Figure 5-5. The concentration profiles of three ionic species and the distribution of electric field are presented in two cases, with different externally applied voltage $\Delta\Phi$ (12V and 24V). The NPP model is solved using a commercial FEM software COMSOL, which is used to compare with the new model in Figure 5-4 and Figure 5-5.

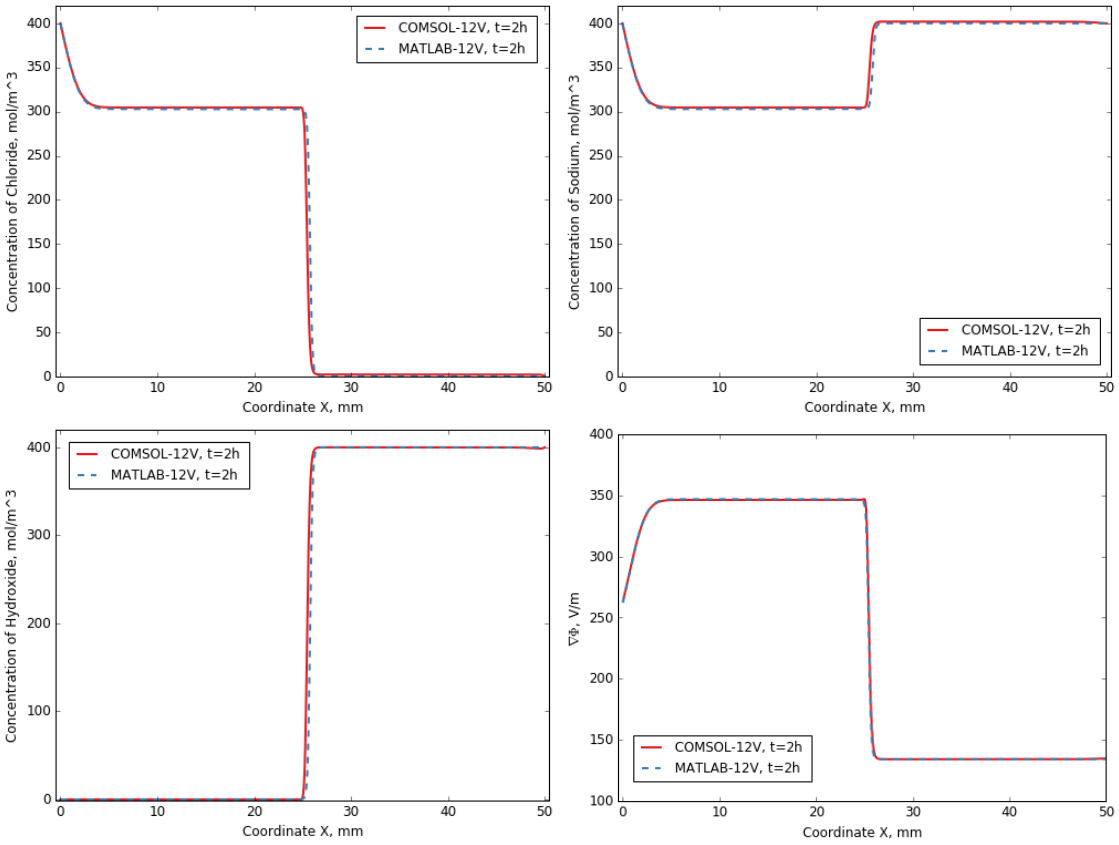

Figure 5-4. Comparison of results from NPP models and the proposed new model ($\Delta\Phi$=12V)

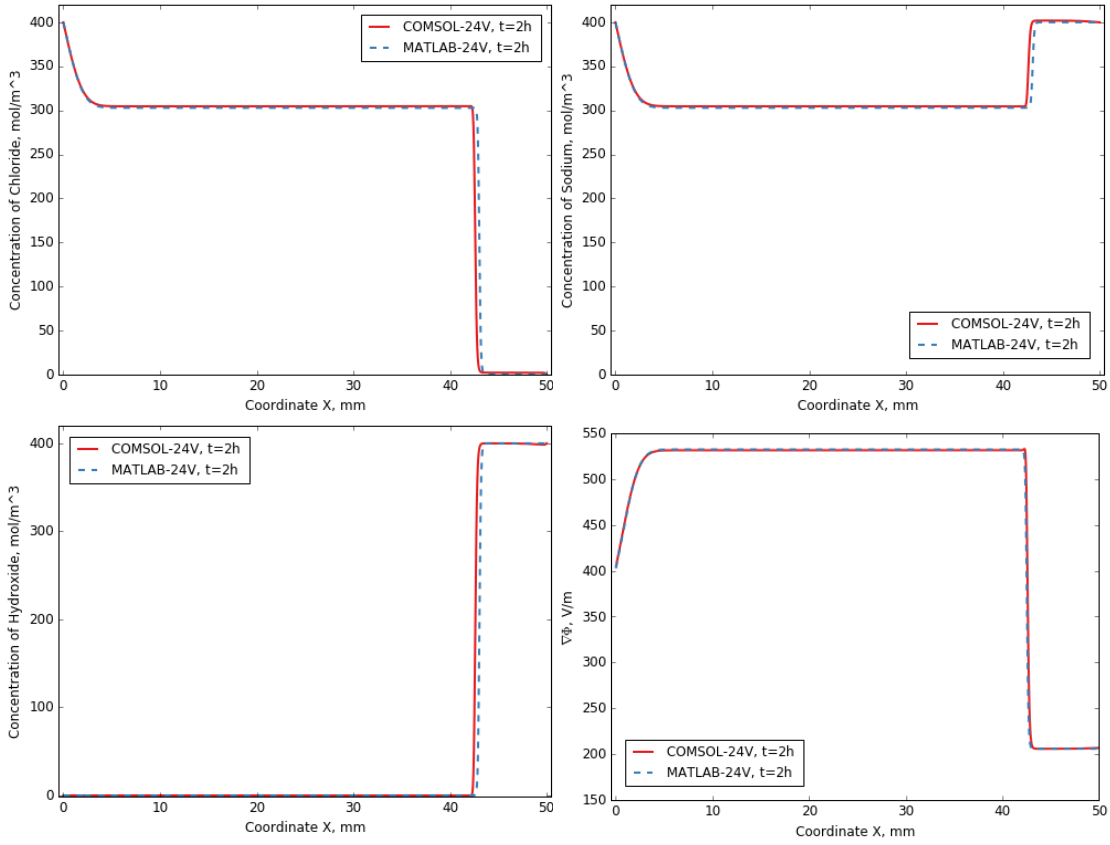

Figure 5-5. Comparison of results from NPP models and the proposed new model ($\Delta\Phi$=24V)

As can be seen from Figure 5-4 and Figure 5-5, the numerical results obtained from the NPP models and the proposed new model are almost the same, which means the new electro-neutrality condition can be used to replace the Poisson's equation without losing the multi-species coupling effect. The ionic transport is migration dominated with the front-like evolution of ionic concentration profiles. And the electrostatic potential gradient, i.e. electric field, is regionally dependent. When the externally applied voltage is increased from 12V to 24V, the difference between concentration profiles from two models gets bigger and can be visibly recognised in Figure 5-5. Although no significant differences are found between electrostatic potential gradient profiles in two cases. This indicates that the high voltage externally applied may have great influences on the validity of the electro-neutrality condition $\sum_1^N z_k C_k = 0$. It is also interesting to notice

that, the concentration profile curves calculated from MATLAB for the proposed new model are slightly smoother than those calculated from COMSOL for the NPP model, especially in the area where the electrostatic potential gradient changes abruptly. The reason is due to the replacement of Poisson's equation, which involves calculation of large numbers. Overall, the proposed model with the new electro-neutrality condition is proved to be a reliable way to replace the NPP model to simulate the multi-component ionic transport in concrete.

5.3 Conclusions

A new one-dimensional numerical model for the multi-component ionic transport in concrete is proposed in this study, with considering a new electro-neutrality condition. From the present study the following conclusion can be drawn:

- Advantages and disadvantages of the traditional methods used to determine the local electrostatic potential, i.e. electro-neutrality condition and Poisson's equation, are discussed. The reason why there is a difference between numerical results from the models using electro-neutrality conditions and those from NPP models is pointed out.
- A numerical demonstration is carried out to prove that the involvement of the proportionality constant of a large number in the Poisson's equation is unnecessary, even the Poisson's equation is the fundamental law of nature.
- A new electro-neutrality condition is presented, which avoids the numerical difficulties caused by the Poisson's equation, and remain the non-linearity of the electric field distribution at the same time. The new model is promising in solving the multi-component ionic transport problems especially in microscopic scale.

Chapter Six - Study of Chloride Penetration into Surface-treated Cement-based Materials

In this Chapter, a one-dimensional numerical investigation on the chloride diffusion in a sealer-treated mortar considering the penetration of sealer induced porosity gradient is presented. The governing equations are solved using a commercial FEM software COMSOL. Effect of chloride binding and electrochemical interaction in the pore solution on chloride diffusion is not considered here. Based on the simulation results, differences between cement sealers and coatings are examined and discussed.

6.1 Surface Treatment of Concrete Structure

Among all the protective methods used to extend the service life of reinforced concrete structures, surface treatment considered as a barrier system has been proved to be an efficient way to limit the chloride penetration (Basheer *et al.*, 1997; de Vries & Polder, 1997; Ibrahim *et al.*, 1997; Maslehuddin *et al.*, 2005).

Materials used for surface treatment can be classified into three groups (Buenfeld & Zhang, 1998; Zhang & Buenfeld, 2000a): (1) coatings that can be seen as a distinct dense physical layer on the concrete surface, and generally vary in thickness from about 0.2mm to about 1.75mm (Perkins, 2002); (2) sealers that not only form a physical film on the concrete surface, but also penetrates the concrete, lining or blocking pores; (3) penetrants that penetrate the concrete surface without leaving a significant surface coating. Coatings and sealers are mostly used to reduce the concrete deterioration by limiting penetration of water and hazardous species such as chloride (Safiuddin & Soudki, 2011).

There are a large number of experimental and field studies that have reported the performance of various types of materials used for surface treatment (Al-Zahrani *et al.*, 2002; Almusallam *et al.*, 2003; Brenna *et al.*, 2013; Dai *et al.*, 2010; Dang *et al.*, 2014; De Muynck *et al.*, 2008; Delucchi, Barbucci & Cerisola, 1997; Diamanti *et al.*, 2013; Khanzadeh Moradllo, Shekarchi & Hoseini, 2012; Medeiros & Helene, 2009; Moon, Shin & Choi, 2007; Pigino *et al.*, 2012; Safiuddin & Soudki, 2011; Seneviratne, Sergi & Page, 2000; Thompson *et al.*, 1997; Uni, 2004; Yang, Wang & Weng, 2004). However, little work has been done to study how chloride diffusion is impeded by different types of surface treatments. Theoretical model is needed to study the chloride distribution profile in surface-treated cementitious materials in order to understand better the protective mechanisms of different surface treatments.

Zhang et al. (Zhang, McLoughlin & Buenfeld, 1998) assumed that all surface treatments can be regarded as coating layers on the untreated substrate concrete as shown in Figure 6-1, then conventional single-species Fick's law was used to modelling chloride penetration into surface-treated concrete which was considered as a composite system with two layers. Their results showed that both parameters of surface treatment layer and substrate layer, like water percolated porosity and diffusion efficient, affected the chloride distribution profile. However, many factors may affect these parameters, such as the diffusion coefficient changes with chemical reaction, chloride binding and electrochemical effect. Yoon et al. (Yoon *et al.*, 2012) applied the extended Nernst-Plank/Poisson's equation to simulation of ionic transport in surface-treated mortar samples tested by RCPT (Rapid Chloride Permeability Test). Distinguished pore

structures between surface coating layer and substrate layer were considered by using separate tortuosity and hence diffusion coefficient.

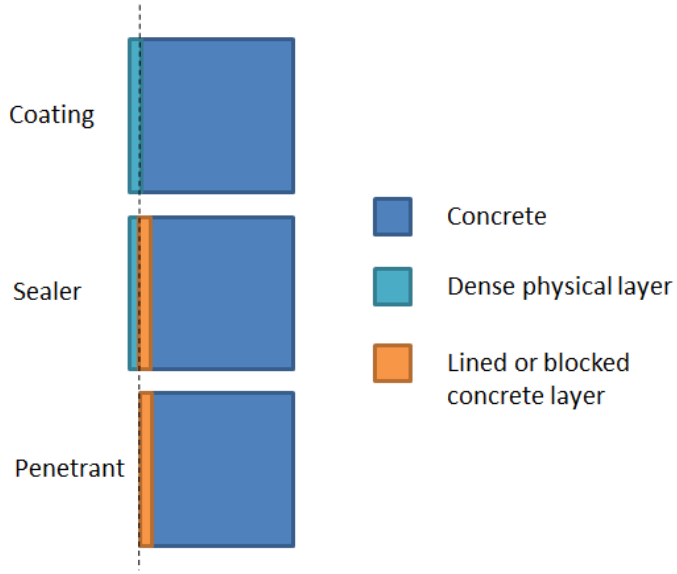

Figure 6-1. Different types of surface treatment (reproduced from (Zhang, McLoughlin & Buenfeld, 1998))

Properties of the surface treatment layer and the substrate layer were assumed constant with time and depth in the previous models. However, when a sealer or a penetrant is used, the pore structure of substrate near the interface between surface treatment layer and substrate layer may change with depth because of the penetration effect. Thus, model considering this pore change in the circumstance of sealers and penetrants is required.

6.2 Mathematical Model of Chloride Diffusion with Varying porosity

As illustrated in Figure 6-1, sealer-treated mortars should be modelled mathematically as three layers, which are one thin surface coating layer, one mortar layer with pores lined by the penetration of sealers and one substrate layer respectively.

The homogenization technique is used here to describe the diffusion mechanisms in porous medium (Samson, Marchand & Beaudoin, 1999). Assume that surface-treated mortar samples are fully saturated during the nature chloride diffusion test and there are no chemical reactions or binding effect between ionic species in the pore solution and the solid pore structure. The mass conservation equation derived at the microscopic scale is then averaged over the representative elementary volume (REV). After this process, the one-dimensional transport equation becomes:

$$\frac{\partial(C \cdot \phi)}{\partial t} = -\frac{\partial(\phi \cdot J)}{\partial x} = -\frac{\partial}{\partial x}\left(-D \cdot \phi \cdot \frac{\partial C}{\partial x}\right) \qquad (6\text{-}1)$$

where C is chloride concentration in the pore solution (mol/L), J is flux of chloride in the pore solution, ϕ is the porosity for a fully saturated material, D is the chloride diffusion coefficient (m^2/s). Because ionic transport is waterborne, Zhang et al. (Zhang, McLoughlin & Buenfeld, 1998) suggested using water-percolated porosity to define pores contributing to chloride diffusion which can be occupied by water and also form continuous water paths. The porosity ϕ used for surface treatment layer and mortar layer here will be taken as percolated porosity. Eq. (6-1) now can be applied to simulate the chloride transport in both surface treatment layer and mortar substrate layer with different material parameters.

6.3 Porosity Gradient in Sealer Penetration Layer

When a penetration sealer is used, it is reasonable to assume that the porosity of substrate increases gradually from the interface to the penetration depth of sealer. In this study, an exponential function defined by three parameters (A, B and C) is used to model the porosity increasing gradient in the penetration part of a sealer-treated mortar. The porosities in the surface coating part and in the pure mortar substrate are chosen to be constant equal to $\emptyset_s$ and $\emptyset_c$ respectively:

$$\left.\begin{array}{cc} \phi(x) = \phi_s & 0 \le x \le t_s \\ \phi(x) = A - B \cdot e^{-C \cdot x} & t_s < x < t_s + t_p \\ \phi(x) = \phi_c & x \ge t_s + t_p \end{array}\right\} \qquad (6\text{-}2)$$

where t_s is the thickness of surface coating part, t_p is the penetration depth of sealer. Parameters in the exponential function are determined after choosing $\emptyset_s$, $\emptyset_c$, t_s and t_p to ensure the continuity of the equation.

6.4 Numerical Simulation of Nature Chloride Diffusion Test

In the case of nature diffusion test, mortar samples treated by surface treatments are immersed in 1M NaCl solution for almost one year and then chloride profiles are determined (Zhang & Buenfeld, 2000a). Surfaces that are not surface treated are sealed to ensure a one-dimensional diffusion. Thickness of the sample along the diffusion direction is 0.05m. The initial condition is then set as:

$$C = 0, at\ x > 0, t = 0 \qquad (6\text{-}3)$$

The boundary conditions are:

$$C = C_0 = 1\, mol/L, at\ x = 0, t \ge 0 \qquad (6\text{-}4)$$

$$-\mathbf{n}\cdot(-\phi\cdot D\cdot\nabla C)=0,\ at\ x=0.05\ m, t\geq 0 \qquad (6\text{-}5)$$

Values of other reference parameters used in the following simulation are given in Table 6-1.

Table 6-1. Default values of the parameters used in the model

Parameters	Value	Description
D_s	$7.3\times10^{-12}\ m^2/s$	Diffusion coefficient of surface coating layer
D_c	$1.4\times10^{-11}\ m^2/s$	Diffusion coefficient of substrate layer
ϕ_s	0.12	Porosity of surface coating layer
ϕ_c	0.2	Porosity of substrate layer
t_s	$0.001m$	Thickness of surface coating part
t_p	$0.008m$	Penetration depth of sealer

6.5 Results

6.5.1 Chloride Concentration Profiles in Sealer-treated Mortars

Figure 6-2 gives chloride concentration profiles in sealer treated mortar substrate at different times. It can be seen that the interface chloride concentration measured at the depth of t_s also increases with time compared to the results obtained from the model of coating treatments by (Buenfeld & Zhang, 1998). Since films on the surface of mortar formed by sealers are thinner and less dense than physical layer formed by coating, smaller resistance to chloride diffusion is offered by the surface layer of sealers. Hence, higher interface chloride concentration is expected in sealer treated mortar which has

been proved by the experiments carried out by (Zhang & Buenfeld, 2000a). As shown in Figure 6-2 interface chloride concentration reaches approximately 0.9 mol/L with a 1 mol/L boundary concentration after 320 days nature diffusion test which demonstrates this phenomenon. It is also noteworthy that the time to reach a relatively high interface chloride concentration is short even though the concentration gradient in the substrate decreases slowly with time. This is probably due to the penetration of sealer which decreases the porosity of substrate near the interface area and increases the resistance to chloride diffusion, as discussed in the following section.

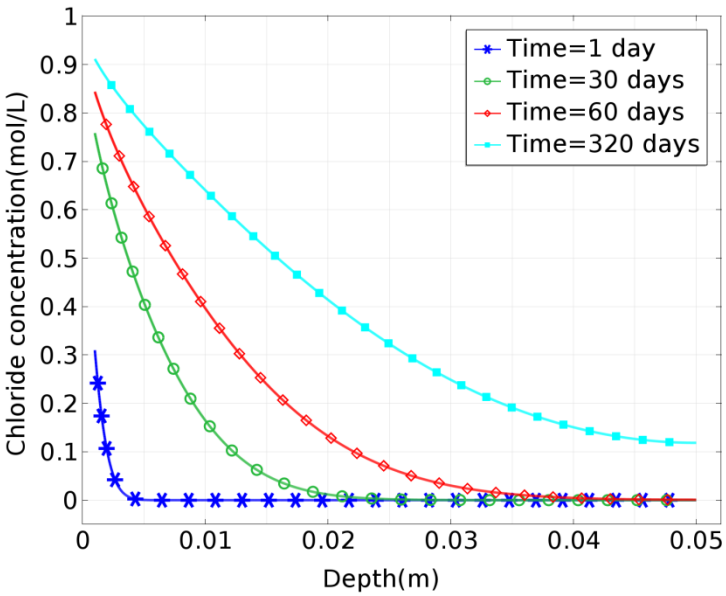

Figure 6-2. Chloride concentration profiles in sealer treated mortar substrate

6.5.2 Effect of Penetration of Sealer

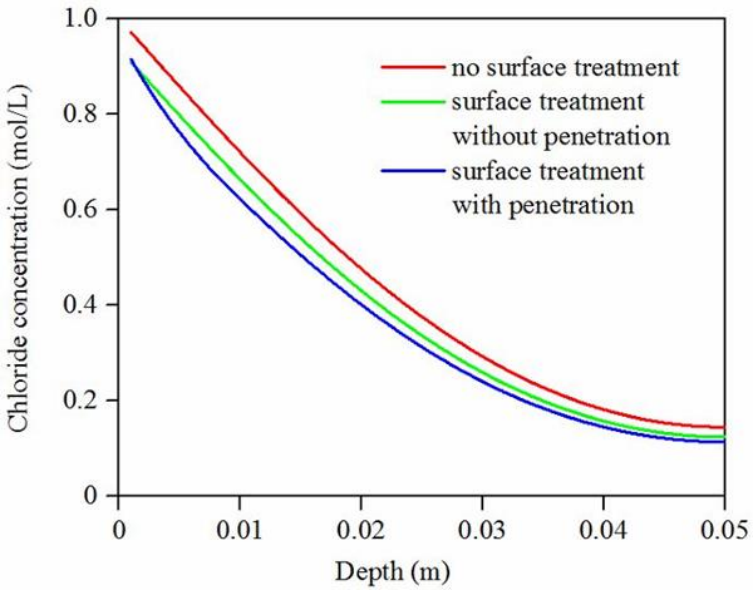

Figure 6-3. Effect of penetration of sealer on chloride concentration in mortar substrate after 320-day test

Normally films formed on mortar surface by sealers are different from the physical dense layer formed by coatings. In order to assess the effect of penetration of sealers, simulations are performed using the same material parameters in the surface coating layer for simplicity. The only difference is that the weather penetration induced porosity gradient equation (6-2) is considered. The results are shown in Figure 6-3. It is noticed that both types of surface treatments help to impede chloride diffusion in mortars. Interface chloride concentration in mortar substrate considering penetration of sealer is slightly higher than that in mortar substrate without considering penetration. In the sealer penetration zone (t_s to $t_s + t_p$), chloride diffusion in substrate treated by penetration sealer is slower at the interface where the porosity in the point is considered to be equal to $\emptyset_s$ .Then the chloride diffusion rate increases along the depth with increasing of the porosity.

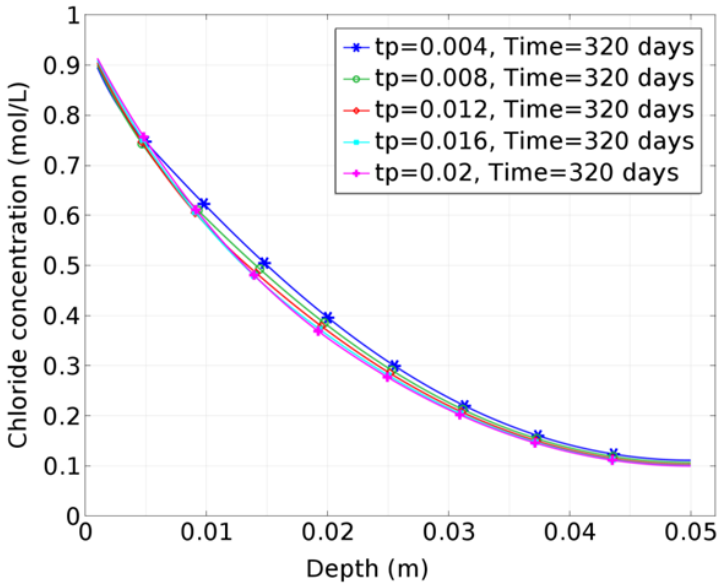

Figure 6-4. Chloride concentration profiles in mortar substrate with various t_p

Figure 6-4 shows the dependence of chloride concentration profiles on the penetration depth of sealer t_p. It is observed that higher t_p leads to higher interface chloride concentration but lower chloride diffusion rate in general. This is because as t_p increases, the average value of porosity of mortar substrate decreases. This enhances the resistance of substrate to chloride diffusion. In the surface layer, chloride accumulates at the interface which leads to higher interface concentration. In the substrate layer, higher resistance leads to lower chloride transport rate. It can also be seen that the effect of t_p on chloride concentration profiles of sealer treated mortars is not significant. It is probably because the difference between the values of parameters such as porosity and diffusion coefficient chosen for surface layer and substrate layer is not big enough. Hence the difference of the porosity gradient is not significant for various t_p .

6.5.3 Unit System Converting

The chloride content obtained from experiments is normally expressed as the total chloride content by weight of mortar in g/g by using the grinding technique. In order to compare the results from simulation with the results from experiments, one needs to convert the concentration unit system (mol/L) into weight percentage unit system. Assume that the specimen is fully saturated before the content test and only chloride in the pore solution is taken into account. Entire volume of a mortar sample is divided into two parts, liquid phase (pore solution) and solid phase which is assumed impermeable. The converting equation is:

$$wp = \frac{C \cdot M_{cl} \cdot \phi}{\rho_{mor}} \tag{6-6}$$

where wp is chloride content in weight percentage (g/g); ρ_{mor} is the density of mortar sample, assumed to be $2000 g/L$ here; M_{cl} is the molar mass of chlorine. In this work, porosity here is considered to be the ratio of water-percolated pore solution volume to bulk volume of mortar. As shown in Eq.(6-6) chloride content profiles expressed by weight percentage have a linear proportional relation with the porosity of mortar substrate. Thus in the case of sealer-treated mortars, sealer penetration induced porosity change needs to be considered in unit converting process.

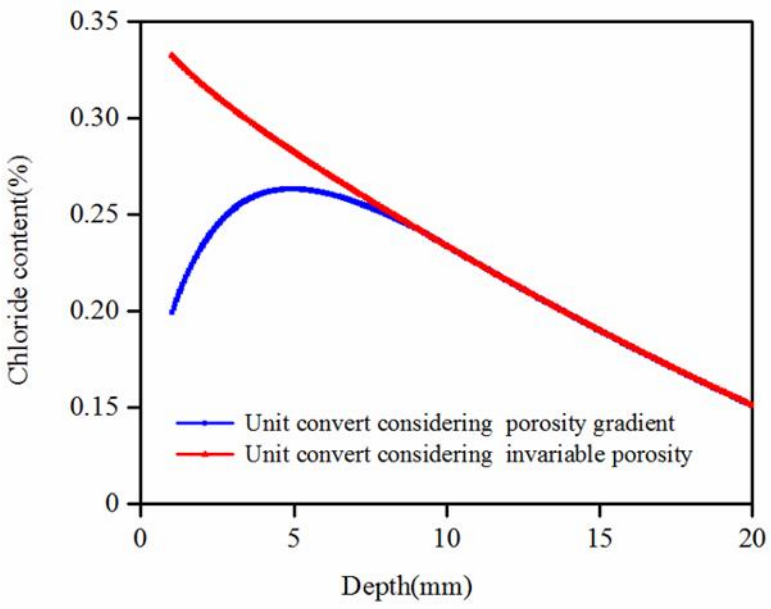

Figure 6-5. Comparison between chloride content profiles in mortar substrate considering porosity gradient and invariable porosity after 320-day test (After converting unit)

Figure 6-5 shows the comparison between chloride content profiles after converting unit system in mortar substrate considering porosity gradient and invariable porosity. It is found that the chloride content in the sealer-treated mortar substrate may be overestimated if the varying porosity is ignored, especially near the interface area. When the porosity increasing gradient is taken into account, there is an upward trend in chloride content from the interface. However, the chloride content reaches a peak at the depth about 5mm while the penetration depth of sealer is 8mm. This is due to the simultaneous decreasing of chloride concentration, which is also linear proportional related to chloride content.

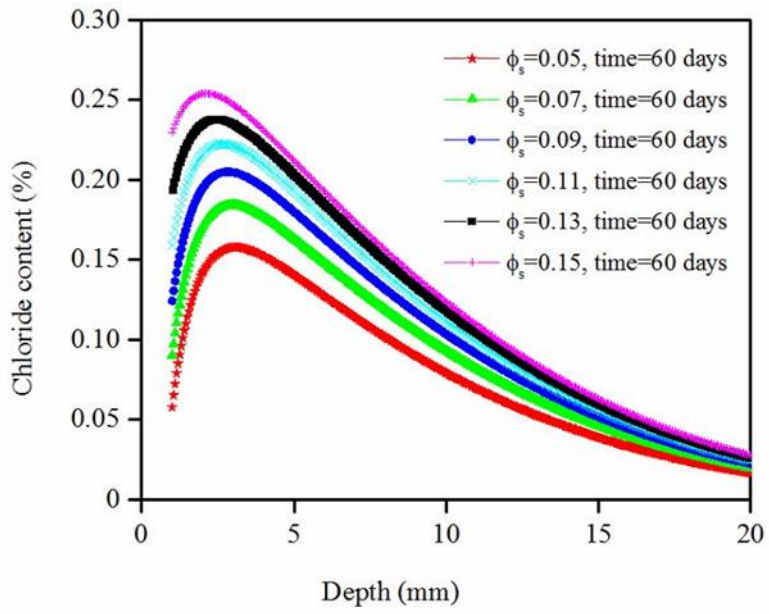

Figure 6-6. Chloride content profiles in mortar substrate with various $\emptyset_s$ (After converting unit)

The porosity of surface coating layer $\emptyset_s$ is an important factor in controlling chloride diffusion into a surface-treated cementitious material. The effect of $\emptyset_s$ on chloride distribution profiles is mainly on the interface chloride concentration with the diffusion coefficient D_s unchanged. Figure 6-6 plots chloride content in mortar substrate with various $\emptyset_s$. The interface chloride content increases as $\emptyset_s$ increases, which is expected. It is also noted that the rising part of the chloride content curve near the interface area is smoother with high $\emptyset_s$. The reason is because the difference between $\emptyset_s$ and $\emptyset_c$ decreases with an increases of $\emptyset_s$.

It should be mentioned here that the chloride content profiles obtained from field structure also have the same rising part from the surface, in which the maximum chloride concentration is observed at the deeper part of the material (Marchand & Samson, 2009). Varying porosity caused by environment effects such as carbonation and leaching may be one of the possible reasons.

6.5.4 Parametric Study

The influence of other parameters on the chloride penetration in sealer-treated concrete are shown in Figure 6-7 to Figure 6-10, the figures show the similar trend compared to that of concrete treated with coatings.

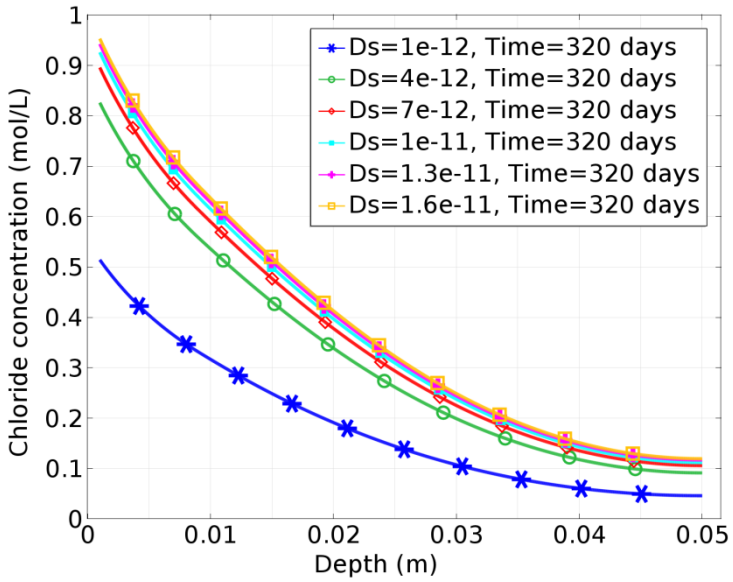

Figure 6-7. Chloride concentration profiles in mortar substrate with various D_s

Figure 6-7 and Figure 6-8 illustrate that the interface chloride concentration increases with an increase in D_s and with a decrease in t_s. Note that $\emptyset_s$ has a comparable effect on the interface chloride concentration to D_s, implying that any methods which reduce t_s and D_s (including aspects of surface treatment formulation and good workmanship, but also include substrate drying) will be effective at increasing resistance to chloride penetration (Buenfeld & Zhang, 1998).

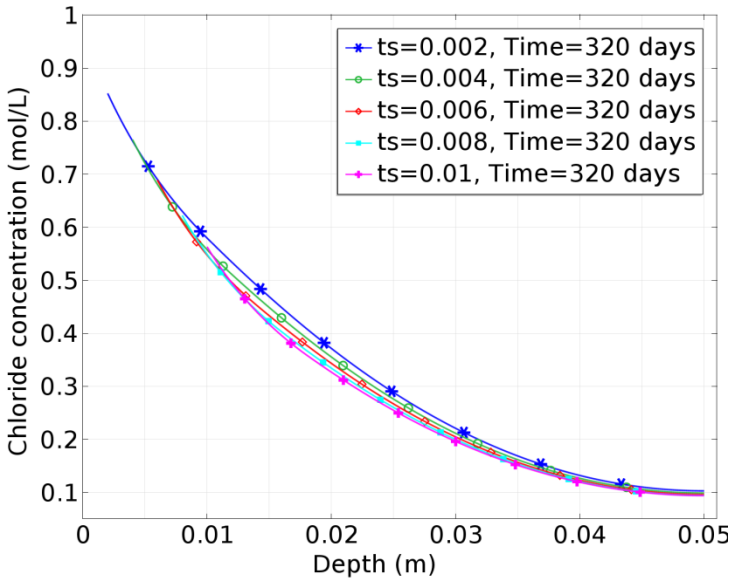

Figure 6-8. Chloride concentration profiles in mortar substrate with various t_s

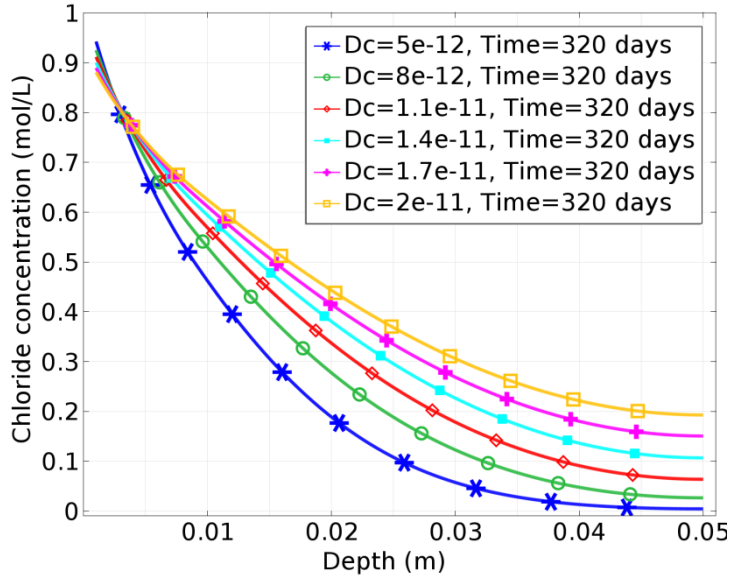

Figure 6-9. Chloride concentration profiles in mortar substrate with various D_c

It is interesting to note that concrete substrate with a lower diffusion coefficient leads to a higher chloride concentration in the area near the surface treatment, but a lower concentration at a greater depth as depicted by Figure 6-9. From the point of view of corrosion initiation, a rebar located near the surface treatment in a concrete with low diffusion coefficient may have a higher corrosion risk than in poor quality substrate.

However, a poor-quality concrete with a high diffusion coefficient would suffer deeper chloride penetration. The dependence of chloride distribution on $\emptyset_c$ is given by Figure 6-10. The porosity in the substrate can reduce the interface concentration. This is because as chloride diffuses through the interface it is diluted by the large volume of pore solution in the substrate.

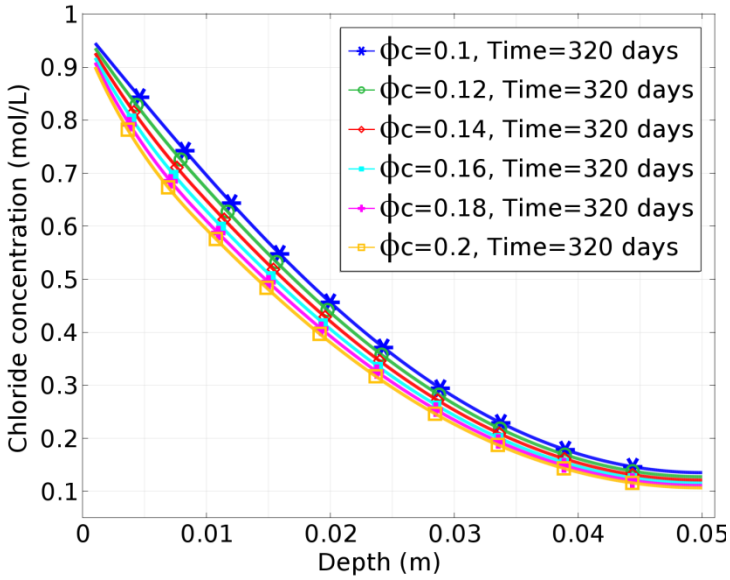

Figure 6-10. Chloride concentration profiles in mortar substrate with various ϕ_c

6.6 Conclusions

In this numerical study, a mathematical model considering varying porosity along depth of the mortar substrate has been developed to simulate one-dimensional chloride diffusion into a sealer-treated mortar. From the present numerical simulation, the following conclusions can be drawn:

- Comparing to surface coating materials, a sealer not only provides a physical layer on the mortar surface, but also penetrates the mortar which decreases the porosity of mortar substrate near the interface area and increases the resistance to chloride diffusion. An exponent distribution of the varying porosity is used

to model the effect of the penetration of sealer on the chloride profiles. The simulation results demonstrate that chloride concentration at the interface between physical coating layer and the mortar substrate in a sealer-treated mortar is higher than that of a coating-treated mortar. However, the chloride concentration gradient is higher near the interface area in a sealer-treated mortar substrate, which implies that chloride diffusion is slower due the penetration induced porosity change. According to the simulation results, it is necessary to take both chloride concentrations at the interface and at the penetration depth of sealer into consideration when performance of a sealer is assessed.

- Generally, a higher penetration depth of sealer leads to higher interface chloride concentration but lower chloride diffusion rate in the entire mortar substrate. But the effect of penetration depth of sealer on chloride profiles is not significant with the exponent porosity distribution assumption.
- In the process of converting the chloride concentration profiles in a sealer-treated mortar substrate into chloride content expressed as the total chloride content by the weight of mortar, if the varying porosity is ignored, the chloride content in the sealer-treated mortar substrate may be overestimated. When the porosity increasing gradient is taken into account, there is an upward trend in the chloride content from the interface to the penetration depth of sealer, instead of a typical error function shape. The existence of porosity gradient near the concrete surface may also explain the chloride content obtained from the field samples which has the same rising part near the surface.

Chapter Seven - Conclusions and Future Work

This thesis presents a numerical study on the multi-component ionic transport in concrete based on the microscopic scale. The main results and contributions, limitations of this research, along with the discussion of the possible improvements for future work are presented in this Chapter.

7.1 Summary and Key Findings

Chapter Three presented a numerical investigation on the effects of the EDL on the ionic transport in cement paste when subjected to an externally applied electric field. Instead of using the zeta potential and the Boltzmann equation to determine the ionic distribution close to the charged surface, the present model uses Nernst-Planck and Poisson's equations coupled with a constant amount of surface charge on the pore walls as the EDL boundary conditions. In addition, the simulation is extended to a two-dimensional geometry. The present numerical model gives almost the same ionic distributions of both counter-ions and co-ions along the axis perpendicular to the charge surface as described by the Boltzmann equation, which proves that this model is valid to evaluate the effects of the EDL on the migration of ionic species in concrete. When positive surface charges were applied, the negatively charged ionic species have higher concentrations in the EDL effect zones than in the bulk zone; while the positively charged ionic species have lower concentrations in the EDL effect zones than in the bulk zone. However, in terms of the average concentration along the y-axis, the effect of the EDL seems not to be very significant as the difference is within 2%. Also, the change of the amount of externally applied electric potential has little influence on the

EDL effects but has great influence on the shape of the wave front of ionic profiles. Overall, it was shown that the EDL has little effect on the migration speed of ions but a significant effect on the ionic flux.

A two-phase multi-component ionic transport model has been developed in Chapter Four to extend the study on EDL effect in Chapter Three. The model was applied to investigate the effect of surface charges at the solid-liquid interface on the ionic transport in a cement paste when it is subjected to an externally applied electric field. The surface charge in the present model is considered by modifying the Nernst-Planck equation in which the electrostatic potential is dependent not only on the externally applied electric field but also on the dissimilar diffusivity of different ionic species including the surface charges. The simulation results showed that the surface charge has a significant influence on the concentration distribution of ionic species but only in the region close to the charge surface. A positive surface charge increases the concentration of negatively charged ions but decreases the concentration of positively charged ions. The overall migration speed of ionic species in the two-phase model is found to be slower than that in the single-phase model because of the effect of tortuosity when the solid phase is involved. The surface charge at the solid-liquid interfaces seems to have very little influence on the overall migration speed of ionic species. This is mainly due to the layer of effect zone of EDL that is very thin when compared to its bulk solution zone. Also, the surface charge has great influence on the chloride flux; but it is also only in the region close to the charge surface. A positive charge surface increases the x-component of chloride flux at the rear point of a solid particle but decreases the x-component of chloride flux at the front point of a solid particle.

Chapter Five proposed a new one-dimensional numerical model for the multi-component ionic transport in concrete, with considering a new electro-neutrality condition. Advantages and disadvantages of the traditional methods used to determine the local electrostatic potential, i.e. electro-neutrality condition and Poisson's equation, are discussed. The reason why there is a difference between numerical results from the models using electro-neutrality conditions and those from NPP models is pointed out. A numerical demonstration is carried out to prove that the involvement of the proportionality constant of a large number in the Poisson's equation is unnecessary, even the Poisson's equation is the fundamental law of nature. A new electro-neutrality condition is then presented, which avoids the numerical difficulties caused by the Poisson's equation, and remain the non-linearity of the electric field distribution at the same time. The new model is promising in solving the multi-component ionic transport problems especially in microscopic scale.

In Chapter Six, a mathematical model considering varying porosity along depth of the mortar substrate has been developed to simulate one-dimensional chloride diffusion into a surface-treated mortar. Comparing to surface coating materials, a sealer not only provides a physical layer on the mortar surface, but also penetrates the mortar which decreases the porosity of mortar substrate near the interface area and increases the resistance to chloride diffusion. An exponent distribution of the varying porosity is used to model the effect of the penetration of sealer on the chloride profiles. The simulation results demonstrate that chloride concentration at the interface between physical coating layer and the mortar substrate in a sealer-treated mortar is higher than that of a coating-treated mortar. However, the chloride concentration gradient is higher near the interface area in a sealer-treated mortar substrate, which implies that chloride diffusion

is slower due the penetration induced porosity change. According to the simulation results, it is necessary to take both chloride concentrations at the interface and at the penetration depth of sealer into consideration when performance of a sealer is assessed. In the process of converting the chloride concentration profiles in a sealer-treated mortar substrate into chloride content expressed as the total chloride content by the weight of mortar, if the varying porosity is ignored, the chloride content in the sealer-treated mortar substrate may be overestimated. When the porosity increasing gradient is taken into account, there is an upward trend in the chloride content from the interface to the penetration depth of sealer, instead of a typical error function shape. The existence of porosity gradient near the concrete surface may also explain the chloride content obtained from the field samples which has the same rising part near the surface.

In summary, the key findings of this thesis are as follows,

- The impact of Electric Double Layer (EDL) on the ionic transport in cement-based materials when subjected to an externally applied electric field has been investigated in this study. A two-dimensional two-phase multi-component ionic transport model has been developed to replace the traditional one-dimensional model based on the Boltzmann equation. The present new model uses Nernst-Planck and Poisson's equations coupled with a constant amount of surface charge on the pore walls as the EDL boundary conditions. Some important features about the effect of surface charge on the concentration distribution, migration speed and flux of individual ionic species are discussed.
- A new electro-neutrality condition is presented to determine the local electrostatic potential in the multi-component ionic migration model. The

fundamental reason why there are differences between numerical results from the models using electro-neutrality conditions and those from NPP models is pointed out, which has rarely been discussed before. Adopting the new electro-neutrality condition can eliminate the numerical difficulties caused by the Poisson's equation, and remain the non-linearity of the electric field distribution. The new electro-neutrality condition is promising in solving the multi-component ionic transport problems especially in microscopic scale.

- A one-dimensional numerical investigation on the chloride ingress in a surface-treated mortar with considering the penetration of sealer induced porosity gradient was performed. The numerical model was carefully treated to apply governing equations of ionic transport to this situation of two pore structures, with every parameter clearly defined on the microscopic scale. When the varying porosity is taken into account, there is an upward trend in the chloride content from the interface to the penetration depth of sealer, instead of a typical error function shape. The existence of porosity gradient near the concrete surface can also explain the chloride content obtained from the field samples which has the same rising part near the surface.

7.2 Limitations and Future Work

Some limitations worth noting of this study will be discussed in this section. These limitations are a direction for future work and also problems to be addressed in the follow-up research.

- It is generally recognised that chloride ions bind physically and chemically on to the pore surfaces when travelling through the cement matrix. Chloride binding not only can significantly reduce the transport speed of free chloride ions in the pore solution but also can alter the pattern of chloride concentration profiles. This binding effect is not considered in this study for simplicity to focus on the influence of EDL effect. In future numerical work, chloride binding should be taken into account along with the EDL effect before comparing the simulation results to the experimental results.
- The study of EDL effect on ionic transport in concrete in this thesis is mainly on the microscopic level. Whether the EDL phenomenon has considerable impact on the ionic transport on the macroscopic level and how to measure the impact in an experimental way if it does, are two problems needed to be further investigated in the future work.
- In Chapter Five a new electro-neutrality condition for multi-component ionic transport model is presented, which can help eliminate the numerical difficulties caused by the Poisson's equation. The numerical study in Chapter Five only proves the applicability of this new model. In the follow-up work, the new model can be used to study phenomena like Polarization and electrode reaction.

References

AASHTO-T259 (2006) 'Standard Method of test for Resistance of Concrete to Chloride Ion Penetration'. *American Association of State Highway and Transportation Officials*,

Adenot, F. & Buil, M. (1992) 'Modelling of the corrosion of the cement paste by deionized water'. *Cement and Concrete Research*, 22 (2), pp. 489-496.

Al-Zahrani, M., Al-Dulaijan, S., Ibrahim, M., Saricimen, H. & Sharif, F. (2002) 'Effect of waterproofing coatings on steel reinforcement corrosion and physical properties of concrete'. *Cement and Concrete Composites*, 24 (1), pp. 127-137.

Almusallam, A., Khan, F., Dulaijan, S. & Al-Amoudi, O. (2003) 'Effectiveness of surface coatings in improving concrete durability'. *Cement and Concrete Composites*, 25 (4), pp. 473-481.

Alonso, C., Andrade, C., Castellote, M. & Castro, P. (2000) 'Chloride threshold values to depassivate reinforcing bars embedded in a standardized OPC mortar'. *Cement and Concrete Research*, 30 (7), pp. 1047-1055.

Andrade, C. (1993) 'Calculation of chloride diffusion coefficients in concrete from ionic migration measurements'. *Cement and Concrete Research*, 23 (3), pp. 724-742.

Andrade, C., Castellote, M. & d'Andrea, R. (2011) 'Measurement of ageing effect on chloride diffusion coefficients in cementitious matrices'. *Journal of Nuclear Materials*, 412 (1), pp. 209-216.

Andrade, C., Sanjuán, M., Recuero, A. & Rio, O. (1994) 'Calculation of chloride diffusivity in concrete from migration experiments, in non steady-state conditions'. *Cement and Concrete Research*, 24 (7), pp. 1214-1228.

Ann, K. Y. & Song, H. W. (2007) 'Chloride threshold level for corrosion of steel in concrete'. *Corrosion Science*, 49 (11), pp. 4113-4133.

Appelo, C. A. J. & Wersin, P. (2007) 'Multicomponent diffusion modeling in clay systems with application to the diffusion of tritium, iodide, and sodium in opalinus clay'. *Environmental science & technology*, 41 (14), pp. 5002-5007.

Arnold, J., Kosson, D. S., Garrabrants, A., Meeussen, J. C. L. & van der Sloot, H. A. (2013) 'Solution of the nonlinear Poisson–Boltzmann equation: Application to ionic diffusion in cementitious materials'. *Cement and Concrete Research*, 44 pp. 8-17.

Arya, C., Bioubakhsh, S. & Vassie, P. (2013) 'Chloride penetration in concrete subject to wet/dry cycling: influence of moisture content'. *Proceedings of the ICE - Structures and Building*, 167 (2), pp. 94-107.

Arya, C., Vassie, P. & Bioubakhsh, S. (2013) 'Chloride penetration in concrete subject to wet–dry cycling: influence of pore structure'. *Proceedings of the ICE - Structures and Building*,

ASTM-C1202 (2010) 'Standard Test Method for Electrical Indication of Concrete's Ability to Resist Chloride Ion Penetration'.

Atkinson, A. & Nickerson, A. (1984) 'The diffusion of ions through water-saturated cement'. *Journal of Materials Science*, 19 (9), pp. 3068-3078.

Audenaert, K., Yuan, Q. & De Schutter, G. (2010) 'On the time dependency of the chloride migration coefficient in concrete'. *Construction and Building Materials*, 24 (3), pp. 396-402.

Baroghel-Bouny, V., Belin, P., Maultzsch, M. & Henry, D. (2007) 'AgNO3 spray tests: advantages, weaknesses, and various applications to quantify chloride ingress into concrete. Part 1: Non-steady-state diffusion tests and exposure to natural conditions'. *Materials and structures*, 40 (8), pp. 759-781.

Baroghel-Bouny, V., Wang, X., Thiery, M., Saillio, M. & Barberon, F. (2012) 'Prediction of chloride binding isotherms of cementitious materials by analytical model or numerical inverse analysis'. *Cement and Concrete Research*, 42 (9), pp. 1207-1224.

Basheer, P., Basheer, L., Cleland, D. & Long, A. (1997) 'Surface treatments for concrete: assessmentmethods and reported performance'. *Construction and Building Materials*, 11 (7), pp. 413-429.

Bentz, D. P. & Garboczi, E. J. (1992) 'Modelling the leaching of calcium hydroxide from cement paste: effects on pore space percolation and diffusivity'. *Materials and structures*, 25 (9), pp. 523-533.

Bentz, D. P., Garboczi, E. J. & Lagergren, E. S. (1998) 'Multi-scale microstructural modeling of concrete diffusivity: Identification of significant variables'. *Cement Concrete and Aggregates*, 20 pp. 129-139.

Berman, H. A. (1972) *Determination of chloride in hardened Portland cement paste, mortar, and concrete*. No. FHWA-RD-72-12 Intrm Rpt.. Available.

Boddy, A., Bentz, E., Thomas, M. & Hooton, R. (1999) 'An overview and sensitivity study of a multimechanistic chloride transport model'. *Cement and Concrete Research*, 29 (6), pp. 827-837.

Brenna, A., Bolzoni, F., Beretta, S. & Ormellese, M. (2013) 'Long-term chloride-induced corrosion monitoring of reinforced concrete coated with commercial polymer-modified mortar and polymeric coatings'. *Construction and Building Materials*, 48 (0), pp. 734-744.

Broomfield, J. P. (2006) *Corrosion of steel in concrete: understanding, investigation and repair*. CRC Press.

Brunauer, S., Odler, I., Yudenfreund, M., Feldman, R., Sereda, P. & Seligmann, P. D. (1970) 'The new model of hardened Portland cement paste'. *Highway Research Record*,

Buenfeld, N. & Zhang, J. (1998) 'Chloride diffusion through surface-treated mortar specimens'. *Cement and Concrete Research*, 28 (5), pp. 665-674.

Buenfeld, N. R., Glass, G. K., Hassanein, A. M. & Zhang, J.-Z. (1998) 'Chloride transport in concrete subjected to electric field'. *Journal of Materials in Civil Engineering*, 10 (4), pp. 220-228.

Caré, S. & Hervé, E. (2004) 'Application of a n-phase model to the diffusion coefficient of chloride in mortar'. *Transport in porous media*, 56 (2), pp. 119-135.

Carmeliet, J., Hens, H., Roels, S., Adan, O., Brocken, H., Cerny, R., Pavlik, Z., Hall, C., Kumaran, K. & Pel, L. (2004) 'Determination of the liquid water diffusivity from transient moisture transfer experiments'. *Journal of Thermal Envelope and Building Science*, 27 (4), pp. 277-305.

Carslaw, H. S., Jaeger, J. C. & Feshbach, H. (1962) 'Conduction of heat in solids'. *Physics Today*, 15 pp. 74.

Castellote, M., Llorente, I. & Andrade, C. (2006) 'Influence of the composition of the binder and the carbonation on the zeta potential values of hardened cementitious materials'. *Cement and Concrete Research*, 36 (10), pp. 1915-1921.

Chapman, D. L. (1913) 'LI. A contribution to the theory of electrocapillarity'. *The London, Edinburgh, and Dublin Philosophical Magazine and Journal of Science*, 25 (148), pp. 475-481.

Chatterji, S. (1996) 'Double layer and expressed solutions and ion transport through cement based materials. Part 1. Fundamentals'. *World cement*, 27 (8), pp. 74-75.

Chatterji, S. & Kawamura, M. (1992) 'Electrical double layer, ion transport and reactions in hardened cement paste'. *Cement and Concrete Research*, 22 (5), pp. 774-782.

Chen, H.-J., Huang, S.-S., Tang, C.-W., Malek, M. A. & Ean, L.-W. (2012) 'Effect of curing environments on strength, porosity and chloride ingress resistance of blast furnace slag cement concretes: A construction site study'. *Construction and Building Materials*, 35 pp. 1063-1070.

Chung-Chia, Y. (2004) 'Relationship between Migration Coefficient of Chloride Ions and Charge Passed in Steady State'. *ACI Materials Journal*, 101 (2), pp. 124-130.

Collepardi, M., Marcialis, A. & Turriziani, R. (1972) 'Penetration of chloride ions into cement pastes and concretes'. *Journal of the American Ceramic Society*, 55 (10), pp. 534-535.

Crank, J. (1975) *The Mathematics of Diffusion.* Oxford University Press.

Dai, J.-G., Akira, Y., Wittmann, F. H., Yokota, H. & Zhang, P. (2010) 'Water repellent surface impregnation for extension of service life of reinforced concrete structures in marine environments: The role of cracks'. *Cement and Concrete Composites*, 32 (2), pp. 101-109.

Dang, Y., Xie, N., Kessel, A., McVey, E., Pace, A. & Shi, X. (2014) 'Accelerated laboratory evaluation of surface treatments for protecting concrete bridge decks from salt scaling'. *Construction and Building Materials*, 55 (0), pp. 128-135.

De Muynck, W., Cox, K., Belie, N. D. & Verstraete, W. (2008) 'Bacterial carbonate precipitation as an alternative surface treatment for concrete'. *Construction and Building Materials*, 22 (5), pp. 875-885.

de Vries, I. J. & Polder, R. (1997) 'Hydrophobic treatment of concrete'. *Construction and Building Materials*, 11 (4), pp. 259-265.

Dehghanpoor Abyaneh, S., Wong, H. S. & Buenfeld, N. R. (2013) 'Modelling the diffusivity of mortar and concrete using a three-dimensional mesostructure with several aggregate shapes'. *Computational materials science*, 78 pp. 63-73.

Dehghanpoor Abyaneh, S., Wong, H. S. & Buenfeld, N. R. (2014) 'Computational investigation of capillary absorption in concrete using a three-dimensional mesoscale approach'. *Computational materials science*, 87 (Supplement C), pp. 54-64.

Delagrave, A., Marchand, J., Ollivier, J.-P., Julien, S. & Hazrati, K. (1997) 'Chloride binding capacity of various hydrated cement paste systems'. *Advanced Cement based materials*, 6 (1), pp. 28-35.

Delucchi, M., Barbucci, A. & Cerisola, G. (1997) 'Study of the physico-chemical properties of organic coatings for concrete degradation control'. *Construction and Building Materials*, 11 (7), pp. 365-371.

Dhir, R. K., Jones, M. R. & Ng, S. L. D. (1998) 'Prediction of total chloride content profile and concentration/time-dependent diffusion coefficients for concrete'. *Magazine of concrete research*, 50 pp. 37-48.

Diamanti, M. V., Brenna, A., Bolzoni, F., Berra, M., Pastore, T. & Ormellese, M. (2013) 'Effect of polymer modified cementitious coatings on water and chloride permeability in concrete'. *Construction and Building Materials*, 49 (0), pp. 720-728.

Dormieux, L., Kondo, D. & Ulm, F.-J. (2006) *Microporomechanics*. John Wiley & Sons.

Elakneswaran, Y., Nawa, T. & Kurumisawa, K. (2009a) 'Electrokinetic potential of hydrated cement in relation to adsorption of chlorides'. *Cement and Concrete Research*, 39 (4), pp. 340-344.

Elakneswaran, Y., Nawa, T. & Kurumisawa, K. (2009b) 'Zeta potential study of paste blends with slag'. *Cement and Concrete Composites*, 31 (1), pp. 72-76.

Elakneswaran, Y., Nawa, T. & Kurumisawa, K. (2009c) 'Influence of surface charge on ingress of chloride ion in hardened pastes'. *Materials and structures*, 42 (1), pp. 83-93.

Ersoy, B., Dikmen, S., Uygunoğlu, T., İçduygu, M. G., Kavas, T. & Olgun, A. (2013) 'Effect of mixing water types on the time-dependent zeta potential of Portland cement paste'. *Science and Engineering of Composite Materials*, 20 (3), pp. 285-292.

Feng, P., Miao, C. & Bullard, J. W. (2014) 'A Model of Phase Stability, Microstructure and Properties During Leaching of Portland Cement Binders'. *Cement and Concrete Composites*,

Florea, M. V. A. & Brouwers, H. J. H. (2012) 'Chloride binding related to hydration products: Part I: Ordinary Portland Cement'. *Cement and Concrete Research*, 42 (2), pp. 282-290.

Friedmann, H., Amiri, O. & Aït-Mokhtar, A. (2008a) 'Shortcomings of geometrical approach in multi-species modelling of chloride migration in cement-based materials'. *Magazine of concrete research*, 60 pp. 119-124.

Friedmann, H., Amiri, O. & Aït-Mokhtar, A. (2008b) 'Shortcomings of geometrical approach in multi-species modelling of chloride migration in cement-based materials'. *Magazine of concrete research*, 60 (2), pp. 119-124.

Friedmann, H., Amiri, O. & Aït-Mokhtar, A. (2008c) 'Physical modeling of the electrical double layer effects on multispecies ions transport in cement-based materials'. *Cement and Concrete Research*, 38 (12), pp. 1394-1400.

Friedmann, H., Amiri, O. & Aït-Mokhtar, A. (2012) 'Modelling of EDL effect on chloride migration in cement-based materials'. *Magazine of concrete research*, 64 (10), pp. 909-917.

Friedmann, H., Amiri, O., Aıt-Mokhtar, A. & Dumargue, P. (2004) 'A direct method for determining chloride diffusion coefficient by using migration test'. *Cement and Concrete Research*, 34 (11), pp. 1967-1973.

Frizon, F., Lorente, S., Ollivier, J. P. & Thouvenot, P. (2003) 'Transport model for the nuclear decontamination of cementitious materials'. *Computational materials science*, 27 (4), pp. 507-516.

Gao, J. M., Qian, C. X., Liu, H. F., Wang, B. & Li, L. (2005) 'ITZ microstructure of concrete containing GGBS'. *Cement and Concrete Research*, 35 (7), pp. 1299-1304.

Garboczi, E. & Bentz, D. (1992) 'Computer simulation of the diffusivity of cement-based materials'. *Journal of Materials Science*, 27 (8), pp. 2083-2092.

Garboczi, E. & Bentz, D. (1996) 'Modelling of the microstructure and transport properties of concrete'. *Construction and Building Materials*, 10 (5), pp. 293-300.

Garboczi, E. J., Schwartz, L. M. & Bentz, D. P. (1995) 'Modeling the influence of the interfacial zone on the DC electrical conductivity of mortar'. *Advanced Cement based materials*, 2 (5), pp. 169-181.

Geiker, M., Nielsen, E. P. & Herfort, D. (2007) 'Prediction of chloride ingress and binding in cement paste'. *Materials and structures*, 40 (4), pp. 405-417.

Glass, G. & Buenfeld, N. (1997) 'The presentation of the chloride threshold level for corrosion of steel in concrete'. *Corrosion Science*, 39 (5), pp. 1001-1013.

Glass, G. & Buenfeld, N. (2000) 'The influence of chloride binding on the chloride induced corrosion risk in reinforced concrete'. *Corrosion Science*, 42 (2), pp. 329-344.

Glasser, F. P., Marchand, J. & Samson, E. (2008) 'Durability of concrete—degradation phenomena involving detrimental chemical reactions'. *Cement and Concrete Research*, 38 (2), pp. 226-246.

Gollop, R. S. & Taylor, H. F. W. (1995) 'Microstructural and microanalytical studies of sulfate attack III. Sulfate-resisting portland cement: Reactions with sodium and magnesium sulfate solutions'. *Cement and Concrete Research*, 25 (7), pp. 1581-1590.

Gouy, G. (1910) 'Constitution of the electric charge at the surface of an electrolyte'. *J. phys*, 9 (4), pp. 457-467.

Gummerson, R., Hall, C., Hoff, W., Hawkes, R., Holland, G. & Moore, W. (1979) 'Unsaturated water flow within porous materials observed by NMR imaging'.

Halamickova, P., Detwiler, R. J., Bentz, D. P. & Garboczi, E. J. (1995) 'Water permeability and chloride ion diffusion in Portland cement mortars: relationship to sand content and critical pore diameter'. *Cement and Concrete Research*, 25 (4), pp. 790-802.

Hall, C. (1989) 'Water sorptivity of mortars and concretes : a review'. *Mag. Concr. Res*, 41 (147), pp. 51-61.

Hall, C. (2007) 'Anomalous diffusion in unsaturated flow: Fact or fiction?'. *Cement and Concrete Research*, 37 (3), pp. 378-385.

Hazrati, K., Pel, L., Marchand, J., Kopinga, K. & Pigeon, M. (2002) 'Determination of isothermal unsaturated capillary flow in high performance cement mortars by NMR imaging'. *Materials and structures*, 35 (10), pp. 614-622.

He, F., Shi, C., Yuan, Q., Chen, C. & Zheng, K. (2012) 'AgNO3-based colorimetric methods for measurement of chloride penetration in concrete'. *Construction and Building Materials*, 26 (1), pp. 1-8.

Hobbs, D. (1999) 'Aggregate influence on chloride ion diffusion into concrete'. *Cement and Concrete Research*, 29 (12), pp. 1995-1998.

Hocine, T., Amiri, O., Ait-Mokhtar, A. & Pautet, A. (2012) 'Influence of cement, aggregates and chlorides on zeta potential of cement-based materials'. *Advances in cement research*, 24 (6), pp. 337-348.

Hoffman, J. D. & Frankel, S. (2001) *Numerical methods for engineers and scientists.* CRC press.

Hong, K. & Hooton, R. (2000) 'Effects of fresh water exposure on chloride contaminated concrete'. *Cement and Concrete Research*, 30 (8), pp. 1199-1207.

Hong, K. & Hooton, R. D. (1999) 'Effects of cyclic chloride exposure on penetration of concrete cover'. *Cement and Concrete Research*, 29 (9), pp. 1379-1386.

Ibrahim, M., Al-Gahtani, A., Maslehuddin, M. & Almusallam, A. (1997) 'Effectiveness of concrete surface treatment materials in reducing chloride-induced reinforcement corrosion'. *Construction and Building Materials*, 11 (7), pp. 443-451.

Jensen, O. M., Hansen, P. F., Coats, A. M. & Glasser, F. P. (1999) 'Chloride ingress in cement paste and mortar'. *Cement and Concrete Research*, 29 (9), pp. 1497-1504.

Jiang, L., Song, Z., Yang, H., Pu, Q. & Zhu, Q. (2013) 'Modeling the chloride concentration profile in migration test based on general Poisson Nernst Planck equations and pore structure hypothesis'. *Construction and Building Materials*, 40 pp. 596-603.

Jiřičková, M. & Černý, R. (2006) 'Chloride binding in building materials'. *Journal of Building Physics*, 29 (3), pp. 189-200.

Johannesson, B., Yamada, K., Nilsson, L. & Hosokawa, Y. (2007) 'Multi-species ionic diffusion in concrete with account to interaction between ions in the pore solution and the cement hydrates'. *Materials and structures*, 40 (7), pp. 651-665.

Justnes, H. (1998) 'A review of chloride binding in cementitious systems'. *NORDIC CONCRETE RESEARCH-PUBLICATIONS-*, 21 pp. 48-63.

Kari, O., Elakneswaran, Y., Nawa, T. & Puttonen, J. (2013) 'A model for a long-term diffusion of multispecies in concrete based on ion–cement-hydrate interaction'. *Journal of Materials Science*, 48 (12), pp. 4243-4259.

Kayyali, O. & Haque, M. (1995) 'The Cl−/OH− ratio in chloride-contaminated concrete—a most important criterion'. *Magazine of concrete research*, 47 (172), pp. 235-242.

Khanzadeh Moradllo, M., Shekarchi, M. & Hoseini, M. (2012) 'Time-dependent performance of concrete surface coatings in tidal zone of marine environment'. *Construction and Building Materials*, 30 (0), pp. 198-205.

Krabbenhøft, K. & Krabbenhøft, J. (2008) 'Application of the Poisson–Nernst–Planck equations to the migration test'. *Cement and Concrete Research*, 38 (1), pp. 77-88.

Kwon, S.-J. & Song, H.-W. (2010) 'Analysis of carbonation behavior in concrete using neural network algorithm and carbonation modeling'. *Cement and Concrete Research*, 40 (1), pp. 119-127.

Labbez, C., Pochard, I., Jönsson, B. & Nonat, A. (2011) 'C-S-H/solution interface: Experimental and Monte Carlo studies'. *Cement and Concrete Research*, 41 (2), pp. 161-168.

Li, L.-y. (2014) 'A pore size distribution-based chloride transport model in concrete'.

Li, L.-Y., Xia, J. & Lin, S.-S. (2012) 'A multi-phase model for predicting the effective diffusion coefficient of chlorides in concrete'. *Construction and Building Materials*, 26 (1), pp. 295-301.

Li, L. & Page, C. (1998) 'Modelling of electrochemical chloride extraction from concrete: influence of ionic activity coefficients'. *Computational materials science*, 9 (3), pp. 303-308.

Li, L. & Page, C. (2000) 'Finite element modelling of chloride removal from concrete by an electrochemical method'. *Corrosion Science*, 42 (12), pp. 2145-2165.

Liu, Q.-f., Easterbrook, D., Yang, J. & Li, L.-y. (2015) 'A three-phase, multi-component ionic transport model for simulation of chloride penetration in concrete'. *Engineering Structures*, 86 pp. 122-133.

Liu, Q.-f., Li, L.-y., Easterbrook, D. & Yang, J. (2012) 'Multi-phase modelling of ionic transport in concrete when subjected to an externally applied electric field'. *Engineering Structures*, 42 pp. 201-213.

Liu, Q.-f., Xia, J., Easterbrook, D., Yang, J. & Li, L.-y. (2014) 'Three-phase modelling of electrochemical chloride removal from corroded steel-reinforced concrete'. *Construction and Building Materials*, 70 (0), pp. 410-427.

Liu, Q. (2014) *Multi-phase modelling of multi-species ionic migration in concrete*. Plymouth University

Liu, Y. & Shi, X. (2012) 'Ionic transport in cementitious materials under an externally applied electric field: Finite element modeling'. *Construction and Building Materials*, 27 (1), pp. 450-460.

Lockington, D., Parlange, J.-Y. & Dux, P. (1999) 'Sorptivity and the estimation of water penetration into unsaturated concrete'. *Materials and structures*, 32 (5), pp. 342-347.

Lorente, S., Carcassè, M. & Ollivier, J. (2003) 'Penetration of ionic species into saturated porous media: the case of concrete'. *International journal of energy research*, 27 (10), pp. 907-917.

Loser, R., Lothenbach, B., Leemann, A. & Tuchschmid, M. (2010) 'Chloride resistance of concrete and its binding capacity–comparison between experimental results and thermodynamic modeling'. *Cement and Concrete Composites*, 32 (1), pp. 34-42.

Lothenbach, B., Bary, B., Le Bescop, P., Schmidt, T. & Leterrier, N. (2010) 'Sulfate ingress in Portland cement'. *Cement and Concrete Research*, 40 (8), pp. 1211-1225.

Lu, X., Li, C. & Zhang, H. (2002) 'Relationship between the free and total chloride diffusivity in concrete'. *Cement and Concrete Research*, 32 (2), pp. 323-326.

Luping, T. (1996) *Chloride transport in concrete-measurement and prediction*. Chalmers University of Technology.

Luping, T. & Nilsson, L.-O. (1993) 'Chloride binding capacity and binding isotherms of OPC pastes and mortars'. *Cement and Concrete Research*, 23 (2), pp. 247-253.

Maheswaran, T. & Sanjayan, J. G. (2004) 'A semi-closed-form solution for chloride diffusion in concrete with time-varying parameters'. *Magazine of concrete research*, 56 pp. 359-366.

Marchand, J. & Samson, E. (2009) 'Predicting the service-life of concrete structures–limitations of simplified models'. *Cement and Concrete Composites*, 31 (8), pp. 515-521.

Marchand, J., Samson, E., Maltais, Y. & Beaudoin, J. (2002) 'Theoretical analysis of the effect of weak sodium sulfate solutions on the durability of concrete'. *Cement and Concrete Composites*, 24 (3), pp. 317-329.

Martın-Pérez, B., Zibara, H., Hooton, R. & Thomas, M. (2000) 'A study of the effect of chloride binding on service life predictions'. *Cement and Concrete Research*, 30 (8), pp. 1215-1223.

Maslehuddin, M., Alidi, S., Mehthel, M., Shameem, M. & Ibrahim, M. (2005) 'Performance evaluation of repair systems under varying exposure conditions'. *Cement and Concrete Composites*, 27 (9), pp. 885-897.

McCarter, W., Ezirim, H. & Emerson, M. (1992) 'Absorption of water and chloride into concrete'. *Magazine of concrete research*, 44 (158), pp. 31-37.

Medeiros, M. H. & Helene, P. (2009) 'Surface treatment of reinforced concrete in marine environment: Influence on chloride diffusion coefficient and capillary water absorption'. *Construction and Building Materials*, 23 (3), pp. 1476-1484.

Mehta, P. K. & Monteiro, P. J. (2006) *Concrete: microstructure, properties, and materials*. vol. 3. McGraw-Hill New York.

Mercado, H., Lorente, S. & Bourbon, X. (2012) 'Chloride diffusion coefficient: A comparison between impedance spectroscopy and electrokinetic tests'. *Cement and Concrete Composites*, 34 (1), pp. 68-75.

Moon, H. Y., Shin, D. G. & Choi, D. S. (2007) 'Evaluation of the durability of mortar and concrete applied with inorganic coating material and surface treatment system'. *Construction and Building Materials*, 21 (2), pp. 362-369.

Morandeau, A., Thiéry, M. & Dangla, P. (2014) 'Investigation of the carbonation mechanism of CH and C-S-H in terms of kinetics, microstructure changes and moisture properties'. *Cement and Concrete Research*, 56 (0), pp. 153-170.

Moranville, M., Kamali, S. & Guillon, E. (2004) 'Physicochemical equilibria of cement-based materials in aggressive environments—experiment and modeling'. *Cement and Concrete Research*, 34 (9), pp. 1569-1578.

Nägele, E. (1985) 'The zeta-potential of cement'. *Cement and Concrete Research*, 15 (3), pp. 453-462.

Narsilio, G., Li, R., Pivonka, P. & Smith, D. (2007) 'Comparative study of methods used to estimate ionic diffusion coefficients using migration tests'. *Cement and Concrete Research*, 37 (8), pp. 1152-1163.

Newman, J. & Thomas-Alyea, K. E. (2012) *Electrochemical systems*. John Wiley & Sons.

Nguyen, P. T. & Amiri, O. (2014) 'Study of electrical double layer effect on chloride transport in unsaturated concrete'. *Construction and Building Materials*, 50 pp. 492-498.

Nielsen, E. P. & Geiker, M. R. (2003) 'Chloride diffusion in partially saturated cementitious material'. *Cement and Concrete Research*, 33 (1), pp. 133-138.

Nilsson, L. & Ollivier, J. (1995) 'Chloride transport due to wick action in concrete', *RILEM International workshop on chloride penetration into concrete*. RILEM Publications SARL, pp. 315-324.

NT-BUILD443 (1995) 'Concrete, hardened: accelerated chloride penetration'. *Nordtest method*,

NT-BUILD492 (1999) 'Concrete, mortar and cement-based repair materials: chloride migration coefficient from non-steady-state migration experiments'. *Nordtest method*, 492 pp. 10.

Oh, B. H. & Jang, S. Y. (2004) 'Prediction of diffusivity of concrete based on simple analytic equations'. *Cement and Concrete Research*, 34 (3), pp. 463-480.

Pack, S.-W., Jung, M.-S., Song, H.-W., Kim, S.-H. & Ann, K. Y. (2010) 'Prediction of time dependent chloride transport in concrete structures exposed to a marine environment'. *Cement and Concrete Research*, 40 (2), pp. 302-312.

Page, C. L. (1975) 'Mechanism of corrosion protection in reinforced concrete marine structures'. *Nature*, 258 (5535), pp. 514-515.

Page, C. L., Short, N. R. & El Tarras, A. (1981) 'Diffusion of chloride ions in hardened cement pastes'. *Cement and Concrete Research*, 11 (3), pp. 395-406.

Perkins, P. (2002) *Repair, protection and waterproofing of concrete structures.* CRC Press.

Pfeifer, D. W., McDonald, D. B. & Krauss, P. D. (1994) 'The rapid chloride permeability test and its correlation to the 90-day chloride ponding test'. *PCI Journal*, 39 (1),

Pigino, B., Leemann, A., Franzoni, E. & Lura, P. (2012) 'Ethyl silicate for surface treatment of concrete – Part II: Characteristics and performance'. *Cement and Concrete Composites*, 34 (3), pp. 313-321.

Planel, D., Sercombe, J., Le Bescop, P., Adenot, F. & Torrenti, J.-M. (2006) 'Long-term performance of cement paste during combined calcium leaching–sulfate attack: kinetics and size effect'. *Cement and Concrete Research*, 36 (1), pp. 137-143.

Polder, R. B. & Peelen, W. H. (2002) 'Characterisation of chloride transport and reinforcement corrosion in concrete under cyclic wetting and drying by electrical resistivity'. *Cement and Concrete Composites*, 24 (5), pp. 427-435.

Powers, T. C. & Brownyard, T. L. (1946) 'Studies of the physical properties of hardened Portland cement paste', *ACI Journal Proceedings*. ACI.

Probstein, R. F. (2005) *Physicochemical hydrodynamics: an introduction.* John Wiley & Sons.

Quincke, G. (1861) 'Ueber die Fortführung materieller Theilchen durch strömende Elektricität'. *Annalen der Physik*, 189 (8), pp. 513-598.

Reddy, B., Glass, G., Lim, P. & Buenfeld, N. (2002) 'On the corrosion risk presented by chloride bound in concrete'. *Cement and Concrete Composites*, 24 (1), pp. 1-5.

Roels, S., Carmeliet, J., Hens, H., Adan, O., Brocken, H., Cerny, R., Pavlik, Z., Ellis, A. T., Hall, C. & Kumaran, K. (2004) 'A comparison of different techniques to quantify moisture content profiles in porous building materials'. *Journal of Thermal Envelope and Building Science*, 27 (4), pp. 261-276.

Rozière, E., Loukili, A., El Hachem, R. & Grondin, F. (2009) 'Durability of concrete exposed to leaching and external sulphate attacks'. *Cement and Concrete Research*, 39 (12), pp. 1188-1198.

Rubin, J. (1983) 'Transport of reacting solutes in porous media: Relation between mathematical nature of problem formulation and chemical nature of reactions'. *Water Resources Research*, 19 (5), pp. 1231-1252.

Sabir, B., Wild, S. & O'Farrell, M. (1998) 'A water sorptivity test for martar and concrete'. *Materials and structures*, 31 (8), pp. 568-574.

Saetta, A. V., Scotta, R. V. & Vitaliani, R. V. (1993) 'Analysis of chloride diffusion into partially saturated concrete'. *ACI Materials Journal*, 90 (5),

Safiuddin, M. & Soudki, K. (2011) 'Sealer and coating systems for the protection of concrete bridge structures'. *International Journal of Physical Sciences*, 6 (37), pp. 8187-8198.

Samson, E., Lemaire, G., Marchand, J. & Beaudoin, J. J. (1999) 'Modeling chemical activity effects in strong ionic solutions'. *Computational materials science*, 15 (3), pp. 285-294.

Samson, E. & Marchand, J. (1999) 'Numerical solution of the extended Nernst–Planck model'. *Journal of Colloid and Interface Science*, 215 (1), pp. 1-8.

Samson, E., Marchand, J. & Beaudoin, J. (1999) 'Describing ion diffusion mechanisms in cement-based materials using the homogenization technique'. *Cement and Concrete Research*, 29 (8), pp. 1341-1345.

Samson, E., Marchand, J. & Beaudoin, J. (2000) 'Modeling the influence of chemical reactions on the mechanisms of ionic transport in porous materials: an overview'. *Cement and Concrete Research*, 30 (12), pp. 1895-1902.

Samson, E., Marchand, J. & Snyder, K. (2003) 'Calculation of ionic diffusion coefficients on the basis of migration test results'. *Materials and structures*, 36 (3), pp. 156-165.

Samson, E., Marchand, J., Snyder, K. A. & Beaudoin, J. J. (2005) 'Modeling ion and fluid transport in unsaturated cement systems in isothermal conditions'. *Cement and Concrete Research*, 35 (1), pp. 141-153.

Santhanam, M., Cohen, M. D. & Olek, J. (2002) 'Mechanism of sulfate attack: a fresh look: part 1: summary of experimental results'. *Cement and Concrete Research*, 32 (6), pp. 915-921.

Santhanam, M., Cohen, M. D. & Olek, J. (2003) 'Mechanism of sulfate attack: a fresh look: Part 2. Proposed mechanisms'. *Cement and Concrete Research*, 33 (3), pp. 341-346.

Šavija, B., Luković, M. & Schlangen, E. (2014) 'Lattice modeling of rapid chloride migration in concrete'. *Cement and Concrete Research*, 61–62 (0), pp. 49-63.

Schmidt, T., Lothenbach, B., Romer, M., Neuenschwander, J. & Scrivener, K. (2009) 'Physical and microstructural aspects of sulfate attack on ordinary and limestone blended Portland cements'. *Cement and Concrete Research*, 39 (12), pp. 1111-1121.

Seneviratne, A., Sergi, G. & Page, C. (2000) 'Performance characteristics of surface coatings applied to concrete for control of reinforcement corrosion'. *Construction and Building Materials*, 14 (1), pp. 55-59.

Sergi, G., Yu, S. & Page, C. (1992) 'Diffusion of chloride and hydroxyl ions in cementitious materials exposed to a saline environment'. *Magazine of concrete research*, 44 (158), pp. 63-69.

Shane, J., Mason, T., Jenning, H., Alexander, M., Arliguie, G., Ballivy, G., Bentur, A. & Marchand, J. (1999) 'Conductivity and microstructure of the interfacial transition zone measured by impedance spectroscopy'. *RILEM REPORT*, pp. 173-204.

Shi, X., Xie, N., Fortune, K. & Gong, J. (2012) 'Durability of steel reinforced concrete in chloride environments: An overview'. *Construction and Building Materials*, 30 pp. 125-138.

Spiesz, P. & Brouwers, H. (2013) 'The apparent and effective chloride migration coefficients obtained in migration tests'. *Cement and Concrete Research*, 48 pp. 116-127.

Stanish, K., Hooton, R. & Thomas, M. (1997) 'Testing the chloride penetration resistance of concrete: a literature review'. *FHWA contract DTFH61*, pp. 19-22.

Stern, O. (1924) 'The theory of the electrolytic double-layer'. *Z. Elektrochem*, 30 (508), pp. 1014-1020.

Sun, G., Zhang, Y., Sun, W., Liu, Z. & Wang, C. (2011) 'Multi-scale prediction of the effective chloride diffusion coefficient of concrete'. *Construction and Building Materials*, 25 (10), pp. 3820-3831.

Suryavanshi, A., Scantlebury, J. & Lyon, S. (1998) 'Corrosion of reinforcement steel embedded in high water-cement ratio concrete contaminated with chloride'. *Cement and Concrete Composites*, 20 (4), pp. 263-281.

Tang, L. P. & Nilsson, L.-O. (1993) 'Rapid determination of the chloride diffusivity in concrete by applying an electric field'. *ACI Materials Journal*, 89 (1), pp. 49-53.

Taylor, H., Famy, C. & Scrivener, K. (2001) 'Delayed ettringite formation'. *Cement and Concrete Research*, 31 (5), pp. 683-693.

Taylor, H. F. (1997) *Cement Chemistry*. Thomas Telford.

Thompson, J. L., Silsbee, M., Gill, P. & Scheetz, B. (1997) 'Characterization of silicate sealers on concrete'. *Cement and Concrete Research*, 27 (10), pp. 1561-1567.

Toumi, A., François, R. & Alvarado, O. (2007) 'Experimental and numerical study of electrochemical chloride removal from brick and concrete specimens'. *Cement and Concrete Research*, 37 (1), pp. 54-62.

Tournassat, C. & Steefel, C. I. (2015) 'Ionic transport in nano-porous clays with consideration of electrostatic effects'. *Rev Mineral Geochem*, 80 pp. 287-329.

Truc, O., Ollivier, J.-P. & Nilsson, L.-O. (2000a) 'Numerical simulation of multi-species diffusion'. *Materials and structures*, 33 (9), pp. 566-573.

Truc, O., Ollivier, J.-P. & Nilsson, L.-O. (2000b) 'Numerical simulation of multi-species transport through saturated concrete during a migration test — MsDiff code'. *Cement and Concrete Research*, 30 (10), pp. 1581-1592.

Uni, E. (2004) '1504-2. Products and systems for the protection and repair of concrete structures'.[in *Definitions, requirements, quality control and evaluation of conformity–Part 2*. (Accessed:Uni, E.

Van Brakel, J. & Heertjes, P. (1974) 'Analysis of diffusion in macroporous media in terms of a porosity, a tortuosity and a constrictivity factor'. *International Journal of Heat and Mass Transfer*, 17 (9), pp. 1093-1103.

Viallis-Terrisse, H., Nonat, A. & Petit, J.-C. (2001) 'Zeta-Potential Study of Calcium Silicate Hydrates Interacting with Alkaline Cations'. *Journal of Colloid and Interface Science*, 244 (1), pp. 58-65.

von Helmholtz, H. (1879) 'The Double Layer'. *Wied. Ann*, 7 pp. 337.

Wang, L. & Ueda, T. (2011) 'Mesoscale modeling of water penetration into concrete by capillary absorption'. *Ocean Engineering*, 38 (4), pp. 519-528.

Wang, Y., Li, L.-y. & Page, C. (2005) 'Modelling of chloride ingress into concrete from a saline environment'. *Building and environment*, 40 (12), pp. 1573-1582.

Wang, Y., Li, L. & Page, C. (2001) 'A two-dimensional model of electrochemical chloride removal from concrete'. *Computational materials science*, 20 (2), pp. 196-212.

Winslow, D. & Liu, D. (1990) 'The pore structure of paste in concrete'. *Cement and Concrete Research*, 20 (2), pp. 227-235.

Xi, Y. & Bazant, Z. P. (1999) 'Modeling chloride penetration in saturated concrete'. *Journal of Materials in Civil Engineering*, 11 (1), pp. 58-65.

Xia, J. & Li, L.-y. (2013) 'Numerical simulation of ionic transport in cement paste under the action of externally applied electric field'. *Construction and Building Materials*, 39 pp. 51-59.

Yang, C.-C. & Weng, S.-H. (2013) 'A three-phase model for predicting the effective chloride migration coefficient of ITZ in cement-based materials'. *Magazine of concrete research*, 65 pp. 193-201.

Yang, C., Wang, L. & Weng, T. (2004) 'Using charge passed and total chloride content to assess the effect of penetrating silane sealer on the transport properties of concrete'. *materials chemistry and physics*, 85 (1), pp. 238-244.

Yang, C. C. & Chiang, C. (2009) 'Relation between the chloride migration coefficients of concrete from the colourimetric method and the chloride profile method'. *Journal of the Chinese institute of engineers*, 32 (6), pp. 801-809.

Ying, J., Xiao, J., Shen, L. & Bradford, M. A. (2013) 'Five-phase composite sphere model for chloride diffusivity prediction of recycled aggregate concrete'. *Magazine of concrete research*, 65 pp. 573-588.

Yoon, S., Oh, S.-g., Ha, J. & Monteiro, P. M. (2012) 'The effects of surface treatments on rapid chloride permeability tests'. *materials chemistry and physics*, 135 (2–3), pp. 699-708.

Yu, S. & Page, C. (1996) 'Computer simulation of ionic migration during electrochemical chloride extraction from hardened concrete'. *British Corrosion Journal*, 31 (1), pp. 73-75.

Yuan, Q., Shi, C., De Schutter, G., Audenaert, K. & Deng, D. (2009) 'Chloride binding of cement-based materials subjected to external chloride environment–a review'. *Construction and Building Materials*, 23 (1), pp. 1-13.

Zhang, J.-Z. & Buenfeld, N. (1997) 'Presence and possible implications of a membrane potential in concrete exposed to chloride solution'. *Cement and Concrete Research*, 27 (6), pp. 853-859.

Zhang, J.-Z. & Buenfeld, N. (2000a) 'Chloride profiles in surface-treated mortar specimens'. *Construction and Building Materials*, 14 (6), pp. 359-364.

Zhang, J.-Z. & Buenfeld, N. (2000b) 'Measuring the membrane potential across cement-based materials'. *Materials and structures*, 33 (8), pp. 492-498.

Zhang, J.-Z., McLoughlin, I. & Buenfeld, N. (1998) 'Modelling of chloride diffusion into surface-treated concrete'. *Cement and Concrete Composites*, 20 (4), pp. 253-261.

Publications

- Ganlin Feng*, Longyuan Li, Boksun Kim, Qingfeng Liu (2016). “Multiphase modelling of ionic transport in cementitious materials with surface charges.” Computational Materials Science. Vol. 111, pp.339-349. DOI: 10.1016/j.commatsci.2015.09.060.
- Qing-feng Liu, Gan-lin Feng*, Jin Xia, Jian Yang, Long-yuan Li (2018). “Ionic transport features in concrete composites containing various shaped aggregates: a numerical study.” Composite Structures. Vol. 183, pp.371-380. DOI: 10.1016/j.compstruct.2017.03.088.
- Ganlin Feng*, Longyuan Li, Boksun Kim (2015). “The effect of an Electric Double Layer on chloride penetration in cement paste.” The 2015 World Congress on Advances in Structural Engineering and Mechanics, ASEM15, Incheon, Korea, August 25-29.
- Ganlin Feng*, Longyuan Li (2016). “Numerical Simulation of Migration-dominated Ionic Transport in Concrete.” Presented at The International Conference on Durability of Concrete Structure, ICDCS16, Shenzhen, China, June 30.